The Dissertation Committee for Nikhil Ulhas Kundargi

certifies that this is the approved version of the following dissertation:

Novel Channel Sensing and Access Strategies in Opportunistic Spectrum Access Networks

Committee:

Ahmed Tewfik, Supervisor

Jeffrey Andrews

Lili Qiu

Sujay Sanghavi

Sriram Vishwanath

Novel Channel Sensing and Access Strategies in Opportunistic Spectrum Access Networks

by

Nikhil Ulhas Kundargi, B.E.

Dissertation

Presented to the Faculty of the Graduate School of

The University of Texas at Austin

in Partial Fulfillment

of the Requirements

for the Degree of

DOCTOR OF PHILOSOPHY

THE UNIVERSITY OF TEXAS AT AUSTIN

May 2012

Acknowledgments

It is a pleasure to thank those who have made this thesis possible. First and foremost, I am greatly privileged to have worked with my adviser Professor Ahmed Tewfik. He instilled in me the joy of being a researcher. I owe a great debt of gratitude for his insightful mentoring, constant encouragement, and farsighted guidance. I am grateful to my doctoral committee members Prof. Jeffrey Andrews, Prof. Sriram Vishwanath, Prof. Sujay Sanghavi and Prof. Lili Qiu for their helpful and constructive inputs to this thesis. I would also like to thank my qualifying examination committee members at the University of Minnesota, Prof. Nihar Jindal, Prof. Emad Ebbini, Prof. Douglas Hawkins, Prof. Mostafa Kaveh and Prof. Tian He for their help in formulating the thesis. I am grateful to my colleagues at National Instruments and Qualcomm during my internships for their insights into modern telecommunications industry, especially Sam Shearman. Also, I am thankful to my colleague Yingxi for his companionship during countless hours of brainstorming. My senior labmates Vikrham, Seshan, Cheolhong have made it easier for me to follow in their footsteps and Dan, Youngchun, Vimal, Vijay, Neeraj, Rahul, Mostafa, Brice, Guido have been great colleagues. My PhD buddies Ajay, Devdatta, Salil B, Shruti P, Esha have shared their war stories to keep me going. My friends Shruti K, Sajal, Siddharth, Neha, Raghav, Harsh, Pranav B, Pranav K, Anush, Nikhil G, Salil V, Purva, Sudarshan, Madhura, Rahul, Anuj, Nachiket, Khushbu, Sandeep and countless others have lightened my burden and made the last few years some of the most enjoyable ones of my life. My undergraduate friends Anup, Amogh, Kaustubh, Harshad, Neil inspired me to pursue this path. Lastly and most importantly, I am indebted to my parents and to my sister for being extremely supportive of my graduate studies.

Novel Channel Sensing and Access Strategies in Opportunistic Spectrum Access Networks

Nikhil Ulhas Kundargi, Ph.D.
The University of Texas at Austin, 2012

Supervisor: Ahmed Tewfik

Traditionally radio spectrum was considered a commodity to be allocated in a fixed and centralized manner, but now the technical community and the regulators approach it as a shared resource that can be flexibly and intelligently shared between competing entities. In this thesis we focus on novel strategies to sense and access the radio spectrum within the framework of Opportunistic Spectrum Access via Cognitive Radio Networks (CRNs). In the first part we develop novel transmit opportunity detection methods that effectively exploit the gray space present in packet based networks. Our methods proactively detect the maximum safe transmit power that does not significantly affect the primary network nodes via an implicit feedback mechanism from the Primary network to the Secondary network. A novel use of packet interarrival duration is developed to robustly perform change detection in the primary network's Quality of Service. The methods are validated on real world IEEE 802.11 WLANs. In the second part we study the inferential use of Goodness-of-Fit tests for spectrum sensing applications. We provide the first comprehensive framework for decision fusion of an ensemble of goodness-of-fit tests through use of p-values. Also, we introduce a generalized $\mathbf{\Phi}$-divergence statistic to formulate goodness-of-fit tests that are tunable via a single parameter. We show that under uncertainty in the noise statistics or non-Gaussianity in the noise, the performance of such non-parametric tests is significantly superior to that of

conventional spectrum sensing methods. Additionally, we describe a collaborative spatially separated version of the test for robust combining of tests in a distributed spectrum sensing setting. In the third part we develop the sequential energy detection problem for spectrum sensing and formulate a novel Sequential Energy Detector. Through extensive simulations we demonstrate that our doubly hierarchical sequential testing architecture delivers a significant throughput improvement of 2 to 6 times over the fixed sample size test while maintaining equivalent operating characteristics as measured by the Probabilities of Detection and False Alarm. We also demonstrate the throughput gains for a case study of sensing ATSC television signals in IEEE 802.22 systems.

Table of Contents

List of Figures

Chapter 1

Introduction

In this chapter, we will provide a brief introduction to Cognitive Radio Networks and the philosophy of Opportunistic Spectrum Access and lay the framework in which to understand the contributions of this thesis. The explosive growth of wireless devices, technologies and services in the civilian and military fields has made radio spectrum into a precious commodity. Historically the spectrum regulatory framework has been formulated in a manner that radio spectrum is treated as a national resource to be licensed out to users by the government. These licensees are promised exclusive rights to the use of this spectrum and an unlicensed transmissions by other parties are considered illegal. The finite amount of available spectrum has resulted in a situation where the innovative wireless services being proposed have no spectrum available on which they can be deployed.

1.1 Spectrum Availability and Spectrum Utilization

The apparent shortage of spectrum that can be allocated motivated the scientific community and the regulatory agencies such as the Federal Communications Commission (FCC) to closely examine the current spectrum utilization. These efforts revealed a surprising dichotomy between the amount of spectrum that becomes available for licensing on one hand and the actual utilization of the spectrum that has already been allotted out on the other hand. In order to illustrate this situation, we will refer to a number of spectrum utilization studies that have been conducted over the last few years. Figure 1.1 shows the current

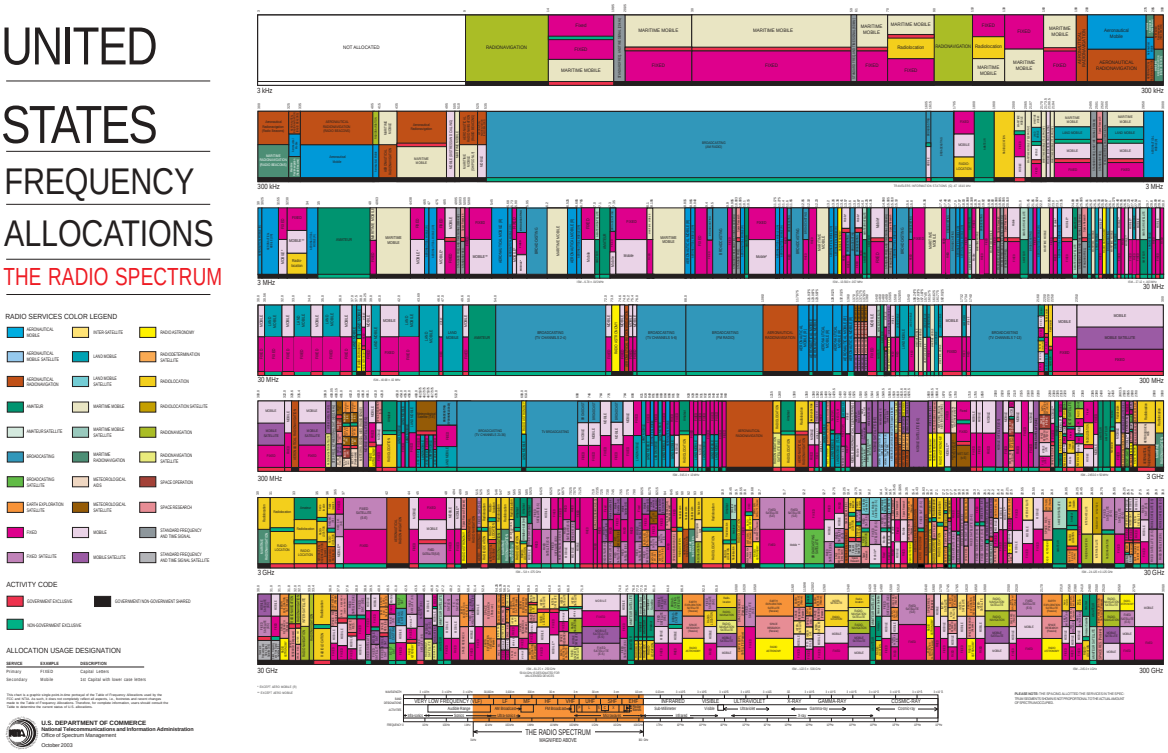

Figure 1.1: Allocation of Spectrum in the United States

allocation of licensed and unlicensed spectrum by the Federal Communications Commission in the United States. It is seen that the spectrum pie has been cut into many small pieces and split among many licensees.

On the other hand, hardly any of the spectrum is heavily utilized and most frequencies are lying vacant for most of the time. Multiple studies undertaken in Europe, Asia and urban America all point towards less than 30 percent utilization at peak usage as seen in figures 1.2 and 1.3, also refer to following works and references therein for more details [1–4]. In most rural areas and at off-peak usage periods, the utilization of spectrum is almost negligible. These exciting observations suggested that a paradigm shift was needed in the way spectrum regulation and utilization occurs. The FCC once again took the initiative in these efforts and formulated the Spectrum Policy Task Force (SPTF), which led in turn to the seminal

Notice of Proposed Rulemaking that proposes to allow "cognitive radio technology" towards the purpose of achieving opportunistic spectrum access.

1.2 Cognitive Radio

Cognitive Radios were first proposed by J. Mitola in his doctoral dissertation in 2000 [5]. He defined a cognitive radio as *"A radio that employs model based reasoning to achieve a specified level of competence in radio-related domains"*. Since then, the concept of a cognitive radio has been substantially enhanced as can be seen through the subsequent definitions of a cognitive radio.

1.2.1 Definitions

The FCC defines CR as *"A radio that can change its transmitter parameters based on interaction with the environment in which it operates"* [6].

The IEEE defines CR as *"A type of radio that can sense and autonomously reason about its environment and adapt accordingly. This radio could employ knowledge representation, automated reasoning and machine learning mechanisms in establishing, conducting, or terminating communication or networking functions with other radios. Cognitive radios can be trained to dynamically and autonomously adjust its operating parameters"* [7].

The NTIA which is a US regulatory institution defines it as *"A radio or system that senses its operational electromagnetic environment and can dynamically and autonomously adjust its radio operating parameters to modify system operation, such as maximize throughput, mitigate interference, facilitate interoperability, and access secondary markets"* [8].

It can be seen that the concept of a cognitive radio is extremely versatile. In the past decade there has been a significant amount of research that has furthered our understanding of all aspects of cognitive radios such as spectrum sensing, dynamic spectrum access, design

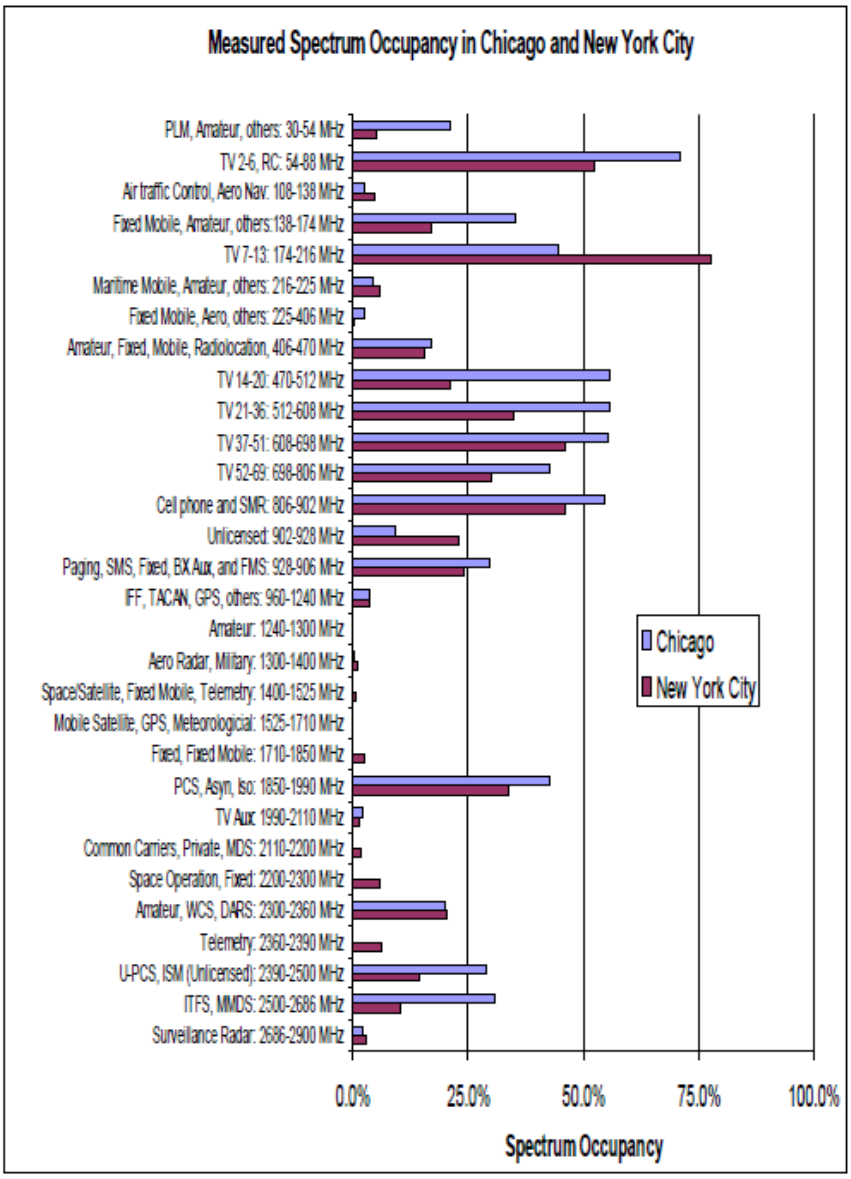

Figure 1.2: Utilization of spectrum in New York and Chicago

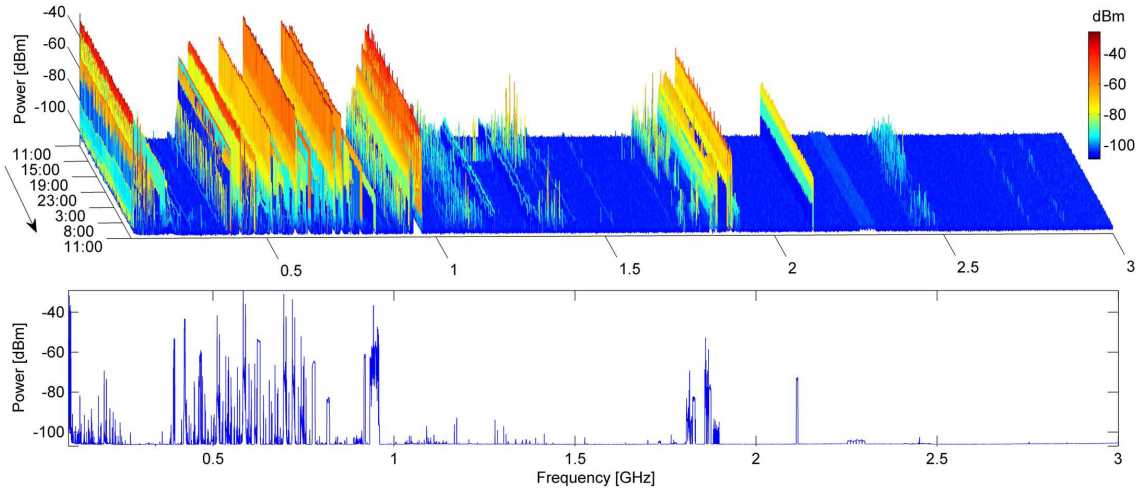

Figure 1.3: Utilization of Spectrum in Paris

of adaptive waveforms, cognitive policy engines, machine learning of radio environment etc. See the following references for further treatment of these issues [9–16]. In this thesis, we only focus on the use of cognitive radio technologies to address the problem of opportunistic spectrum access. Specifically, we propose novel approaches to detect idle channel capacity that has hitherto been not exploited in an opportunistic manner, in addition to addressing challenges in more conventional opportunistic spectrum access settings.

1.3 Opportunistic Spectrum Access

The Opportunistic Spectrum Access (OSA) is a channel access paradigm that uses a cognitive radio to detect underutilization of spectrum, and to access that spectrum in a smart manner such that various constraints on the effects caused by this access are satisfied. The design of an OSA system can be split into three steps [17].

1. Spectrum Opportunity Identification

   In a given OSA approach, the presence of a spectrum opportunity needs to be defined. A number of approaches have been proposed, with the most popular being to designate

the absence of a primary user from the channel under consideration as a spectrum opportunity. This can be naive under certain situations where the primary needs to sense the channel before accessing it.

2. Spectrum Opportunity Exploitation

   Once a spectrum opportunity is detected, it can be exploited in a variety of ways by the secondary user. This is achieved via algorithms that control the power and waveforms of secondary transmission, the medium access protocol between multiple secondary users and networks, e.t.c.

3. Interference Constraints and Regulatory Policies

   The spectrum opportunities are not static. The primary user might suddenly start transmitting on a channel, or the secondary user can be mobile and move into a location where another primary user is using the channel under consideration. Such behavior is controlled by introducing a interference constraint in terms of the time duration for which a secondary is allowed to transmit after the primary occupies the channel, or in terms of bounds on collision probabilities for collision between primary and secondary transmissions in random access systems. These constraints can be self imposed by the cognitive radio standards or they might be mandated by the regulatory bodies. The Interference Temperature is another such constraint that will be introduced in the next chapter.

1.3.1 Key Terms

In this section, we define a number of key terms related to cognitive radios that will be frequently used later throughout this work.

1. Primary User

A primary user is the user licensed to operate on the spectrum under consideration. Such a license is granted by the regulatory body in the territory in which the primary user operates, such as FCC (US), OFCOM (UK), ETSI (EU) e.t.c. It is guaranteed to be free from interference generated by any unlicensed users.

2. Secondary User

   A secondary user is the user that operates in any spectrum band that has not been licensed to it. Such a secondary user is not guaranteed to be free of interference from primary users, and is expected to not generate any significant interference to the primary users using that spectrum.

3. Spectral Hole

   In a spatial Opportunistic Spectrum Access mode, a frequency band not being accessed by any primary users at a given location is called a spectral hole. In practice, primary networks that stay on or off for a long time at a given location such as TV channels are classified as spectral holes.

4. Temporal Hole

   In a temporal Opportunistic Spectrum Access model, the time intervals between successive access of the frequency band by the primary user is called a temporal hole. In practice, primary networks that transmit frequently for relatively short intervals such as cellular networks or Wireless LANs are classified as temporal holes.

5. White Space vs Gray Space

   Temporal holes and Spectral holes can be combined into the concept of white space. A white space OSA model allows the secondary user to transmit *only* when the primary user is absent. A gray space OSA model on the other hand allows the secondary user to transmit at the same time as the primary user, subject to more stringent constraints.

6. Interference Temperature

   The interference temperature is a concept introduced by the FCC to allow gray space use. It is the net additional interference that can be generated at the location of the primary user due to operation of all the secondary users.

7. Overlay OSA

   An overlay OSA approach exploits the available white space. It allows the secondary user to transmit with relatively high power but imposes a constraint on when and where it may transmit.

8. Underlay OSA

   An underlay OSA approach exploits the available gray space. It imposes stringent constraints on the transmission power of the secondary users by making them transmit below the noise floor of the primary users. It does not need to detect White Space via spectrum sensing.

1.4 Organization

Finally, we will briefly preview the structure and organization of the subsequent chapters.

In Chapter 2, we develop a novel suite of transmit opportunity detection methods that effectively exploit the gray space present in high traffic packet networks. Our method adopts a holistic view of the primary network and proactively decides the maximum safe transmit power that does not affect any of the nodes in the primary network. This is achieved via an implicit feedback mechanism from the Primary network to the Secondary network. This is the first time that such a PU-SU feedback link has been shown to naturally arise in the framework of Dynamic Spectrum Access. A novel use of primary packet interarrival duration

is developed to rapidly and robustly perform change detection in the primary network's Quality of Service. We thoroughly validate the efficacy of the methods through exhaustive field testing on real world large scale IEEE 802.11 WLAN deployments.

In Chapter 3 we study the inferential use of goodness of fit tests in a non-parametric setting. The utility of such tests will be demonstrated for the test case of spectrum sensing applications in cognitive radios. We provide the first comprehensive framework for decision fusion of an ensemble of goodness-of-fit testing procedures through an Ensemble Goodness-of-Fit test. Also, we introduce a generalized family of functionals and kernels called **Φ**-divergences which allow us to formulate goodness-of-fit tests that are parameterized by a single parameter. The performance of these tests is simulated under Gaussian and non-Gaussian noise in a MIMO setting. We show that under uncertainty in the noise statistics or non-Gaussianity in the noise, the performance of non-parametric tests in general, and phi-divergence based goodness-of-fit tests in particular, is significantly superior to that of the energy detector with reduced implementation complexity. In particular, the false alarm rates of our proposed tests is maintained at a fixed level over a wide variation in the channel noise distributions. Additionally, we describe a collaborative spatially separated version of the test for robust combining of tests in a distributed spectrum sensing setting and quantify the significant collaboration gains achieved.

In Chapter 4 we develop the sequential energy detection problem in the context of spectrum sensing for cognitive radio networks. We formulate a novel Sequential Energy Detector and provide a comprehensive study of its performance. The sensitivity of the Sequential Test to primary signal variance estimation is addressed for the first time ever. Through extensive simulations it is demonstrated that our Sequential version of the energy detector delivers a significant throughput improvement of 2 to 6 times over the fixed sample size test while maintaining equivalent operating characteristics as measured by the Probabilities of Detection and False Alarm. We also apply our methods to demonstrate the

throughput gains for a case study of sensing ATSC television signals in the framework of the IEEE 802.22 standard.

Chapter 2

Proactive Identification and Utilization of Transmission Opportunities

2.1 Introduction

Cognitive Radio Networks (CRNs) operate on the principle of Dynamic Spectrum Access (DSA) which involves detection and exploitation of underutilized segments of the radio spectrum without causing interference to the licensed spectrum user. The Cognitive Radio (CR) acts as a Secondary User (SU) that coexists with the licensed Primary User (PU). The field of cognitive radios has developed at a rapid pace in the last decade, see for e.g, [1] and [2]. Recent pioneering studies have broadened the focus of CRNs to include prediction of network behavior at the MAC layer [3]. Also, Packet Based Networks (PBNs) are predominant in the implementation of current wireless networks. The traffic characteristics of PBNs are bursty and difficult to predict and attempts to devise time series based prediction models have achieved limited success to date. As the PBNs have become increasingly popular, there has been an accompanying crowding of the spectrum that they use. DSA holds promise for an efficient spectrum use framework in PBNs. But Physical layer (PHY) based DSA methods need a clearly present white space for a contiguous time interval. Due to heavy utilization the above methods will fail to effectively exploit any usable white space. Moreover, a simple ON-OFF model for temporal white space recognition fails when applied to PBNs because it causes unforeseen and harmful effects on the Medium Access Protocol

of the primary network. The novel framework proposed in this chapter is tailored for 'gray space' utilization even in such crowded PBNs without affecting its network layer behavior.

Traditional Dynamic Spectrum Access methods confine themselves to finding transmit opportunities in time, space or coding domain. The interference perceived by the primary user is controlled probabilistically. For example, IEEE 802.22 mandates that the probability of correctly detecting a primary network be more than 99 %. Other proposed time domain CR systems bound the probability of a packet collision to less than 1 %. Another approach that has been widely adopted defines a maximum interference power constraint at the location of the primary receivers. All these methods suffer from the major drawback that there is *no feedback* from the primary network to the secondary network with regards to the actual degradation in the end user experience of the primary system. The detection of safe transmission opportunities and their utilization is an open-loop process.

The complexity of modern wireless communication networks has created a disconnect between theoretical models that attempt to describe and predict the network and the actual behavior of the network in real world. Most performance studies of wireless networks are based on a long list of assumptions that will usually not hold true in a practical deployment of the network. To list a few, queuing theoretic analyses assume the network is in a steady saturation state, packets are often created and transmitted in a deterministic manner, and have uniform sizes, physical layer channels are modeled using simplistic ON/OFF Markov chains, all packet arrivals are assumed to follow a Poisson distribution e.t.c [18, 19]. In short, there is no guarantee that opportunistic access methods that rely on these idealistic models can actually succeed in practical network deployment situations. Our experimental measurements demonstrate the opposite, wherein many of these assumptions are not observed, and the opportunistic channel access methods end up hurting the primary users in an unforeseen manner. We propose to approach this issue from the opposite angle, namely, we make no assumptions about the network type and behavior, and create a network agnos-

tic non-parametric method for opportunistic transmit opportunity utilization by secondary networks. In other words, usually the interferee detects and measures the presence of the interferer through techniques such as measuring the bit errors, frame errors, the signal to interference ratio etc. The question we address here is, How can the interferer measure and hence react to the interference it causes at the interferee ? .

The novel *Pro*active *T*ransmit *O*pportunity Exploitation at the *MAC* Layer (Protomac) framework proposed in this Chapter is tailored for 'gray space' utilization even in such crowded networks without affecting its network layer behavior or causing the primary users to switch to other channels to avoid the secondary interference. In this paper, we propose for the first time a Dynamic Spectrum Access paradigm that intelligently learns the stationarity based behavior of the primary network and manages to extract explicit feedback regarding the effect of secondary transmissions which is in turn exploited to fine tune the secondary transmissions. The principle contributions of this chapter are:

- We propose a Transmit Margin, which dynamically quantifies the additional interference that the primary network can tolerate with no loss in its Quality of Service.
- We demonstrate the stationarity of the primary network at a granularity measured in seconds, and the interlinking between this stationarity and the Quality of Service delivered to the primary nodes.
- We introduce the use of two novel nonparametric tests, the sequential Kolmogorov-Smirnov test and the Parallelized Goodness-of-Fit test, and also derive a group-sequential Kullback-Leibler divergence update method to detect the change in the network stationarity in a fast and robust manner.
- We develop a channel sensing and access algorithm to create a cognitive radio link that operates at a power below the transmit margin by tracking the primary network behavior.

To our knowledge, it represents the first attempt based on the stationarity of the primary network statistics to formulate a new architecture for intelligent cognitive access to the channel which at every step takes into consideration explicit feedback from the Primary Network to the Secondary Network, while still adhering to the transparency principle. This architecture can work in parallel to existing temporal access schemes in the sense that these schemes can now take into account the exact effect that their operation has on the primary network in their area, and change their behavior accordingly. Thus the techniques proposed to be developed here will complement the approaches generally being adopted in the active field of the design of temporal opportunistic spectrum access policies. This will hopefully go a long way towards encouraging primary users to tolerate secondary users that have to date been considered a nuisance.

2.2 Background

2.2.1 Change Detection Based Methods

The quickest change detection problem deals with identification of abrupt changes in the underlying probability distribution of stochastic processes. Its goal is to detect the occurrence of change as quickly as possible while maintaining a specified false alarm rate [20]. Early stage detection of large scale Denial-Of-Service attacks which are initiated at unknown points in time can be achieved by observing abrupt changes in internet network traffic. Various implementation of Cumulative Sum (CUSUM) and Multi-Chart tests for network intrusion detection have been studied in the networking research community [21], [22]. The problem we address is different in that we have prior knowledge of when the distribution is going to change. Thus, whenever we change the CR power, it is certain that the new distribution is going to be different from the prechange distribution. But the degree of the change is an unknown and is tested by Protomac.

2.2.2 Estimation of Network Parameters

In [23], an efficient 802.11 fault diagnosis system using estimation of the round trip delay times and the packet loss rates was implemented. Another interesting method to determine if a packet loss is due to a bad channel or due to a packet collision can be found in [24]. A few popular 802.11 MAC based channel estimators are evaluated in [25]. These approaches differ from the scope of this work in that the node performing the estimation of some network parameter is itself a part of the primary network. In the context of a CRN, the CR has no direct access to the comprehensive network level view and has to infer based on only its restricted local observations.

2.2.3 IEEE 802.22 WRAN Standard

The recently developed IEEE 802.22 Wide Regional Area Network (WRAN) standard is set to be the first commercial implementation of the cognitive radio technology and aims to provide broadband access to rural areas. IEEE 802.22 operates in the underused television bands. It implements sophisticated spectrum sensing and detection protocols that allow it to coexist with the ATSC based digital TV signals. Also, the individual user terminals in IEEE 802.22 are at far-flung locations, while the primary transmitter is a TV broadcast station which can be upto a hundred miles away. Due to the unique design goals of IEEE 802.22, it is not suited for coexistence with a packet based primary network. Also, the corresponding problems of primary user detection will be very differently posed in smaller range WLAN type scenario.

2.2.4 Interference Temperature

The FCC first proposed an Interference Temperature (IT) metric in the context of IEEE 802.22 [26]. IT permits CRs to opportunistically use the primary channel so long as the

aggregate interference caused at the location of primary users does not exceed a predecided threshold. The aggregate interference is quantified in terms of an IT similar to the noise temperature concept. Figure 2.1 shows the potential new opportunities for spectrum access. Thus, adoption of the IT metric opens up a whole new dimension in DSA methods and unlocks previously unusable portions of the spectrum. IT based schemes are now an active research area in cognitive radios and some promising recent developments based on IT can be found in [27], [28], [29], [30]. Such an interference temperature formulation has many theoretical and analytical advantages and holds great promise for implementation in future CRNs. A possible practical obstacle towards implementing the Interference Temperature Metric as envisaged by the FCC is that the IT limit is defined at the location of the primary receiver. But the secondary transmitter has no effective way to measure the current IT at the remote primary's location. It can at most measure the interference temperature at its own location and use it to approximate the IT at the primary receiver's location.

2.2.5 SWIFT

Another related approach is SWIFT [31] in which the secondary user maintains a wideband OFDM CR signal overlaid on an IEEE 802.11 signal by adding and deleting the subcarriers so as to avoid using the subcarriers being used by the narrowband primary network. Our work is different in a number of significant aspects. First, SWIFT is a white space approach and aims to avoid the frequencies used by the PU by dynamically changing SU occupied bins, whereas Protomac is a gray space approach and uses the Transmit Margin (introduced in Section 2.4) to operate on the same bands as the PU by dynamically changing SU transmit power and time. Second, SWIFT computes PU metrics but does not consider the effect of these metrics on Quality of Service (QoS) of the PU. We can complete this link and monitor the QoS because Protomac is based on the underlying stationarity of the PU network and not limited to the instantaneous effect on PU. Since we monitor the longterm stationarity

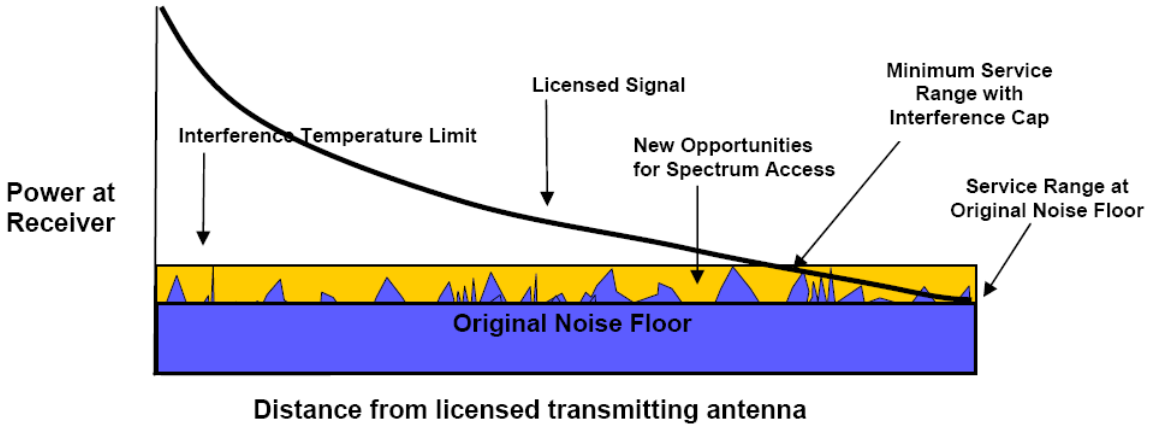

Figure 2.1: FCC's Interference Temperature Metric as proposed by the FCC

of the primary network Protomac is sensitive to effects that manifest after a significant delay. For example, the decision to change the primary modulation scheme is a function of the packet error rate averaged over the past few minutes. SWIFT cannot detect such macro timescale effects which Protomac does. Third, SWIFT assumes a Gaussian distribution of all PU metrics and based on this assumption it uses the Student's t-test to only detect a change in the mean of these statistics. But in reality, these statistics are strongly non-Gaussian, and are usually multimodal whereas Protomac adopts nonparametric non-model-based methods and can detect a change anywhere in the distribution. Our experimental results in Section 2.11.3 show that assuming a Gaussian distribution will be sub-optimal and leads to a severe performance degradation since the distributions can change significantly in shape with only a small change in their mean value. Finally the implementation of SWIFT only proposes but does not actually implement the interarrival time and packet size statistics (see [31] Sec 6). In this paper we present a unified treatment of our previous contributions [32–34] and further significantly develop a holistic sensing and access system model with extensive validation on a real world testbed.

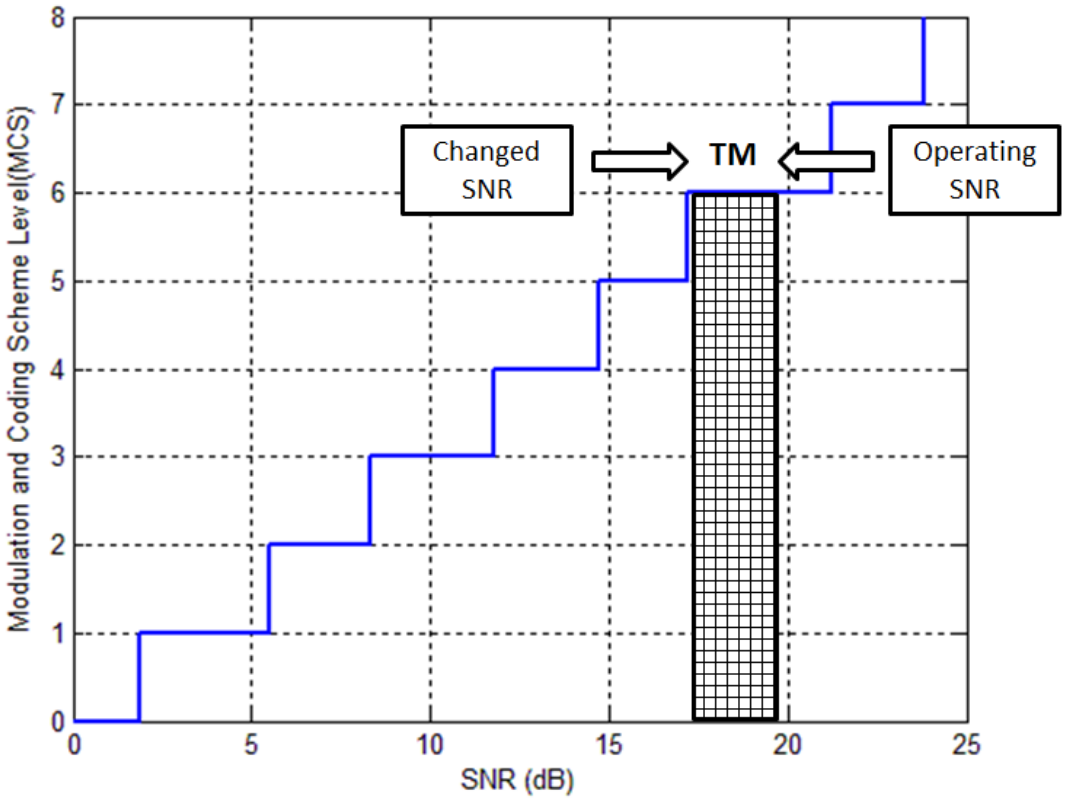

Figure 2.2: Transmit Margin

2.3 Analysis of Network Traffic

The transmissions of the secondary user interfere with the primary network. While designing the secondary system, the aim is to bound the maximum interference power received by the primary users. Conventional Cognitive Radio systems use the sum interference power received at the primary network as the design constraint as explained in Section 2.2.4. This constraint is often formulated as an interference temperature. While mathematically convenient, there are two inherent difficulties in implementing this interference constraint. First the secondary user signal can be significantly attenuated when it reaches the primary user. If we use the unattenuated signal to calculate the interference added, then we will be wasting a lot of available capacity. Second, there is the problem of additivity where each secondary user might individually ensure that it does not exceed the interference constraint locally, but the sum interference due to all such secondary users as measured at the location of the primary user might be much higher than the interference constraint. One possible solution to these problems is to estimate the power spectral density at a remote location as proposed in [35]. We will now introduce another alternate approach which is to modify the level of abstraction from considering a single primary user and instead formulate the problem as an effective interference limit for the entire primary network.

At any given instant the primary network is characterized by its Quality of Service (QoS) metric. The QoS is measured via the available bandwidth, the latency and delay, the throughput etc. At a coarser level, the QoS is captured by a variety of packet statistics which can be calculated from the trace of the packets on the primary channel. Thus, if we have time domain data of when each packet was sent, which primary node sent it to whom, the data rate, SNR and duration of the packets, then we can completely characterize the behavior and state of the primary network. Note that this also allows us to quantify the behavior of the network at the remote node locations as described by their packet statistics. For example, if a certain primary node experiences a higher interference than it can tolerate,

it will not be able to properly decode some of the packets sent to it. This will cause those packets to be retransmitted and a resultant perturbation will be observed in the packet statistics. While this is a special example, we can similarly argue that any perturbation in the network behavior can be detectable after appropriate processing and thresholding. In the next sections we will describe in detail the methods for doing precisely such network state change detection.

2.4 Transmit Margin

We now proceed to motivate and define a Transmit Margin (TM) which is inspired by the IT metric but circumvents the difficulty described above. Consider once more the scenario depicted in Figure 2.2. Notice that the primary receiver requires a certain $SNR_{min} = \frac{P_{Signal,min}}{P_{Noise,max}}$ to maintain its QoS. If the receiver noise level N_0 is lower than $P_{Noise,max}$ or if received signal power $P_{Signal} > P_{Signal,min}$ then the channel can support additional secondary power insertion equal to $SNR_{actual} - SNR_{min}$ without any effect on its Quality-of-Service (QoS).

The IT concept was introduced with a goal of being able to safeguard the QoS experienced by the primary network. This QoS is defined in terms of the network throughput, available bandwidth, latency etc. Thus, the QoS depends on a host of factors each of which either lies within the circle of influence of the Secondary Network or outside its circle of influence. For example, an abrupt spike in primary traffic which leads to a increase in the packet collision rate and decrease in QoS is not controllable by the Secondary Network. But, an increased number of packet retransmissions caused by a rise in the Packet Error Rate (PER) due to a degraded channel quality might be directly attributable to the secondary network's behavior. The Secondary transmission power acts as additive noise to the primary channel and when increased beyond a threshold, it is capable of causing a drop in the primary QoS. The Transmit Margin is defined as the allowable maximum secondary transmission power

which does not degrade the primary network QoS beyond a small tolerable predecided limit. Thus Protomac retains the spirit of the IT concept, but shifts the test criteria from the PHY layer (SNR) to the MAC layer (QoS). The degradation is measured with respect to the base QoS which the Secondary Network observed before starting the transmission attempt. Also, the TM as defined is highly conservative in that a degradation in primary QoS caused by factors outside the secondary's circle of influence will also be treated in the same way as one caused by the secondary behavior, by a reduction of transmit power. The onus is always on the secondary users to ensure that they do not interfere with the primary network. Also, the change in QoS is tested through the network statistics which in turn are a direct indicator of the channel quality as measured at the physical location of the primary system transceivers; this implicitly allows Protomac to control the effect of the secondary network at the remote primary locations. This is the cardinal advantage delivered by the use of a Transmit Margin.

2.5 Network-level Descriptors

Protomac observes the external behavior of the primary network to infer underlying changes. In this section we describe the properties of the primary network that enable Protomac to characterize it reliably. These properties rely on the probability distributions of various observable quantities of the primary network. We will now describe the estimation of the distributions of these primary network statistics.

The primary network observations are preprocessed in two stages. First, the samples are randomized in a group-sequential manner, i.e., only a subset of the samples observed are used. Specifically, every sample is accepted with a predecided probability γ. This sampling scheme reduces the effects of the correlation between successive samples that arises due to the implementation of the protocol, such as a packet transmission being always followed by an acknowledgment after a fixed interval [18, 36]. The results here are obtained for typical

values of γ between 0.6 - 0.9. Second, the probability densities of the relevant statistics are then estimated using kernel density estimation. The density has to be estimated such that the distinct peaks in the density are not masked, while at the same time, it is smooth enough to avoid spurious noise. The choice of the bandwidth h of the kernel used for this density estimation has to be optimally set in order to achieve these goals and is calculated via the procedure described in Section 2.8.9.

2.5.1 Primary Network can be characterized through its observable statistics

The SU node is not associated to the Primary Network and does not have direct access to measure the Quality of Service parameters such as delay, bandwidth etc. Our algorithm characterizes the instantaneous state of the primary network by tracking the metrics of the primary network that the SU *can* observe. Specifically, the SU observes a) the primary packet sizes that it can sense and b) the interarrival duration between consecutive primary packets. These network statistics are summarized via building their probability distribution functions. Although other network statistics can be incorporated into our algorithm, the packet size and interarrival time distributions have the beneficial properties that they are sensitive to the interference caused by the secondary users while being agnostic to the exact implementation of the wireless protocol in the primary network.

2.5.2 Distribution of Statistics is relatively stationary over short time intervals

Through prolonged observation of the primary network statistic, it was observed that the primary network state as described by the above network statistics varies slowly with time. In other words, except for sudden disruptive events, the primary network demonstrates short term time stationarity. This observation underlies and enables our proposed algorithms. Empirically, this stationarity is prominently observed on a time scale of the interval in which 50-200 packet arrivals per interval, i.e. $50/\lambda$ to $200/\lambda$ seconds, where λ is the

average arrival rate of packets on the primary channel. To quantify this time stationarity, we calculated the KL divergence (see Section 2.8 for more details) between consecutive slots and observed the number of consecutive slots over which the density of the network statistic does not diverge significantly. Figure 2.3 shows that these statistics drift only slowly over time, and that the rate of this drift depends on the traffic density of the primary network.

2.5.3 Changes in QoS of Primary Network are mirrored in its Network Statistics

The QoS is captured by a variety of packet statistics which can be calculated from the trace of the packets on the primary channel. Thus, if we have time domain data of when each packet was sent, which primary node sent it to whom, the data rate, SNR and duration of the packets, then we can completely characterize the behavior and state of the primary network. Note that this also allows us to quantify the behavior of the network at the remote node locations as described by their packet statistics. For example, if a certain primary node experiences a higher interference than it can tolerate, it will not be able to properly decode some of the packets sent to it. This will cause those packets to be retransmitted and a resultant perturbation will be observed in the packet statistics. While this is a special example, we can similarly argue that any perturbation in the network behavior can be detectable after appropriate processing and thresholding.Thus the QoS of the Primary Network provides implicit feedback to the SU node about the interference caused by its transmission at the remote location. We have validated this interlinking of PU QoS and the observable PU statistics through a large number of experimental runs and a representative result is shown in Figure 2.4. More results for a variety of operating conditions are available on the authors' website.

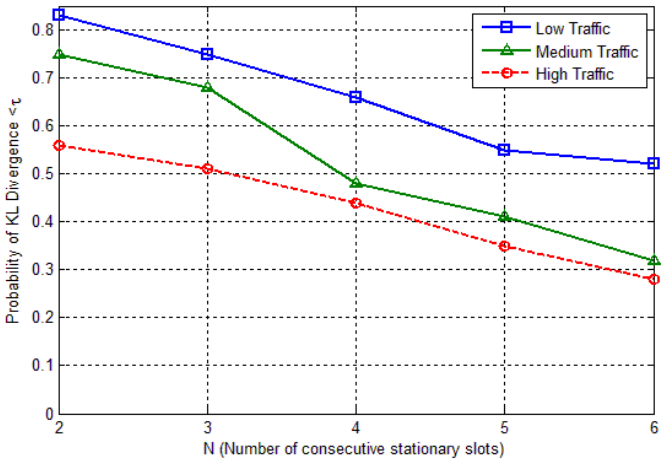

Figure 2.3: Decay of time stationarity over consecutive slots of 100 packet arrivals for a threshold of 1.0

Tx power in mW	Avg. Round Trip Delay in msec	Prob. of KL Div. > 2.0	Prob. of KL Div. > 1.0
0.125	81	0.19	0.33
0.5	54	0.31	0.41
1.125	78	0.27	0.44
2.0	389	0.88	0.968
4.5	813	0.85	0.961
8	NA	AP Disassociated	

Figure 2.4: Dependence of Round-trip delay time and Network Statistics on Secondary Interference

2.6 ProTOMAC: Description and Flowchart

In the previous section, we have presented the underlying principle that we can monitor the effect of secondary system operation on the primary system's Quality of Service via a number of short term stationary network statistics. In this section, we will provide an

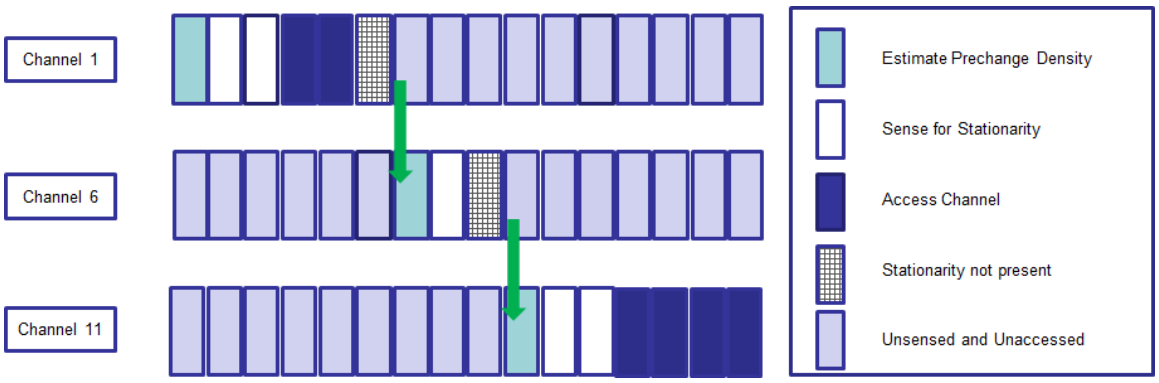

Figure 2.5: Channel Sensing and Access in Protomac

overview of the operation of the proposed system that exploits these observations. The system operates via two interlinked processes, transmit opportunity detection and secondary link control. The basic principle is that the secondary user gradually increases its signal power while simultaneously measuring the degree of change caused in the primary network operation and thus operating within the safe Transmit Margin available to it. The implementation will be described here in the context of an IEEE 802.11 Wireless LAN but it can be easily ported to any packet based network that is based on a random channel access framework.

2.6.1 Secondary Channel Structure

The proposed secondary system superimposes a slotted structure on top of the existing multi-channel primary network, i.e. the primary channel is split up into segments of 50-200 packet slots for the purpose of sensing and access. This length is chosen to match the short-term stationarity of the primary statistics as introduced in the previous section. Note that these secondary slots are independent of whether the primary network is slotted or unslotted and are pertinent only to the secondary access algorithm. Figure 2.5 shows a three channel IEEE 802.11 network divided into slots. Also, Figure 2.6 shows the flowchart of steps that a secondary system goes through while accessing the channel. We will explain the principle

steps that Protomac goes through during channel access.

2.6.1.1 Initialization

At initialization, every CR starts off with a sensing period when it observes the initial state of the primary network without transmitting. During this period, the secondary network calculates the traffic patterns and the rate at which the network statistics are changing is estimated. This estimation of the transition probabilities and the short term stationarity present in the primary network is used as a baseline to measure the effects on the QoS of the primary users. Protomac proceeds to the next step only if the primary network displays stationarity.

2.6.1.2 Channel Access

The Channel Access step is depicted in Figure 2.5. Once the primary network has been deemed to be stationary, the secondary node uses the next slot to build an estimate of the prechange distribution of the network statistics. The secondary node will now wait for an additional N_{sense} slots. During these slots, the KL divergence of the network statistics is calculated per slot, and only if the change is less than the preset threshold, it proceeds to the next stage. The exact values of N_{sense} and the divergence threshold control the aggressiveness of the system. After successfully waiting for N_{sense} slots, the cognitive radio is allowed to start accessing the channel at a power level decided by the Transmit Power Control Loop.

2.6.1.3 Transmit Power Control Loop

Once the CR has determined that a transmit opportunity exists in the channel access cycle, it proceeds to transmit its signal. This is done in a proactive manner, by increasing the interference perceivable to the primary network. The allowable transmit power of each

CR is quantized into discrete levels as $P_1 = \Delta P, P_2 = 2\Delta P, ..., P_{max}$. The CR starts by increasing its power to P_1 and runs the change detection tests that will be described later. If the test detects a change above the threshold, it ceases transmission immediately and during the next access opportunity the transmit power is reduced to by one level while if the test is negative, the transmit power is increased during the next access interval and the process is repeated. After the secondary transmission is over, the channel transition probabilities are updated.

2.6.1.4 Channel Hopping

If Protomac detects a change in the primary network, using the coarse change detection algorithms described in the next section, during any access slot, it immediately ceases transmitting and does not continue to transmit for the remaining slot. It will restart sensing the primary channel transition probabilities, and if these have been degraded, it will randomly hop to one of the other primary channels and restart the Channel Access algorithm in a similar manner to that currently implemented in the IEEE 802.22 standard.

2.7 Network Descriptors

The basic statistical principles underlying the methods proposed in this work can be applied to any network statistic that remain relatively stationary over moderate time periods. In this section, we motivate the adoption of the packet size and the retransmission behavior of the network as suitable statistics for implementation using Protomac.

2.7.1 Packet Size

It is hypothesized that the primary network maintains a relatively constant packet traffic rate, which is a reasonable assumption over a time window of a few minutes [37], [38].

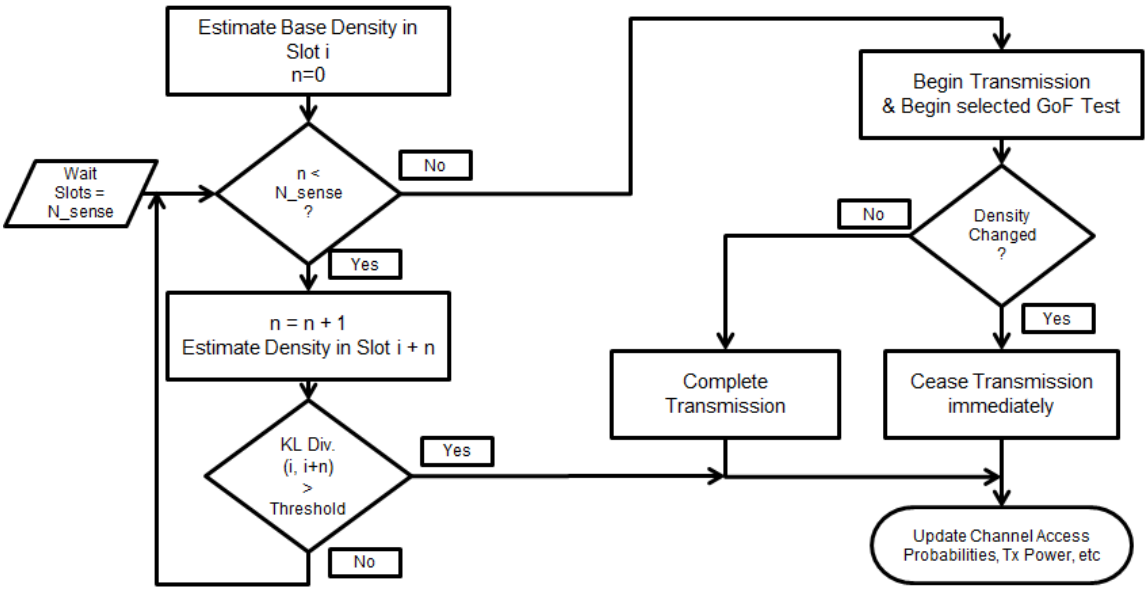

Figure 2.6: Protomac Flowchart

This is reflected by the stationarity of the perceived available bandwidth over time intervals on the order of minutes. The network traffic is succinctly characterized by the histogram of the distribution of the packet sizes. The 802.11 protocol limits the maximum length of the packets to 1548 bytes in practice. A high throughput traffic flow will have a histogram concentrated more towards the higher packet sizes, while a low throughput traffic flow will have a more evenly balanced histogram. The insertion of interference due to the secondary transmitter will cause a shift in the histogram away from the one corresponding to high traffic flow. The two principal reasons for this behavior are,

1. The secondary transmission acts as addition of noise to the channel and increases the bit error rate (BER) for the primary packets. Also, the packet error rate (PER) is proportional to the BER and the packet length. Thus, the bigger packets are more prone to be received in error than the smaller packets.

2. The 802.11 MAC protocol has a fragmentation threshold which controls how longer frames are fragmented into packets. This threshold changes dynamically and decreases

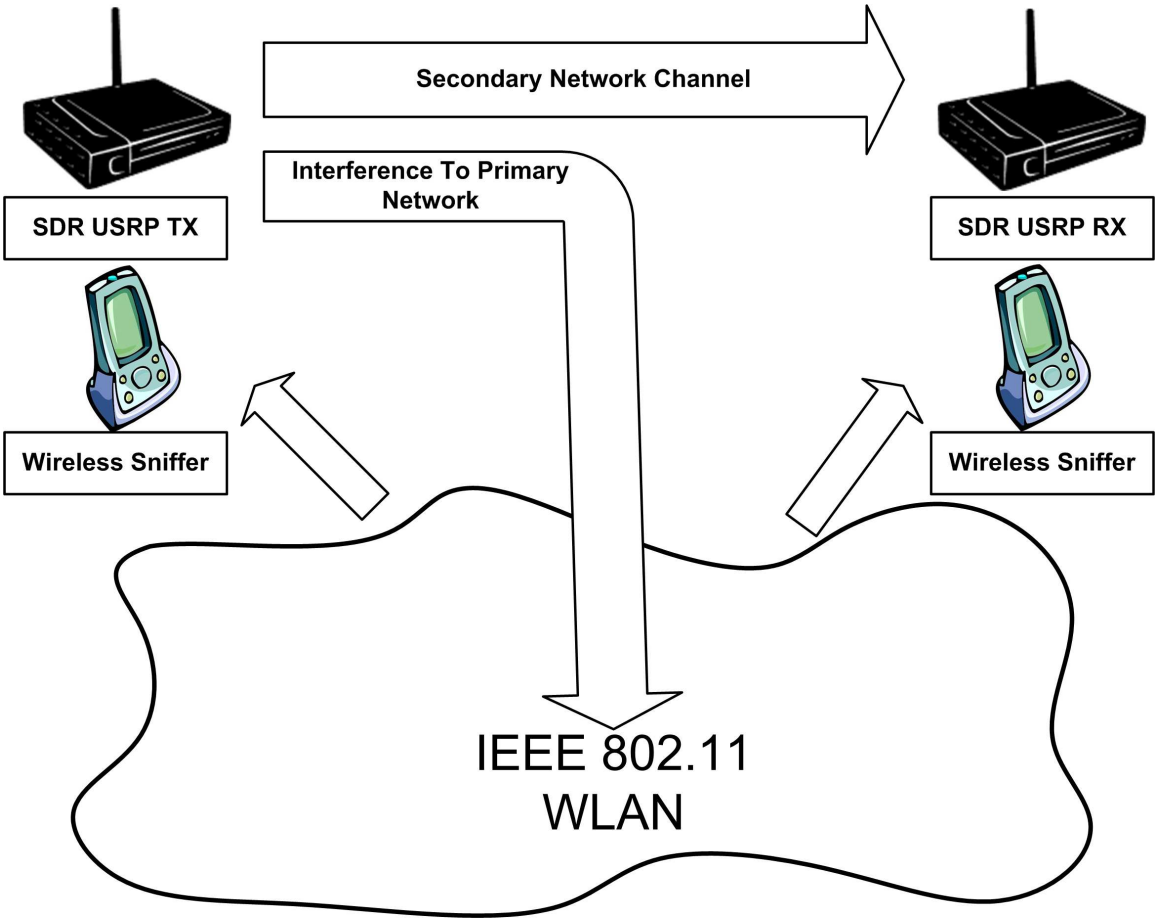

Figure 2.7: Experiment TestBed

when the node perceives an increased PER.

2.7.2 Packet Retry Rate

The 802.11 MAC retransmits a packet if the original transmission is unsuccessful. The packet retry number flag is used to indicate such packets. The retransmissions might be due to traffic congestion or an increased PER in the channel. It is possible to estimate the channel quality from the proportion of packets that have this flag set and to assess the degradation in primary QOS due to secondary user interference. A related alternate approach which has been implemented by the authors tracks the primary channel quality through the lossy intercepted data-ACK packet exchange as seen through secondary channels [39].

2.7.3 Channel Interarrival Time

The distribution of the interarrival period between successive packets on the wireless channel is another statistic that will be used in this work. This statistic is interlinked to the packet size statistic. As the channel quality degrades, the number of packet errors and hence the number of packet retransmissions by the primary network increases. Also, this in turn affects a number of other variables in the MAC schemes, such as Carrier Sense Multiple Access in IEEE 802.11 WLANs, via the carrier sensing, random backoff periods, retry attempts, and changes in modulation and coding type. Thus, a change in the Channel Interarrival Time distribution is an indicator of these various underlying factors. In the rest of the chapter we focus on the packet size statistic and the channel interarrival time statistic.

In the next section, we will cover the two methods that we will use to perform the change detection in the network statistics, 1) Goodness-of-Fit tests and 2) Distributional Divergence Measures.

2.8 Network Statistics Change Detection

In Section 2.5, it was shown that the distributions of the various network statistics change slowly, except for a few abrupt shifts. These shifts are caused due to either secondary transmitting above the Transmit Margin or due to other disturbances originating within the primary network. The Protomac algorithm aims to detect the occurrence of this abrupt change in the network statistics distribution. In this section, we will introduce the techniques for detecting such an abrupt change in the primary network. The change detection is implemented at two levels, coarse change detection and fine change detection. Coarse change detection is used to simultaneously detect the change while the secondary user is transmitting in its access slot. It must be able to detect the change very rapidly, and this is achieved at the cost of an increase in the false alarm rate. We implement coarse change detection using a modified Goodness-of-Fit test and a group sequential Kullback-Leibler divergence update method. On the other hand, the fine change detection technique is used to decide, with high confidence and low false alarms, whether the network statistics distribution has changed after the secondary user finishes its transmission in that slot. We use the Kullback-Leibler (KL) divergence between the old and new distributions as the baseline to decide whether a change has occurred. We will now cover these coarse and fine change detection techniques in more detail and briefly introduce the concept of Goodness-of-Fit testing. We will develop two novel GoF tests, the sequential Kolmogorov-Smirnov test and the Parallelized Goodness-of-Fit test, and derive a fast group-sequential method to update the KL divergence.

2.8.1 Goodness-of-Fit Tests

Goodness-of-fit (GOF) tests are used to check whether the samples are from a given probability distribution [40–42]. Consider a random sample of n independent and identically distributed observations $x_1 < x_2 < x_3 < ... < x_n$ arranged in ascending order. The Goodness

of Fit (GoF) test is a one sided hypothesis test for H0 that this sample was drawn from a distribution with a Cumulative Distribution Function (CDF) F_0. The hypothesis to be tested are formulated as shown.

$$H0 : F(x) = F_0(x) \text{ for all values of x,} \tag{2.1}$$

$$H1 : F(x) \neq F_0(x) \text{ for at least one value of x,} \tag{2.2}$$

where $F(x)$ is the empirical CDF of the sample. Thus, these tests are ideal for testing for deviations from the prechange network statistics distribution. In this work we have implemented a novel suite of multi-chart multi-type GoF tests. There are two families of Goodness of Fit tests: 1) Kolmogorov Smirnov Type tests which use the L1 norm and 2) The Cramer von-Mises type tests which use the L2 norm. The KS test has the following desirable properties:

1. The KS test is preferable if the sample size is small, as the KS statistic is exact even in that case [42]. This proves valuable in formulating a sequential version of the test.

2. The KS test is the only non-parametric goodness-of-fit test with exactly derivable confidence bands [43].

3. The KS statistic is a distribution-free statistic.

2.8.2 Implementation of the Kolmogorov-Smirnov test

Let $X_1, X_2, ..., X_n$ be a random sample of size n drawn from an unknown distribution F(x). We want to test the hypothesis that $F(x) = F_0(x)$. First, the empirical cumulative distribution function (e.d.f) of the n samples is calculated as $S_n(x)$.

$$S_n(x) = \frac{\text{Number of sample observations} \leq x}{n} \tag{2.3}$$

Now, we evaluate the KS distance between the prechange cumulative distribution $F_0(x)$ and the empirical cumulative distribution $S_n(x)$. When plotted graphically, this gives us the greatest vertical distance between the two distributions and is defined as the KS distance D_n,

$$D_n = \sup_x |F_0(x) - S_n(x)|. \tag{2.4}$$

We can also define two additional metrics for a one-sided KS test. D_n^+ and D_n^- are used to formulate one-sided confidence bands for finer testing.

$$D_n^+ = \sup_x [F_0(x) - S_n(x)] \tag{2.5}$$

$$D_n^- = \sup_x [S_n(x) - F_0(x)] \tag{2.6}$$

The distribution-free property of the KS test means that the KS statistics D, D^+, and D^- have a distribution function that is independent of the exact form of $F_0(x)$. In his classic paper, Kolmogorov has proved the existence of a limiting value of D_n [44]. Also, there are formulas which let us calculate the statistic for small finite n and asymptotic approximations as $n \to \infty$, e.g,

$$\lim_{n\to\infty} Pr(\sqrt{n} D_n \leq d) = \sum_{j=-\infty}^{\infty} (-1)^j e^{-2j^2 d^2}. \tag{2.7}$$

The Glivenko-Cantelli theorem [45] states that when $F = F_0$, the KS statistic D_n vanishes as shown,

$$Pr\left(\lim_{n\to\infty} D_n = 0\right) = 1. \tag{2.8}$$

As a result, we can be confident that our test will be strongly consistent against all alternatives and the false hypothesis will be rejected with probability one as we accumulate more and more samples, i.e, as $n \to \infty$.

Let α be the significance level corresponding to the $100(1-\alpha)$ confidence interval. Also, parameter $d_n(\alpha)$ is the critical value for a given α, i.e, it is the probability of incorrectly

rejecting the hypothesis in equation (3.3). We can find the corresponding critical region of the test as shown in (2.9),

$$P\{D_n \geq d_n(\alpha)\} = \alpha. \tag{2.9}$$

Massey gives recursive expressions and tables to calculate the critical value for a given α [46]. Note that α is an indicator of the probability of misdetection of the test, which we investigate in section 2.11.

A confidence band [42] [47] is an alternate way of looking at the problem of testing for goodness-of-fit. We will reverse the traditional use of the confidence band wherein we find the $1-\alpha$ quantile corresponding to d_α of the KS statistic and threshold D_n against the d_α distance. Instead, we will use d_α to set a confidence band for the whole postchange density function. Thus, regardless of the exact form of the prechange density, we get the two equivalent statements in equations (2.10) and (2.12). Equation (2.12) states that the prechange density function $F_0(x)$ lies entirely within a band of $\pm d_\alpha$ from the empirical distribution function $S_n(x)$ with a probability of $1-\alpha$.

$$P\{D_n = \sup_x |S_n(x) - F_0(x)| \geq d_\alpha\} = \alpha \tag{2.10}$$

$$P\{S_n(x) - d_\alpha \leq F_0(x) \leq S_n(x) + d_\alpha\} = 1 - \alpha \text{ for } \forall x \tag{2.11}$$

$$P\{F_0(x) - d_\alpha \leq S_n(x) \leq F_0(x) + d_\alpha\} = 1 - \alpha \text{ for } \forall x \tag{2.12}$$

2.8.3 Sequential Kolmogorov-Smirnov Test

We implement a novel modification of the KS test in Protomac. In section 2.8.2, we have reviewed how to setup a KS test. Here, we propose a sequential version of the KS test. According to the authors' best knowledge, there has been only one previous formulation of a sequential version of the KS test by Hawkins [48]. But, the Hawkins approach proposed a sequential version to tackle the problem of quickest change detection, i.e, the aim was to

estimate the change point of a given time series, not the magnitude of the change. This makes the Hawkins approach unsuitable for the situation under consideration here. We present a novel formulation which works by iteratively estimating the KS statistics in an online manner.

It is important to be able to reach a decision in favor of a hypothesis in a timely and reliable manner. A sequential formulation of the KS test will minimize the time required to reach the decision. In equation (2.4), it is seen that the KS statistic depends on the number of samples n. This dependence implies that as the number of samples increases, the width of the confidence band of the test cumulative distribution decreases. We explain the operation of the sequential test with help of figure.2.8 which shows the plot of two possible drifts in test statistic D_n with increasing n. Also, superimposed on the plot are the $d_n(\alpha)$ contours corresponding to increasing values of α. A significance level for the test, α_{th}, is initialized to a predecided value. The test begins by collecting samples and updating the empirical cumulative distribution function at each step.

In Protomac, the KS test is evaluated in a group-sequential manner for rapid change detection, i.e, in any secondary slot where the SU starts transmitting, it also simultaneously begins to collect samples of primary network statistics to run the test. Starting at 10 samples, the KS statistic is reevaluated after collecting every additional 5 samples. This ensures that if the underlying distribution has undergone a significant change, we can detect it in a faster time, and immediately cease secondary transmission to minimize the effect on the PU. But most goodness-of fit tests have a high variance of the statistic at small sample sizes ($\leq$ 30 samples) and this leads to a very high false alarm rate and the rejection of a large proportion of valid transmit opportunities. The KS statistic exhibits a low sensitivity at these small sample sizes and this sensitivity rapidly improves as the sample size increases above 20. We exploit this behavior through a sequential shrinkage of test significance. At every step in the group sequential process, the significance level of the KS test is decreased in line with

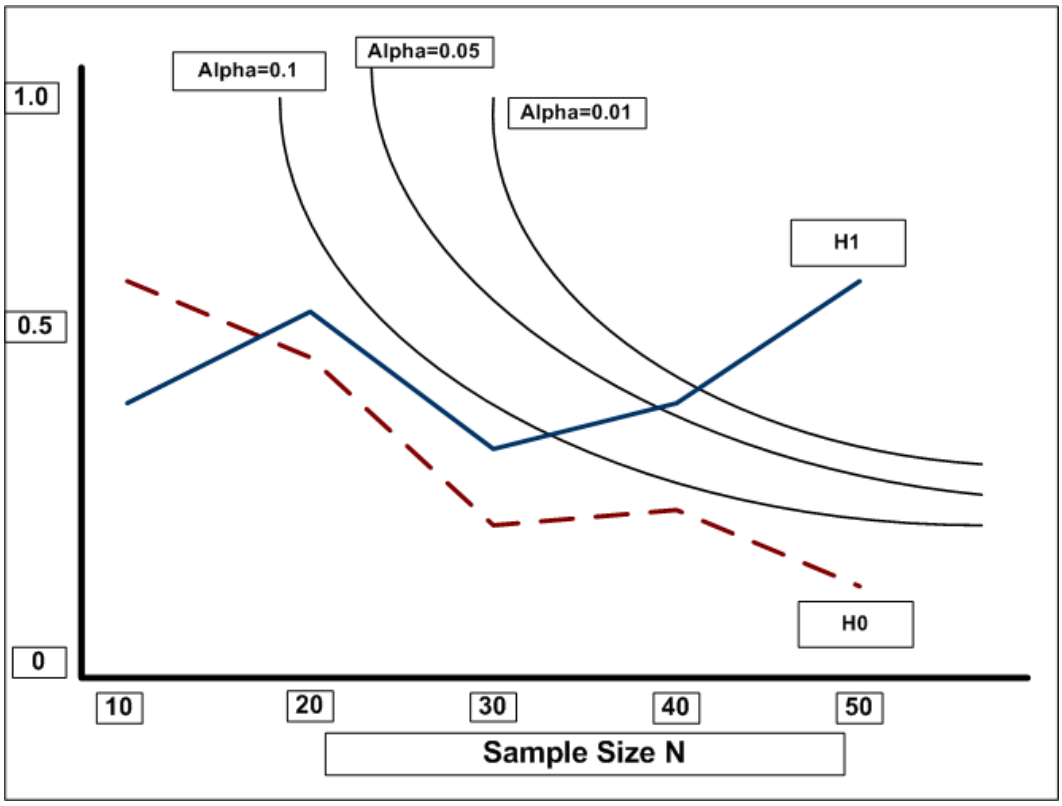

Figure 2.8: Sequential KS Test

the increase in the performance of the KS statistic, i.e., the corresponding confidence band of the KS test centered around the null distribution increases. The implementation details and results for this sequential KS test are given in Section 2.11.

2.8.4 Cramer von-Mises GoF Test

The Cramer von-Mises statistic ω_n^2 is defined in (2.13) and is the integrated squared difference between the original distribution and the empirical distribution [49].

$$\omega_n^2 = n \int_{-\infty}^{\infty} \left(F_n(x) - F_0(x)\right)^2 dF_0(x). \tag{2.13}$$

Substituting $t_i = F_0(x_i)$, we have,

$$\omega_n^2 = n \int_0^1 \left(F_n(t) - t\right)^2 dt, \tag{2.14}$$

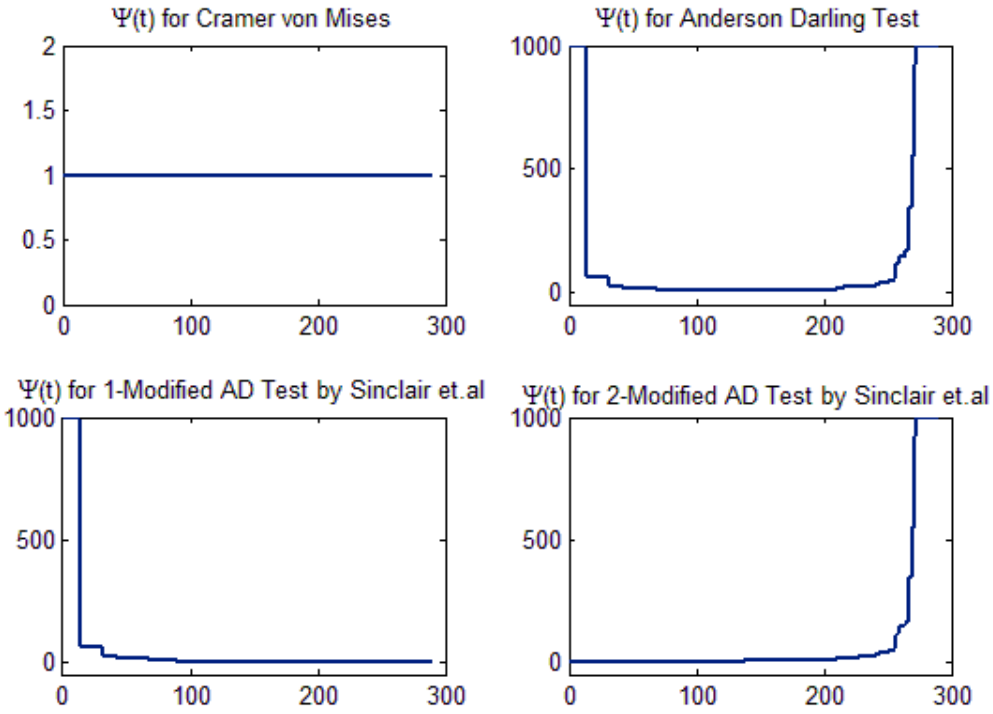

Figure 2.9: $\Psi(t)$ for various GoF tests

where the t_i are Uniform (0,1) random variables. After some manipulation, we obtain the easily computable form as shown in (2.15).

$$\omega_n^2 = n \sum_{k=1}^{n} \left(t_k - \frac{k - 1/2^2}{n} + \frac{1}{12n} \right). \tag{2.15}$$

The Cramer von Mises test is sensitive to deviations in the central region of the distribution function whereas the related Anderson-Darling test is sensitive to the deviations in the upper and lower tails of the distribution and the Viollaz-Rodriguez test can be customized to be sensitive to either the upper tail or the lower tail deviations. Our method forms a suite of these GoF tests as explained in the next section.

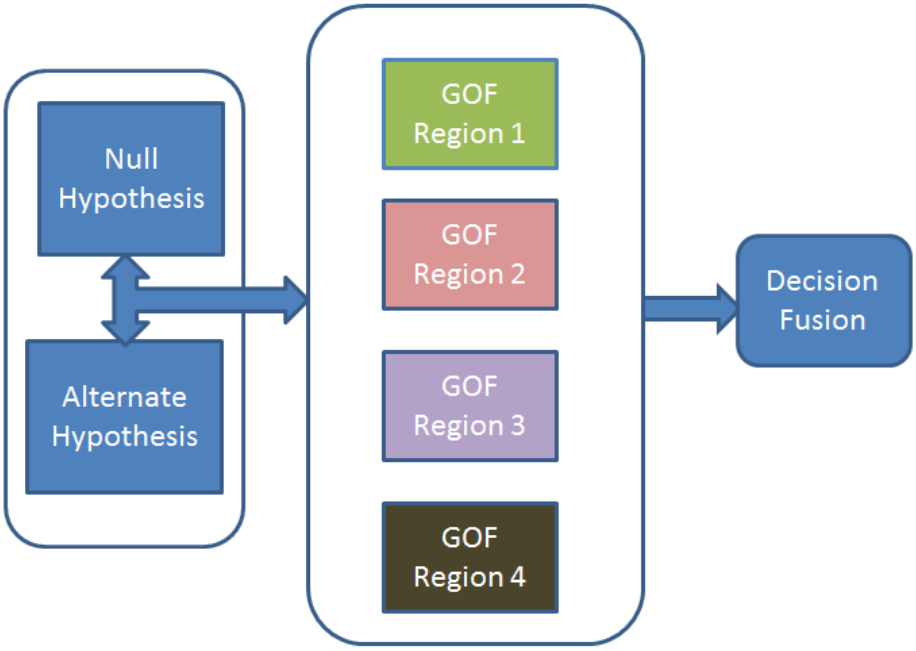

Figure 2.10: Operation of the Parallelized Goodness-of-Fit test that consists of individual tests sensitive to different regions of the underlying density.

2.8.5 Anderson-Darling Test and Related Tests

Consider the variation where the Cramer-von Mises statistic is weighted by a weight function $\Psi(t)$ as in (2.16).

$$W_n^2 = n \int_0^1 (F_n(t) - t)^2 \, \Psi(t) dt. \tag{2.16}$$

The most popular choices of $\Psi(t)$ are $\Psi(t) = 1$ and $\Psi(t) = \frac{1}{t(1-t)}$ corresponding to the CvM test and the Anderson-Darling (AD) test respectively [50, 51]. The modified AD statistic as given by Rodriguez-Viollaz is $\Psi(t) = 1/t$ and $\Psi(t) = 1/(1-t)$. Although an infinite number of choices for $\Psi(t)$ exist, the four choices given above were found to be sufficient for our requirements.

2.8.6 The Parallelized GoF Test

The GoF statistics above form the Generalized Cramer-von Mises family where the weight function $\Psi(t)$ lets us factor in the region where the deviation is most likely to occur. The Cramer-von Mises test is sensitive to deviations in the central region of the distribution function whereas the related Anderson-Darling test is sensitive to the deviations in the upper and lower tails of the distribution and the Viollaz-Rodriguez test can be customized to be sensitive to either the upper tail or the lower tail deviations. Depending on the application, statisticians recommend one of these tests to maximize the test power under the alternative hypothesis H_1. In our case, the alternate distributions are different in shape depending on the exact change caused in the Primary network and on the traffic characteristics which cannot be predicted in advance while formulating the test.

In order to solve this problem of complete lack of a priori knowledge regarding which test will have the highest power, we propose to apply a suite of these GoF tests at the same time. Such a parallelized Goodness-of-Fit test is implemented by performing the Cramer-von Mises test, the Anderson-Darling test and the its two Sinclair-Rodriguez-Viollaz variants simultaneously. The final decision is made via ORing the individual decisions. This has the effect of formulating the parallelized test in a conservative manner and is desirable since cognitive radio networks implement the philosophy that it is critical to robustly detect any possibility of interference with the primary network. The parallelized Goodness-of-Fit test as implemented in Figure 2.10 is highly sensitive across the whole support of the packet statistic distribution since each constituent GoF test is sensitive to a change in certain specific regions of the underlying density of the packet statistics. The performance of this test is described in Section 2.11.

2.8.7 Kullback-Leibler Divergence

Protomac uses fine change detection based on the Kullback-Leibler measure to decide at the end of secondary slot if the primary network statistics have changed. Due to the interference introduced by the secondary users, the initially estimated prechange density changes by an unknown degree to the new postchange density. In this section we will examine ways to measure the degree of this change using the concepts of information theory [52]. There are several ways to measure the unlikeness of two distributions such as Kullback Leibler divergence measures and Chernoff Distance measures. All the divergence measures we cover below are members of a generalized class of information theoretic divergence measures called Ali-Silvey distances but each measure is suited for particular class of applications due to its unique properties [53].

The Kullback-Leibler (KL) divergence was introduced by Kullback in the context of statistical inference [54]. Let F_1 and F_2 be two probability distributions and let $f_1(x)$ and $f_2(x)$ be the corresponding probability density functions. The KL divergence from F_1 to F_2 is defined as,

$$D(F_1 \parallel F_2) = \int f_1(x) log \left(\frac{f_1(x)}{f_2(x)} \right) dx. \tag{2.17}$$

Equation (2.17) shows that the KL divergence is also the expected value of the log-likelihood ratio of the two densities under consideration, where $\Lambda(x) = \frac{f_1(x)}{f_2(x)}$. The expectation is taken with respect to F_1 to get $D(F_1 \parallel F_2)$ as shown,

$$D(F_1 \parallel F_2) = E_{F_1}[log\, \Lambda(x)]. \tag{2.18}$$

Although the KL divergence will be used as a distance measure, note that while the KL divergence follows the additive property, it does not satisfy the triangle inequality nor is it a symmetric measure, i.e,

$$D(F_1 \parallel F_2) \neq D(F_2 \parallel F_1). \tag{2.19}$$

But, the KL divergence is always non-negative and equals zero if and only if the two distributions are equal. Thus we can justifiably use the KL divergence to measure the similarity between two probability distributions, i.e, $D(F_1 \parallel F_2) \geq 0$ and

$$D(F_1 \parallel F_2) = 0 \iff F_1 = F_2. \tag{2.20}$$

A symmetric version of the KL divergence was defined by Jeffreys as in equation (2.21) and is called the J-divergence [55].

$$J(F_1 \parallel F_2) = D(F_1 \parallel F_2) + D(F_2 \parallel F_1). \tag{2.21}$$

For our application, we are interested only in a measure of the distributional difference after we introduce the interference. These measures will be taken for each transmit power level. Thus, we can expect that the asymmetric KL divergence should be sufficient for our needs. Indeed, the experiments demonstrate the superior performance of the KL divergence as compared to the J-divergence. The reason for this is that the prechange density is accurate while the postchange density is only approximate and hence $E_{F_{Pre}}[log\,\Lambda(x)]$ is better than $E_{F_{Post}}[log\,\Lambda(x)]$. The KL divergence of discrete distributions with a probability mass function is calculated as shown,

$$D(F_1 \parallel F_2) = \sum_{x=1}^{N} f_1(x) \log\left(\frac{f_1(x)}{f_2(x)}\right). \tag{2.22}$$

2.8.8 Bhattacharyya Distance

The Chernoff distance between distributions F_1 and F_2 is $C(F_1 \parallel F_2) = -log(\mu(t))$, where $\mu(t)$ is defined in (2.23) [56].

$$\mu(t) = \int [f_1(x)]^{1-t}[f_2(x)]^t\,dx. \tag{2.23}$$

The Chernoff class of distance measures includes a wide subset of divergences. But their evaluation involves solving a difficult optimization problem [57]. The Bhattacharyya distance

is a special easily computed case of the Chernoff distance.

$$B(F_1 \parallel F_2) = -\log \mu\,(1/2). \tag{2.24}$$

It was first proposed by Bhattacharyya and was popularized in the context of information theory [58], [59]. The Bhattacharyya coefficient μ is defined in (2.25).

$$\rho = \mu\,(1/2) = \int \sqrt{f_1(x) f_2(x)}\, dx. \tag{2.25}$$

Also, the Bhattacharyya coefficient and the Bhattacharyya distance are bounded as $0 \leq \rho \leq 1$ and $0 \leq B(F_1 \parallel F_2) < \infty$. The Bhattacharyya coefficient for the case of discrete distributions with a probability mass function is,

$$\rho = \sum_{x=1}^{N} \sqrt{f_1(x)\, f_2(x)}. \tag{2.26}$$

2.8.9 Group Sequential Divergence Updates

We now describe the novel group sequential update of the KL divergence measure. After each change in transmit power, the CR observes the primary network packet statistics to estimate the postchange density. Speed of detection of the occurrence of a significant change in this distribution is a critical aspect of being able to operate without interfering with the primary network. In order to achieve fast detection, we adopt a twofold approach. As a first step, an approximate rough estimate is obtained from a low number of samples. This rough estimate will have significant estimation variance but it allows us to check for a drastic and abrupt change in the distribution. The base threshold used for the rough estimate will be correspondingly higher. After we have obtained the rough estimate and the change is indicated to be within the base threshold, we will continue to collect samples and refine the postchange density estimate. This step is called the density update and is implemented in the form of a group sequential update. Group sequential updates are used in sequential hypothesis testing problems where the data arrives in groups. Also the corresponding threshold is refined as the density estimate becomes more and more accurate.

2.8.9.1 KL Divergence Group Sequential Update

The discrete prechange distribution F_1 follows a mass function $f_1(x)$, while the rough estimate of the postchange distribution F_2 is given by the mass function $f_2(x)$. If a group of observations of size n arrives and the corresponding perturbation in the mass function is $\Delta(x)$, then the updated density under new distribution $\tilde{F}$ is $\tilde{f}_2 = f_2(x) + \Delta(x)$. The KL divergence is updated during runtime using equation (2.27) which is derived later.

$$\begin{aligned} D(F_1 \parallel \tilde{F}_2) = D(F_1 \parallel F_2) - (E_{F_1}[x] - \frac{1}{2}E_{F_1}[x^2] \\ + \frac{1}{3}E_{F_1}[x^3] - \frac{1}{4}E_{F_1}[x^4]... \end{aligned} \tag{2.27}$$

Here we derive Group Sequential KL Divergence Update equation (2.27). Let $\kappa = \sum_{x=1}^{N} f_1(x) \log f_1(x)$. The old KL divergence in equation (2.17) changes to (2.28).

$$\begin{aligned} D(F_1 \parallel \tilde{F}_2) &= \sum_{x=1}^{N} f_1(x) \log \left(\frac{f_1(x)}{\tilde{f}_2(x)} \right) \\ &= \sum_{x=1}^{N} f_1(x) \log f_1(x) - \sum_{x=1}^{N} f_1(x) \log \tilde{f}_2(x) \\ &= \kappa - \sum_{x=1}^{N} f_1(x) \log(f_2(x) + \Delta(x)) \\ &= \kappa - \sum_{x=1}^{N} f_1(x) \log \left(f_2(x) \left(1 + \frac{\Delta(x)}{f_2(x)} \right) \right) \\ &= \kappa - \sum_{x=1}^{N} f_1(x) \log f_2(x) \\ &\quad - \sum_{x=1}^{N} f_1(x) \log \left(1 + \frac{\Delta(x)}{f_2(x)} \right) \\ &= D(F_1 \parallel F_2) - \sum_{x=1}^{N} f_1(x) \log \left(1 + \frac{\Delta(x)}{f_2(x)} \right) \end{aligned} \tag{2.28}$$

We use the Taylor series as given in (2.29) with $\omega(x) = \frac{\Delta(x)}{f_2(x)}$ to get (2.30).

$$\log(1 + x) = \sum_{n=1}^{\infty} -1^{n+1} \frac{x^n}{n}. \tag{2.29}$$

$$D(F_1 \parallel \tilde{F}_2) = D(F_1 \parallel F_2) - \sum_{x=1}^{N} f_1(x)(\omega - \frac{\omega^2}{2} + ...) \tag{2.30}$$

On simplifying further we get equation (2.27). We assume that (2.31) holds, which is valid for small perturbation to $f(x)$.

$$f_2(x) \gg \Delta(x) > 0 \, \forall \, x \in [1, N]. \tag{2.31}$$

2.8.10 Theoretical Performance Bounds

In this section we will examine the theoretical bounds on the performance of Protomac. We would ideally like to correlate the degradation in QoS as perceived by the primary network with the sequence of network statistics that we observe. It was suggested in [59] that the KL divergence be used for the purpose of selection of a signal set in a communication system to minimize the probability of error. A particular signal set is defined to be better than another if the KL-divergence between the distributions under the former is more than that under the latter. This observation enables us to rank the primary network packet density according to its KL divergence from the prechange density. The postchange distribution with a lower KL divergence is superior to a postchange distribution with a higher KL divergence. We can correlate this ranking based on divergence with the ranking based on error performance as shown. Let π_1 and π_2 be the prior probabilities of hypothesis H_1 and H_2 respectively. Then, we define the Bayesian Probability of Error as in equation (2.32). Hypothesis H_1 indicates the postchange distribution is below the Transmit Margin threshold and H_2 indicates that the postchange density is above the Transmit Margin threshold.

$$P_e = \min_{h1} \left(\pi_1 \int_{H_2} f_1(x) \, dx + \pi_2 \int_{H_1} f_2(x) \, dx \right) \tag{2.32}$$

The probability of error reflects the sum of the misclassification errors under the two sets of densities, and can be interpreted as a probability of interference with the primary network.When the postchange density has changed beyond the TM threshold, miss probability

$P_M = P(H_2|H_1)$ and false alarm probability $P_{FA} = P(H_1|H_0)$. Kullback derived the following bound for the KL divergence as in (2.33). This is the limiting bound for the best possible performance of the system and is used to set the thresholds.

$$\begin{aligned} & P_{FA} \log \frac{P_{FA}}{1 - P_M} + (1 - P_{FA}) \log \frac{1 - P_{FA}}{P_M} \\ & \leq D(F_1||F_2). \end{aligned} \tag{2.33}$$

If we fix $P_{FA} = 0$ we get a lower bound on P_M as

$$P_M \geq 2^{-D(F_1||F_2)}. \tag{2.34}$$

2.9 Density Estimation

In section 2.8.7 we reviewed efficient methods to evaluate divergences between distributions. But prior to these calculations, the probability densities under the two hypotheses must be estimated and hence density estimation is a critical aspect of ProTOMAC. Specifically, there are two densities to be estimated, the prechange density and the postchange density at the current transmit power. These two estimators have differing demands; the prechange density requires accuracy while the postchange density must be estimated with reasonable accuracy in the least time. The prechange density is estimated after the channel is observed for a long time to obtain a large sample. Consequently accurate density large sample estimation methods will be adopted. Whereas the postchange density must be estimated from a small sample size while assuring an estimator accuracy that is sufficient to deliver good discriminations of the density deviations.

Assume that the packet samples $X_1, X_2, .., X_n$ are independent realizations of an unknown density function $f(x)$ which is to be estimated as $\hat{f}(x)$. The Kernel Density Estimator

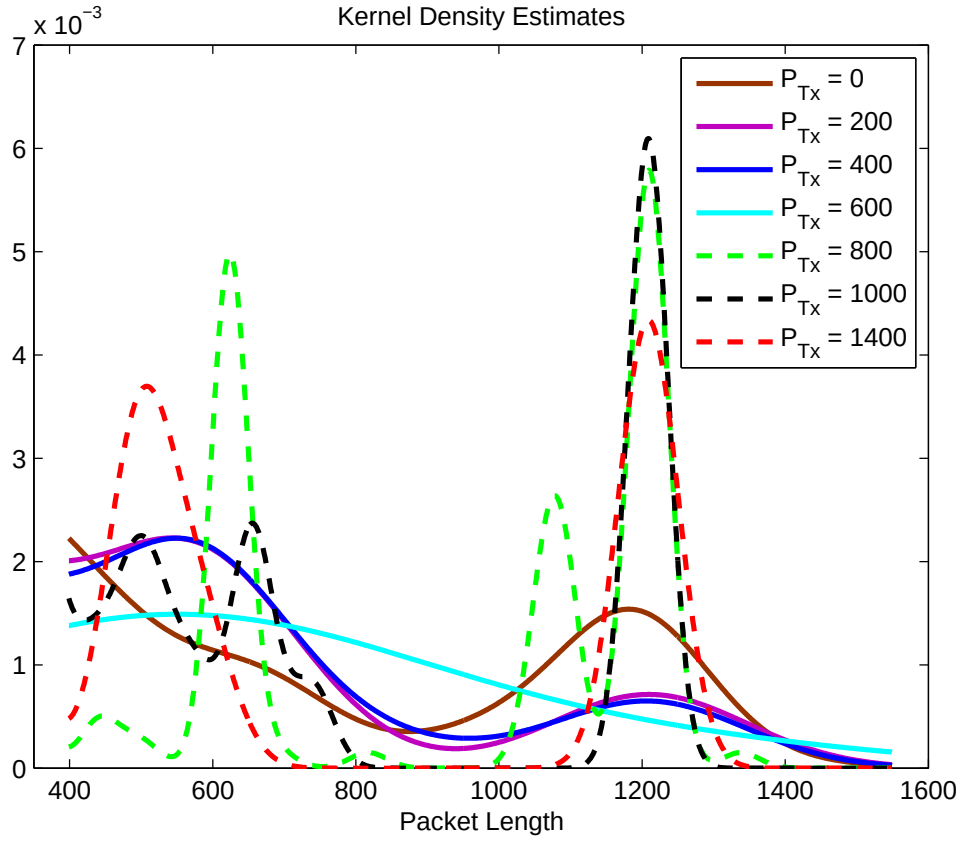

Figure 2.11: KDEs of CAP1 Dataset for increasing Tx Power with full capture duration

(KDE) is given as

$$\hat{f}_h(x) = \frac{1}{n}\sum_{i=1}^{n} K_h(x - X_i), \tag{2.35}$$

where the kernel function K_h is defined as,

$$K_h(u) = \frac{1}{h}K\left(\frac{u}{h}\right). \tag{2.36}$$

Appropriate choice of the kernel function K_h and an optimal selection of the smoothing factor or bandwidth h are the two critical aspects of KDE. The accuracy of the estimated density function is quantified by the Asymptotic Mean Square Integrated Error(AIMSE) criteria defined as

$$AIMSE(h) = \frac{1}{nh}R(K) + h^4\left(\frac{\mu_k(K)}{4}\right)^2 R(f"), \tag{2.37}$$

where the functional $\mu_k(K) = \int x^k K(x)dx$ and $R(K) = \int K^2(x)dx$. The first term in equation (2.37) is the asymptotic integrated variance and the second term is the asymptotic integrated bias. Minimization of the AIMSE gives the optimal bandwidth.

2.9.1 Deheuvel's Rule of Thumb Method

The optimal value of h is obtained by solving equation (2.37) as

$$h_\infty = \left(\frac{R(k)}{\mu_2^2(K)R(f'')}\right)^{\frac{1}{5}} n^{-\frac{1}{5}} \tag{2.38}$$

But $R(f'')$ is an unknown since f itself is the density to be estimated. We get around this difficulty by using the Deheuvel's Rule of Thumb method [60]. It involves approximating f through another reference density function which is rescaled to have a variance equal to the sample variance. Using a standard Gaussian as the reference distribution, the bandwidth is estimated as,

$$\hat{h_{rot}} = 1.06\hat{\sigma}n^{-\frac{1}{5}} \tag{2.39}$$

where $\hat{\sigma}$ is the sample variance.

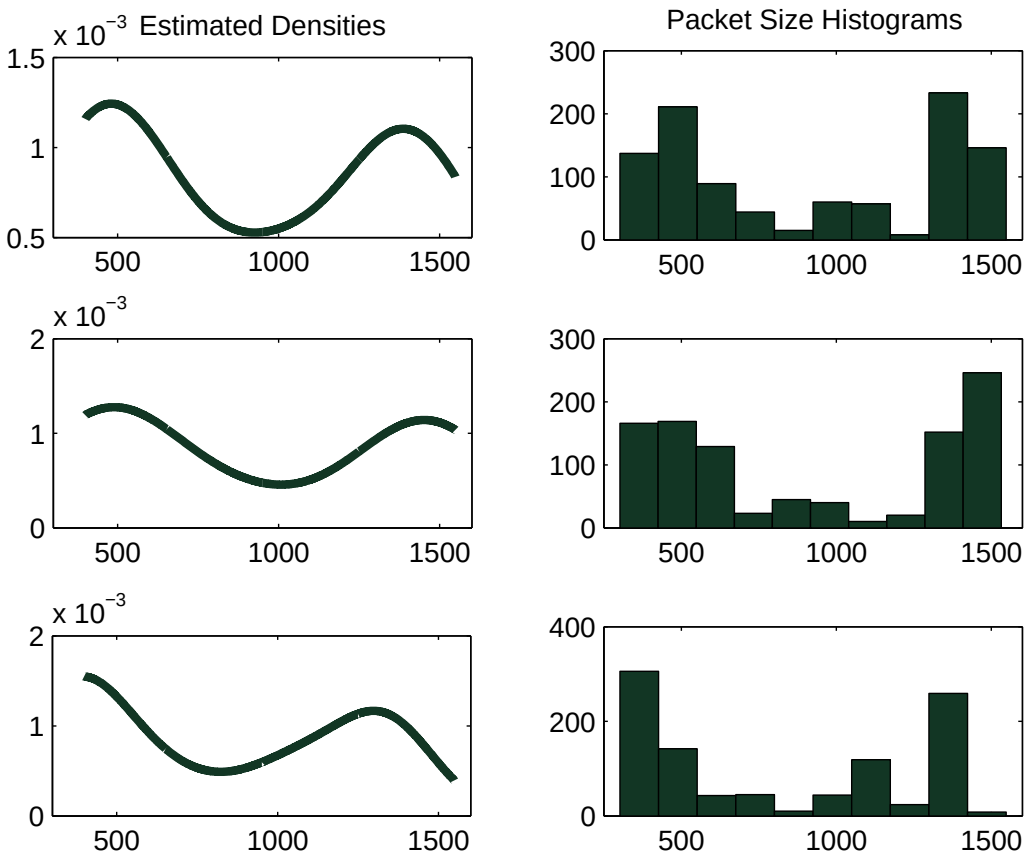

Figure 2.12: Kernel Density Estimates and Packet Length Histograms for CAP3 Dataset using Deheuvel's Method

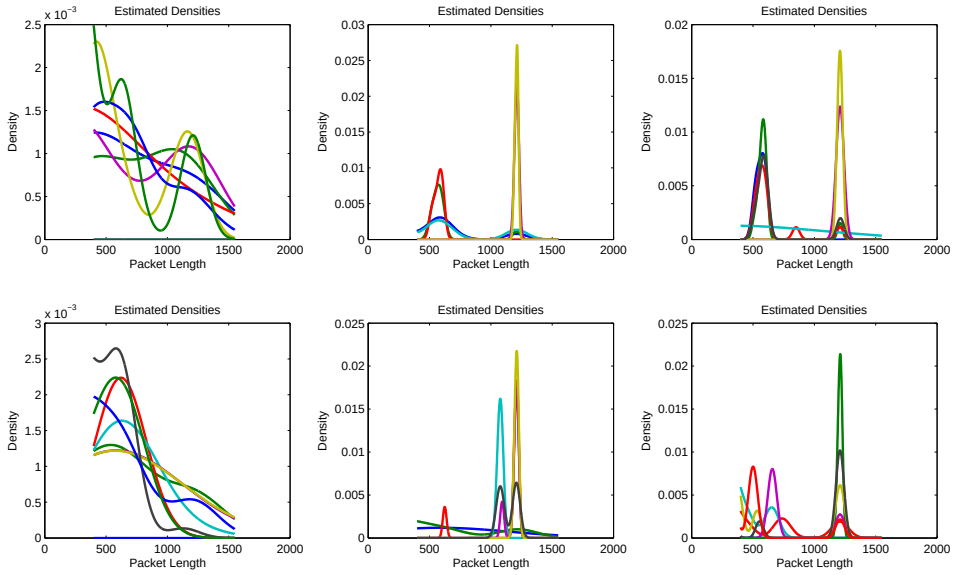

Figure 2.13: Demonstration of Time Stationarity over Captures for 6 increasing Transmission Power Levels

2.10 Experimental Testbed Setup

In this section we describe the experimental testbed based implementation of Pro-TOMAC. Figure 2.7 shows the setup of the testbed. The interactions between the primary and secondary networks are illustrated in the figure. The CRN consists of colocated Wireless Sniffers and Software Radios acting together as the secondary nodes. The primary network is an IEEE 802.11g WLAN network.

2.10.1 Primary Network Configuration

IEEE 802.11 channels lie within the license free Industrial, Scientific and Medical (ISM) band. Also, IEEE 802.11 shares the ISM band with a variety of legacy devices like microwave ovens, Bluetooth and cordless phones. These legacy devices are sources of interference and a host of methods have been developed to avoid or to minimize this interference.

Newer technologies like Bluetooth have complex MAC protocols to allow coexistence with 802.11 [61]. These interference mitigation methods have been designed on a case-by-case ad-hoc basis. The advent of dynamic spectrum use demands generalized non-interfering spectrum access methods. ProTOMAC provides an open-ended and flexible framework for an intelligent radio access mechanism within the philosophy of CRNs.

The testbed has been setup in the laboratory and is co-located with the University's IEEE 802.11g WLAN. The 802.11g network is configured in the Infrastructure mode in which the individual 802.11g basestations (BS) connect to a central Access Point (AP) and form a cell. The presence of multiple overlapping cells creates a dense grid where nodes have the choice to switch to alternate channels or to change association to an adjoining cell. For example, Capture Set 1 consists of data transfer between 28 nodes and 6 APs. Analytical modeling of such an extensive setup is not easily achieved. Instead, we have implemented an empirical approach which dynamically tracks the statistical behavior of the network in a non-parametric non model-based manner as explained in detail in section 2.6. As the secondary node transmits at a low power, the maximum probability of interference is presented to the 802.11 nodes directly within the range of the secondary network.

2.10.2 Secondary Network Configuration

The secondary network consists of two Software Defined Radios (SDR). Each SDR is composed of an Universal Software Radio Peripheral (USRP) manufactured by Ettus Research which has a USB 2.0 based link to a laptop computer [62]. The USRPs are equipped with a RF front-end board RFX2400 capable of simultaneously transmitting and receiving. The RFX2400 has a frequency range of 2.3 to 2.9 GHz and has been designed to operate in the ISM band (2.4 to 2.486 GHz). The USRP is programmed and controlled via the GNU Radio suite of open source software radio and signal processing packages [63]. Also, a 2.4 GHz Intel Core2 Duo machine running the Ubuntu 8 Heron operating system interfaces with

the USRPs.

SDR 1 is configured as the transmitter and broadcasts at 2.412 GHz which is the center frequency of channel 1 in IEEE 802.11. The transmission power is a dynamically controlled variable. RFX2400 based USRPs have a maximum transmit power of 50 mW (17 dBm). SDR 2 is configured as the receiver and positioned at a distance of 1 m to 5 m. Throughout the series of experiments, SDR 2 was able to receive and demodulate the transmitted sequence succesfully. Section 2.12.4 gives details of the secondary link performance. An Intel Wireless 4965 Network Adapter card controlled via the Kismet Wireless Sniffer captured and logged the 802.11 network traffic. The sniffers were colocated with the secondary transmitter and receiver.

2.10.3 Implementation Issues

We demonstrate the performance of ProTOMAC with the help of three representative runs, the outcomes of which are recorded in primary network packet captures labeled CAP1, CAP2 and CAP3. Here we will describe the results in detail using CAP1 with brief comments on the other runs. The three ProTOMAC runs occurred at different times of the day and encountered varied network traffic. Thus, taken together we establish the robustness of ProTOMAC under the gamut of situations that might be encountered in practice. The distribution of the packet sizes and interarrival times was used as the network statistic as in Section 2.3.

2.10.3.1 Study of Network Stationarity

The short term stationarity of the primary network can be shown through a representative example where we observed the IEEE 802.11 network at three different traffic conditions, busy traffic, medium traffic and low traffic. For each case the density of the

packet interarrival times on the primary network was calculated for consecutive slots where each slot consisted of 100 packet arrivals. Then the KL divergence of each slot was found with respect to slots observed at increasing delays and finally the network statistic was deemed to have changed if the calculated KL divergence was higher than a threshold, which was 1.0 in this case. The probability that the network statistic changes over time is then plotted in Figure 2.3. It can be seen that for the low traffic network, there is a 70 % probability that the network statistics are unchanged after 4 consecutive slots, while this probability is still more than 50 % when observed over a 6 slot interval. In other experiments, a stationarity probability of 50-90 % was observed over a 6 slot interval. The exact degree of stationarity changes with every network state and observation time. Protomac works by quantifying this stationarity by the probability of change over consecutive slots, and then by continuously monitoring this transition probability. Protomac stops using the channel and seek another channel if there is a 10 percentage point fall in the underlying network stationarity.

2.11 Experimental Results For Goodness of Fit Tests

2.11.1 Sequential Kolmogorov-Smirnov Test

The method presented in the previous sections was implemented on three datasets of packet captures. Here will explain the results for a representative case of Dataset 2. The secondary transmission power was increased uniformly from zero upto 7 mW in three steps as 2.3mW, 4.6mW and 7mW . Figure 2.14 shows the histograms of the packet sizes for the four transmission power levels. This power was sufficient to cause an inoperable interference to primary base stations within a 1.2 m radius of the secondary transmitter, while the primary base station was tested to work properly at a range of 2.5 m from the secondary transmitter. Also, a secondary receiver could decode the transmissions at 2.3 mW at a distance of upto 12 m to set up a working secondary link. The data rate of the primary network dropped

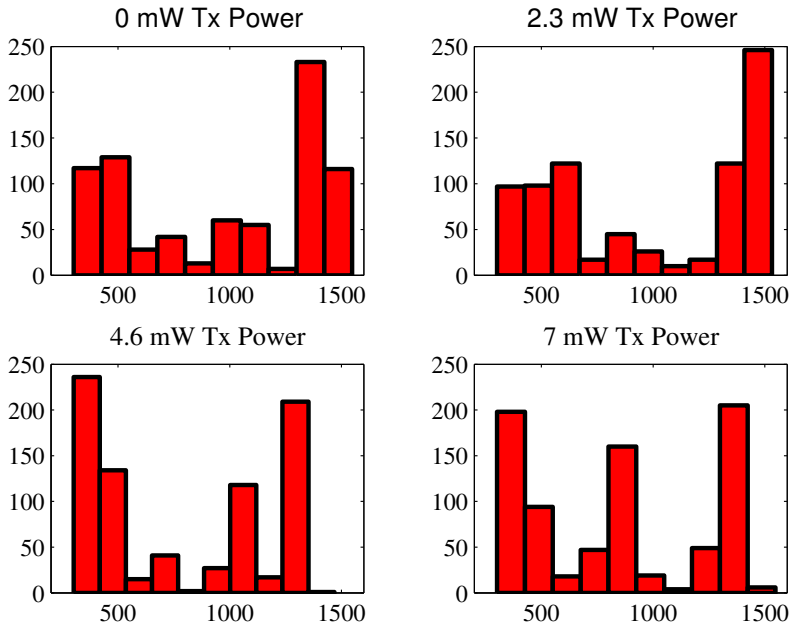

Figure 2.14: Packet Size Histograms for 4 Tx Power levels

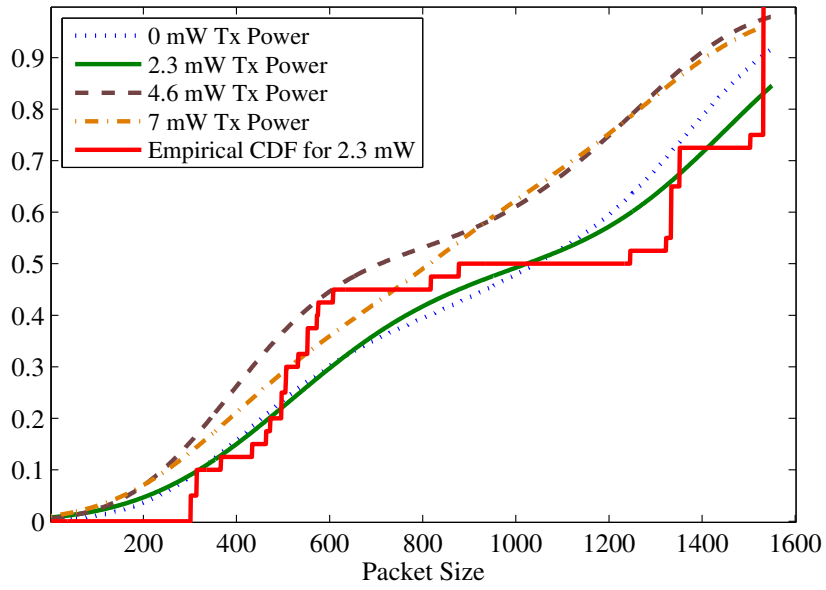

Figure 2.15: Empirical CDF (using 40 samples) for Tx power 2.3 mW

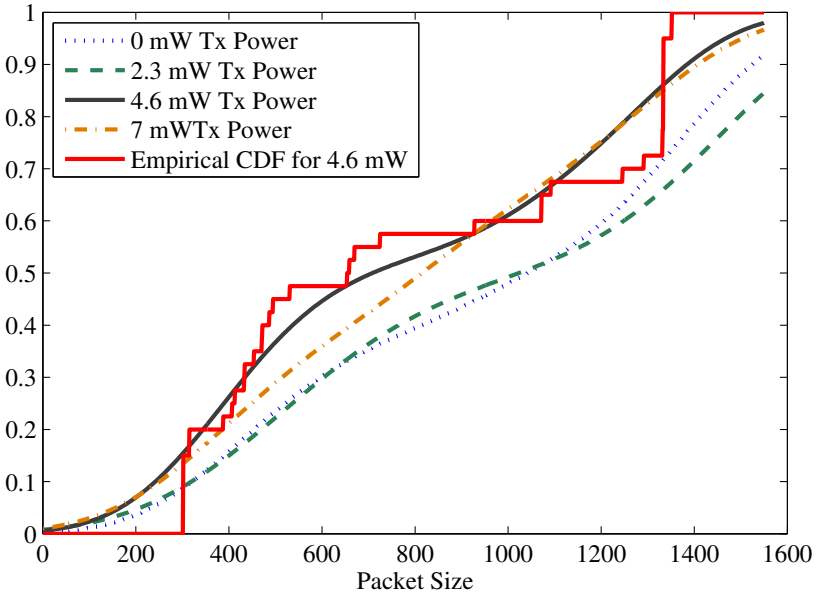

Figure 2.16: Empirical CDF (using 40 samples) for Tx power 4.6 mW

marginally from an initial 0.161 Mbps to 0.156 Mbps for a transmit power of 2.3 mW and to 0.121 Mbps for a transmit power of 4.6 mW. The Adaptive Modulation and Coding (AMC) mode of the primary WLAN was unchanged for all 4 secondary transmit power levels but changed if we attempted to increase the power further. Application of our method allowed a Tx power of 2.3 mW but curtailed the secondary from transmitting at 4.6 mW or at 7 mW. Thus, we were able to safely and reliably create a transmission opportunity and setup an operational secondary link with only a marginal effect on the QOS of the primary network. Similar results and threshold transmit powers were obtained for the other datasets.

Figure 2.15 shows the kernel density estimates of the packet captures. The densities were estimated using the full duration of the captures and are considered to be the baseline accurate estimate of the CDFs. Note the slight shift in the CDF curve when secondary power is increased from 0 to 2.3 mW, while a further increase in power to 4.6 mW and 7 mW causes a sudden large shift in the CDF. During the sequential KS test, the approximated empirical estimate of the packet size CDF is calculated using only the packets captured to

that instant. The empirically calculated CDF using a duration of 40 packets is shown in figures 2.15 and 2.16. Once the empirical CDF is obtained, we run the KS test and obtain the KS distance D_n. The criterion D_n is compared with the distribution tables of the KS statistic to obtain the p-value and the confidence interval.

The Sequential Kolmogorov Smirnov test as explained in section 2.8.3 was implemented on Dataset 2 for a range of sample sizes from 5 packets to 40 packets. The resulting performance over 1000 iterations of the KS test is plotted in Figure 2.17. The standard deviation error bars show that the KS statistic converges to a stable value as the sample size increases. Also, accurate decisions with increased speed can be made by a sequential procedure while bounding the maximum sample size to 40 packets. For a sample duration of 20 to 40 packets, the observed average sensing time was between 140 ms to 290 ms.
We will define a Probability of Misdetection of Transmission Opportunity (P_{MD}) as the probability of deciding the distribution has not changed when in reality it has changed, i.e, when we are transmitting at 4.6 mW or 7 mW. And the Probability of Detection of Transmission Opportunity (P_D) is the probability of accurately deciding that the distribution has not changed, i.e, we are transmitting at 2.3 mW. Figure 2.18 shows the behavior of the P_{MD} and P_D curves as the sample size increases. It is seen that for a given significance level of α, the P_D degrades gracefully with increasing sample size while there is an abrupt steep drop in the P_{MD} of the test after a certain sample size. If we operate in the region after the steep drop, we can sense and utilize existing transmission opportunities with a 50%-75% accuracy while we interfere with the primary with a probability $P_{MD} < 0.1$. This interference rate becomes negligible if we allow slightly larger sample sizes, e.g, for $\alpha = 0.05$ and a 30 sample size test, we detect transmit opportunities with a 64% accuracy with an interference probability of 0.02. Based on these observations, the KS test was run in a sequential manner, i.e, the KS statistic was evaluated repeatedly after collecting the first $n = 15, 20, ...$ samples after beginning the secondary network transmission in the access slot. In addition to this

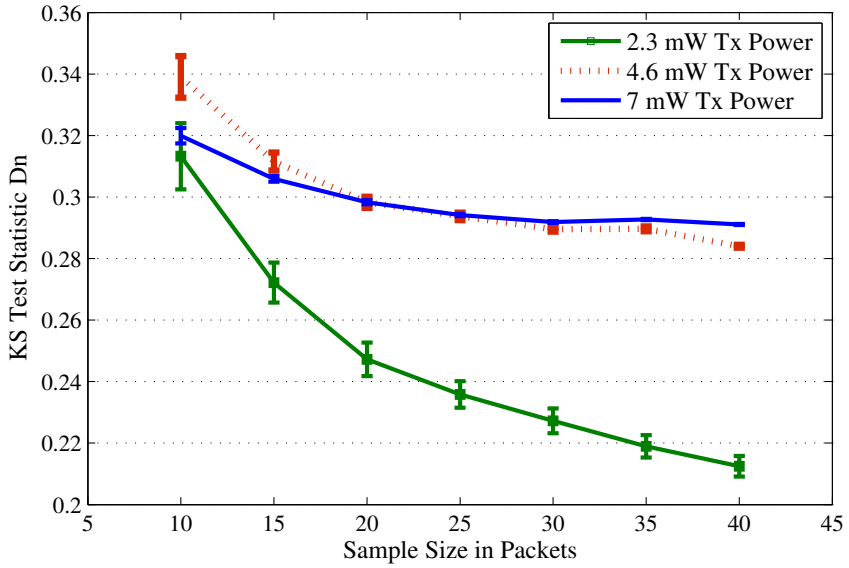

Figure 2.17: Sequential Behavior of KS Test Statistic with increasing Sample Size

the significance level of the test was progressively reduced starting at $\alpha = 0.15$ for $n = 15$, $\alpha = 0.10$ for $n = 20$ to $\alpha = 0.05$ for $n = 25$ and kept steady after that. This is referred to as sequential shrinkage of significance. This ensures that the KS test is able to detect the change at even small sample sizes while maintaining a tolerable false alarm rate. The performance of the KS test is better than that of the other tests we consider at small samples but its selectivity increases very rapidly as the test sample size increases and at higher sample sizes the KS test starts rejecting distributions with even a slight change from the null distribution. Hence we recommend beginning with the KS test and after the first 25 - 30 samples switching to the parallelized Goodness-of-Fit test whose performance we present below.

2.11.2 Parallelized Goodness-of-Fit test

The performance of Cramer-von Mises test, Anderson-Darling test and the Parallelized GoF test is shown in the ROC curves in Figures 2.19, 2.20 and 2.21. In these results

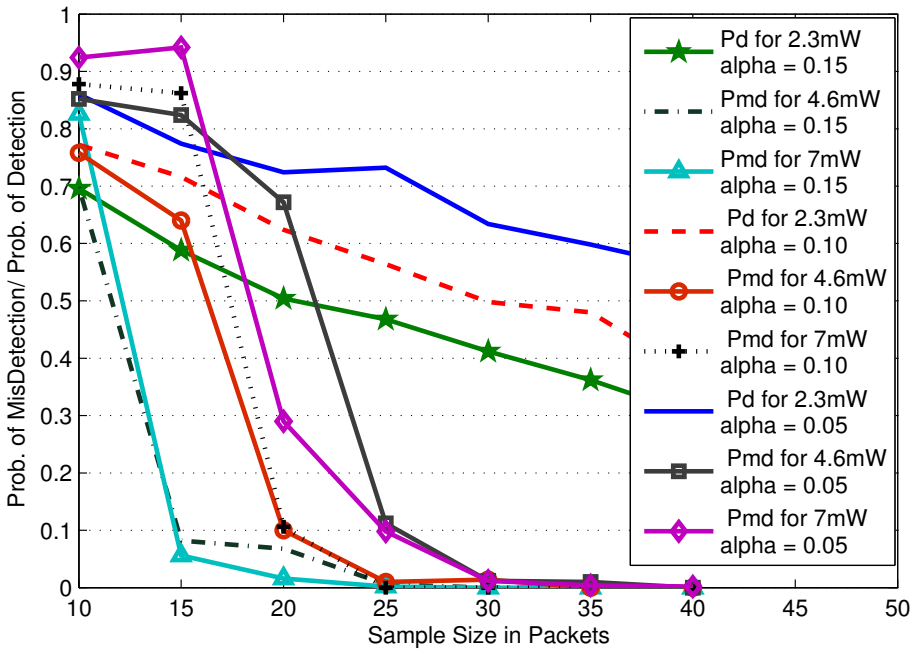

Figure 2.18: ROC Curves for KS Test

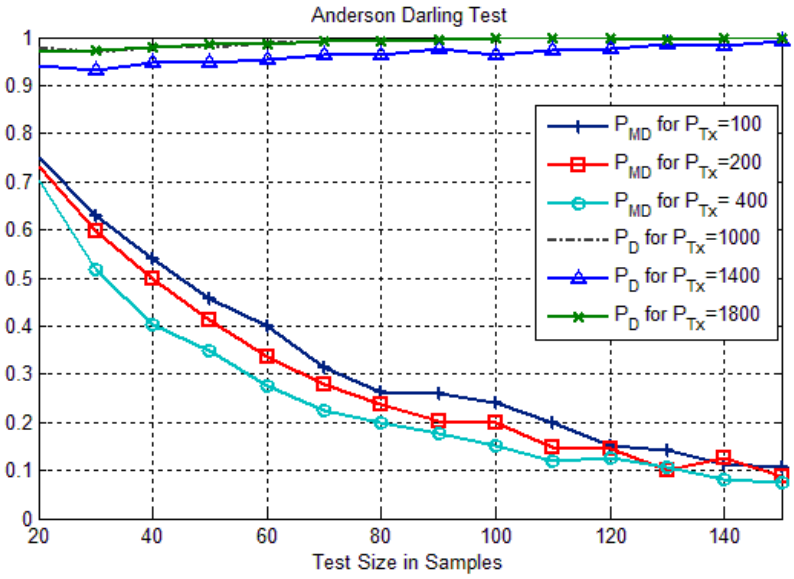

Figure 2.19: ROC Curves for AD Test

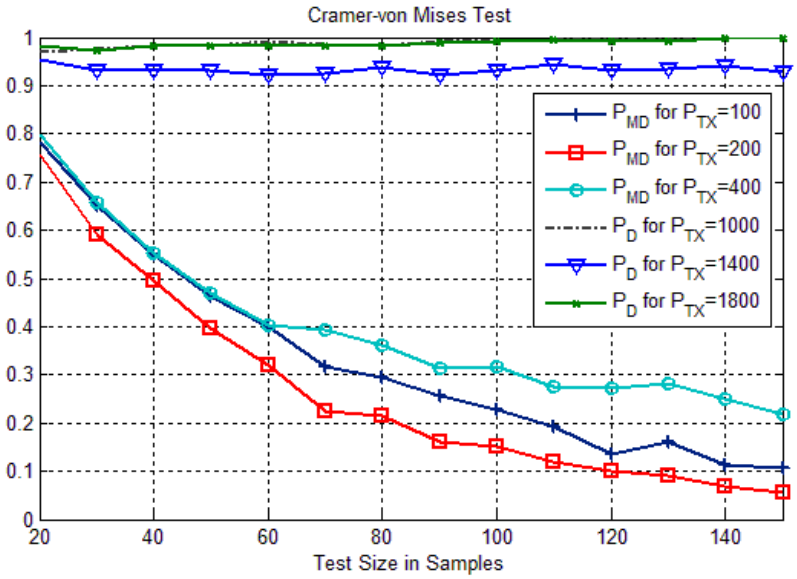

Figure 2.20: ROC Curves for CvM Test

P_{MD} is the probability of misdetection of a transmit opportunity when it exists, that is, when the CR wrongly decides that it is not safe to transmit. P_D is the probability of detection where the CR correctly detects that it transmitting above the transmit margin and backs off. At very small sample sizes, these tests have a very high probability of classifying a valid transmit opportunity as not being valid as is seen in the plots. Also as expected, the Cramer-von Mises test performs better than the Anderson-Darling test when there is a change in the center region of the packet statistics, which occurs for transmit powers of less than 80 μW (400 units) while at powers equal to or above this transmit margin, the change in the density occurs predominantly in the lower tail region and the Anderson-Darling test shows superior performance. As shown in Figure 2.21 which combines the implementation of these two tests, the Parallelized Goodness of Fit test performs well for all transmit power levels. The critical quantity to the primary user is the P_D of the test and is bounded to values above 90 % at all transmit power levels and is often as high as 98-99 % even at small test duration. On the other hand, the P_{MD} of the test decreases rapidly with the increase in

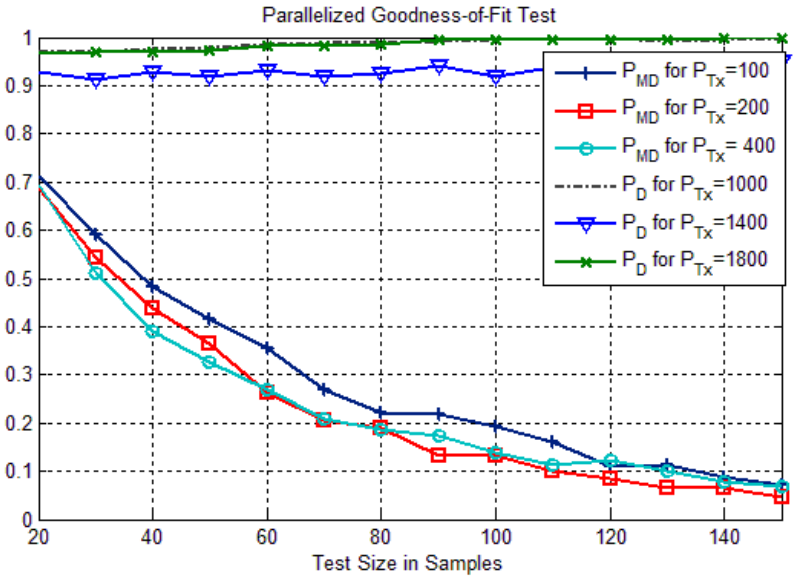

Figure 2.21: ROC Curves for Parallelized Goodness of Fit Test

test duration and saturates at approximately 10% letting us successfully detect and utilize upto 90% of the available transmit opportunities.

2.11.3 Comparison with the SWIFT approach

In Section 2.2 we discussed the SWIFT approach as presented in [31]. It detects changes using the Student's t-test and assumes a Gaussian distribution of the metrics. Figure 2.22 plots the relative performance of the t-test and the Anderson-Darling test which is used in Protomac. These results are obtained by considering the gaps between successive packet transmissions as measured by their interarrival times which acts as the network statistic. It is seen in Figure 2.22a that the Probability of Detection of the Anderson-Darling test is 25 percentage points better than that of the t-test while the AD test Probability of False Alarm is 10 percentage points better for a test size of 50 samples as in Figure 2.22b. Here the statistics are assumed to have changed when the KL divergence is at least 0.5. The underlying non-Gaussianity of the channel interarrival times causes the t-test to show inferior

performance to the nonparametric AD test which does not assume any knowledge of the distribution of the statistics. While the detection performance of Protomac is superior, the secondary network datarates of SWIFT and Protomac cannot be compared in a fair manner as SWIFT uses the white space in the unoccupied 5 GHZ ISM bands through a full power wideband transmission, while Protomac uses the gray space in a single narrowband channel through a low power transmission. Also, Protomac is designed to prevent the primary users from switching to another channel due to high secondary interference on current channel, whereas SWIFT does not check and prevent this behavior, and thus creates artificially vacant channels by driving away some primary traffic off its channel.

2.12 Experimental Results for Divergence Measure based Tests

2.12.1 Baseline Density Estimates

In Figure 2.12, we have plotted the results of using Deheuvel's method as explained in Section 2.9. It shows the kernel density estimates for the different CR transmit powers in CAP3 dataset. The density estimates are marginally affected by the choice of individual kernels but show a high sensitivity to the bandwidth chosen. Application of Deheuvel's method for CAP3 gave a bandwidths between 62 to 68, while an exhaustive search over the range 10 to 200 showed optimal performance for bandwidths between 55 to 65. Deheuvel's method also performs satisfactorily on CAP1 and CAP2 datasets.

Figure 2.11 plots the accurate densities of the primary packet lengths using the full duration of the individual captures in the kernel density estimator. The network statistics do not deviate significantly upto a transmit power level of 600 units. But, there is a sudden and large shift in the density for transmit power levels of 800 to 1400. Thus, in the case studied in CAP1 dataset, the Transmit Margin is 600 units. Also, the corresponding metrics for primary network QOS mirror this threshold. The file transfer rate dropped from 40 kbps

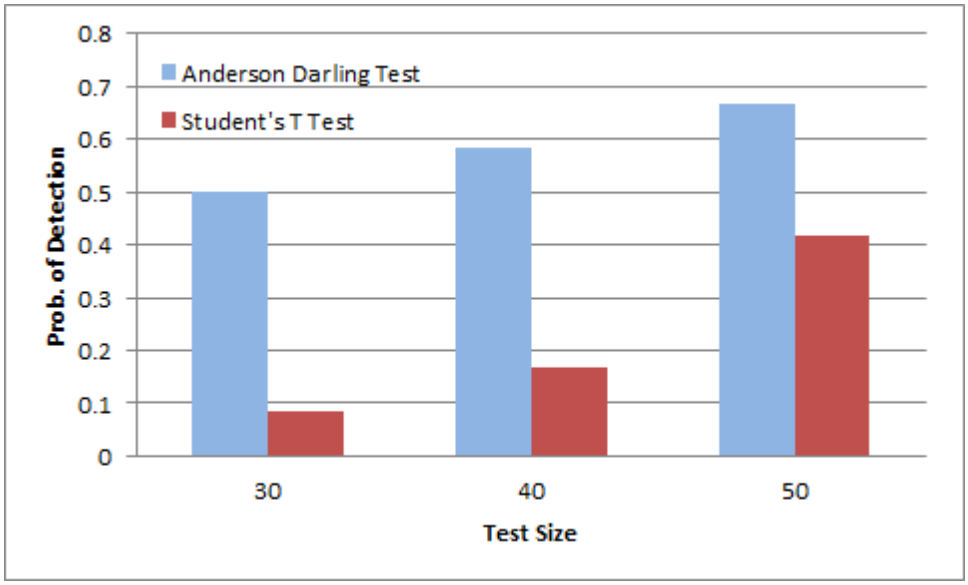

(a)

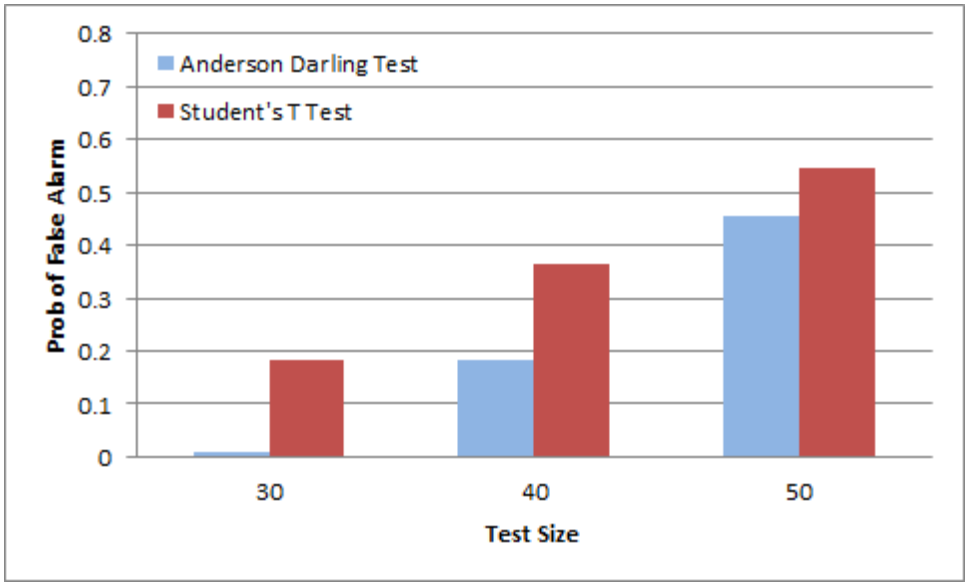

(b)

Figure 2.22: Probability of Detection (a) and Probability of False Alarm (b) for the Student's t test and the Anderson-Darling test for increasing test sample size.

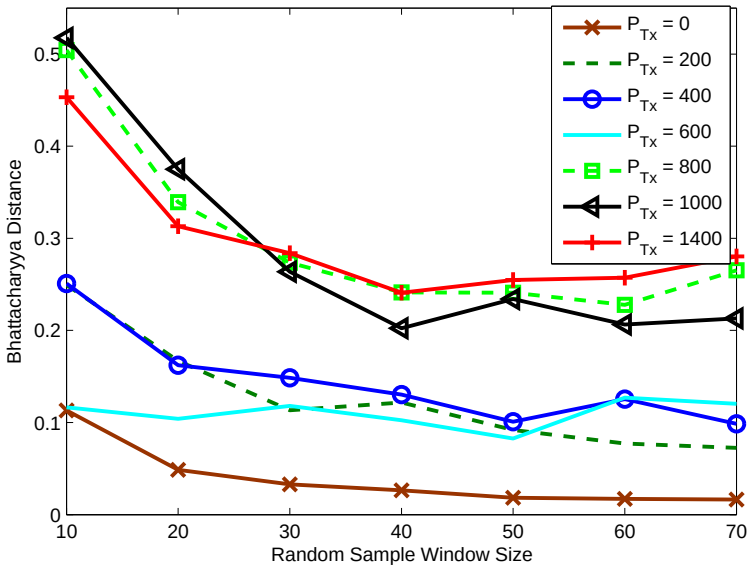

(a) Test Performance under i.i.d assumption with random sampling using Bhattacharyya Distance

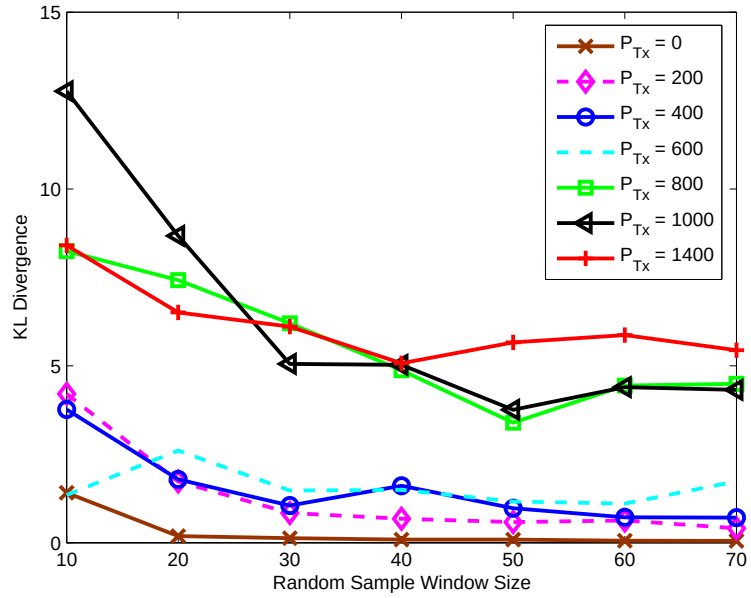

(b) Test Performance under i.i.d assumption with random sampling using KL Divergence

Figure 2.23: ProTOMAC Results for CAP1 Dataset

to 38 kbps at 600 units, 32 kbps at 800 units and 20 kbps at 1000 units. The round trip delay was unchanged in this case till the transmit power was increased to 1400. Also, the Transmission Rate remained unchanged at 54 MBps till it dropped to 36 MBps at a power level of 1000. A similar clear threshold was found for the other datasets. Thus, the Transmit Margin as predicted by ProTOMAC is slightly conservative.

2.12.2 Tests using Randomized Sampling

Now, we will examine the performance of ProTOMAC under various formulations of the group sequential type tests as explained in Section 2.6. If we neglect the underlying non-stationarity and model the data as being drawn from an independent identically distributed (i.i.d)process, then the best bound for the test performance is obtained as shown in Figure 2.23b for the Bhattacharyya Distance and in Figure 2.23a for the KL Divergence measure. It demonstrates the behavior of the divergence between the approximate estimated density of a small size sample and the accurate prechange density as the size of the sample is increased from 10 to 70 packets. These packets are selected via random uniform sampling without replacement from the full capture duration. This sampling model is impractical for actual implementation as we have to wait for the whole duration of the capture before sampling it, which will introduce a large delay. But the performance under the random sampling model is a good comparison benchmark. We note from figure 2.23b that the maximum discrimination between the two densities is possible for the low sample size range, i.e, 20-30 packets, which is a remarkably fast sensing time.

2.12.3 Group Sequential Test

A highly efficient and fast practical modification of the above random sampling scheme is to randomly select without replacement a subset of length M out of the N samples captured till the current instant. This introduces an element of randomization that improves system

performance. Figure 2.26 shows the Bhattacharyya distance for CAP1 dataset with fixed representative random sample lengths of 20, 40 and 100, as plotted in Figures 2.26a, 2.26b and 2.26c respectively, for increasing total capture duration. Also, the corresponding performance of the KL Divergence measures is plotted in Figures 2.26d, 2.26e and 2.26f. Thus, it is a group sequential test implementation with a rough density estimate calculated using 20 samples and progressively refined with the addition of consecutive groups of 10 samples each. During analysis, an empirical threshold of 0.3 for the KL divergence and 3.5 for the Bhattacharyya distance was used. ProTOMAC shows reliable convergence with time as the capture duration increases. It was observed that Bhattacharyya Distance based test had an asymptotic gain of 1.5 while the KL divergence based test had an asymptotic gain of 4. Also, the test statistic is highly conservative at smaller sample sizes. For example, a threshold of a Bhattacharyya Distance 0.3 classifies some safe Transmit Opportunities as unsafe for small capture duration. This classification error reduces rapidly at longer capture duration. Also, there is faster convergence and a reduction in the degree of risk with increasing random sample length. Similar results are obtained if we use the KL divergence as a statistic as shown in Figures 2.26d, 2.26e and 2.26f.

2.12.4 Secondary Link Power Budget

ProTOMAC implements an end-to-end secondary link. A stream of packets is transmitted from SDR 1 to SDR 2 over the secondary channel which has been carved out at the given Transmit Margin. We will now characterize the secondary link behavior and investigate the performance and reliability of the secondary network. In each instance a 1 MB file was transmitted as packets of a fixed size over the link. Binary Phase Shift Keying (BPSK) modulation was implemented with 1 bit per symbol to work at a 500 kbps bitrate. The carrier frequency for the BPSK was set to 2.412 GHz. Figure 2.25a plots the effect of increasing the transmit power on the PER, for different fixed packet sizes. Higher packet

Tx Power	Packet Size (bits)	Bitrate (in MBPS)	PER in %
0.5 mW	100	1	0.46
		2	0.42
		4	4.24
	1000	1	0.6
		2	9.92
		4	35.72
0.32mW	100	1	0.17
		2	3.53
		4	8.7
	1000	1	0.7
		2	7.2
		4	34.1
0.18 mW	100	1	3.04
		2	28.75
		4	NA
	1000	1	5.82
		2	44.14
		4	NA

Figure 2.24: Secondary Link Performance for OFDM modulation

sizes are adversely affected at low transmit margins and experience a PER of upto 35 %. Remarkably, packets smaller than 400 bytes are highly resilient to errors even at very low transmit power and have a PER of 5 %. Figure 2.25b plots curves corresponding to different transmit powers which show degradation of PER with increasing link distance for a fixed packet size of 700 bytes. The PER increases with range as might be expected. This degradation in PER is more pronounced for low transmit margins. With more complex modulation scheme the performance of the secondary link improves significantly as shown in Figure 2.24 for an OFDM modulation scheme with 256 subcarriers.

2.13 Conclusions

We have developed a suite of novel methods which enable us to identify and exploit the opportunistic transmission opportunities present in a crowded Packet Based Network. For the first time, the detection of opportunities has been implemented at the MAC layer. Also,

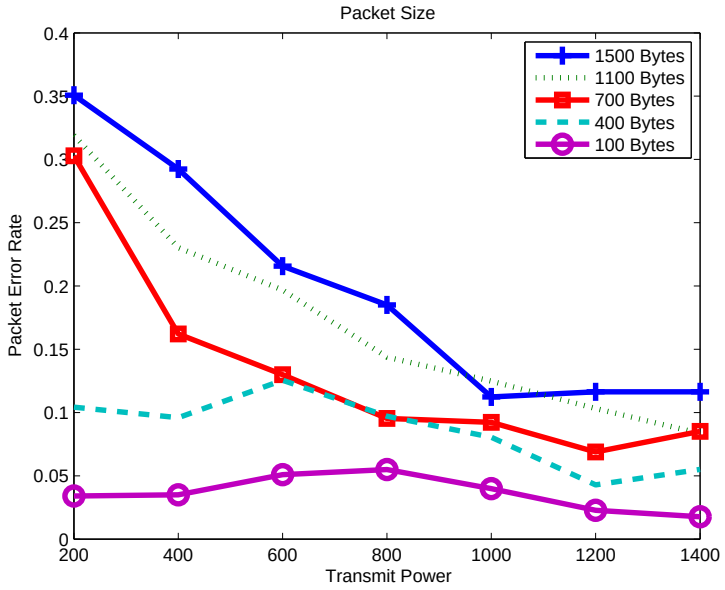

(a) Effect of Packet Size on Secondary Link Performance for BPSK modulation: PER vs Tx Power

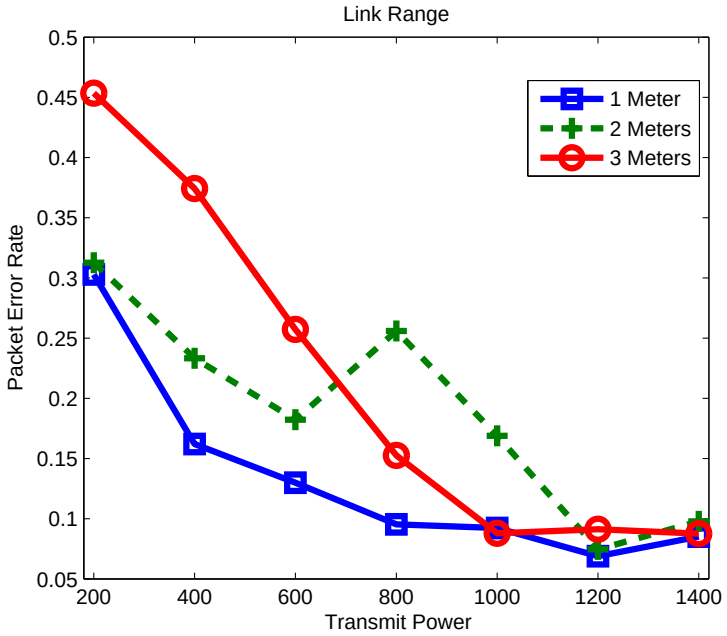

(b) Effect of Link Distance on Secondary Link Performance for BPSK modulation: PER vs Tx Power

Figure 2.25: ProTOMAC Results for CAP1 Dataset

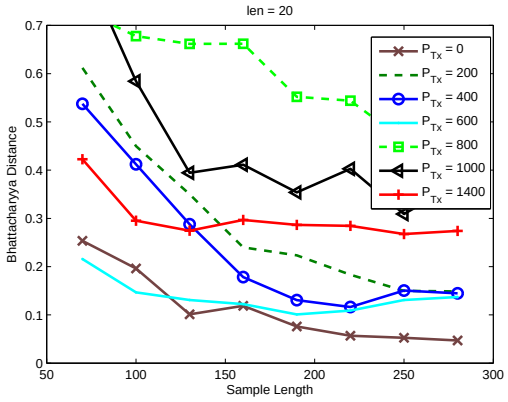

(a) N=20

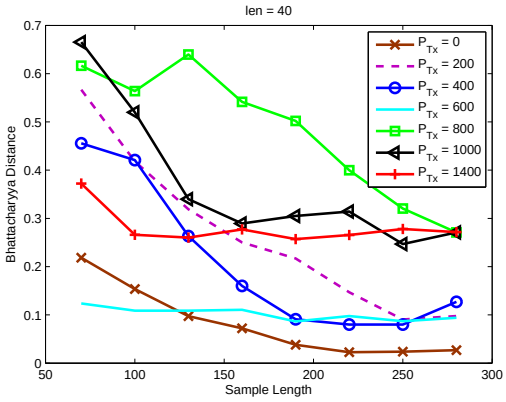

(b) N=40

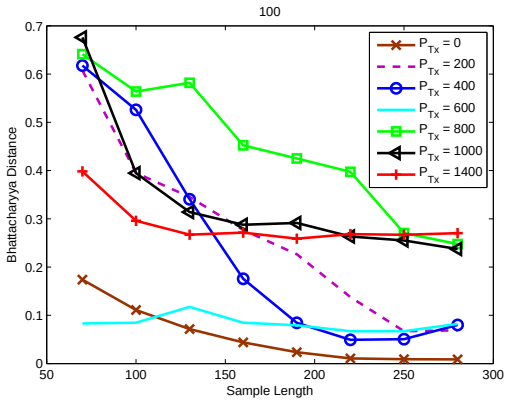

(c) N=100

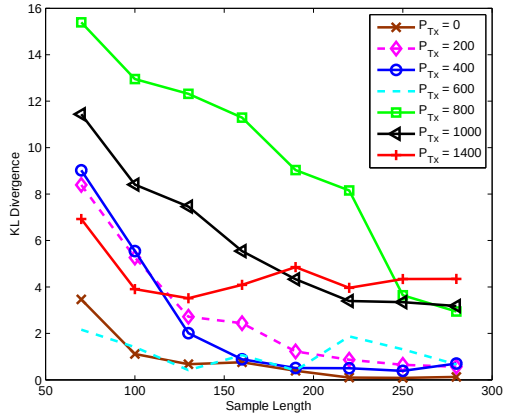

(d) N=20

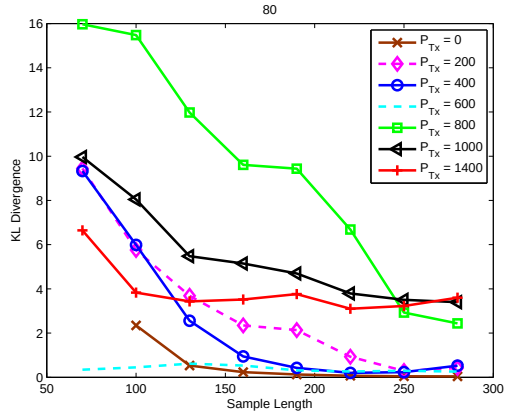

(e) N=40

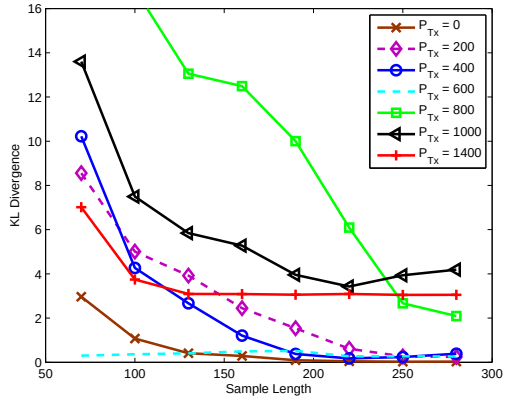

(f) N=100

Figure 2.26: Group Sequential Test Performance for CAP1 Dataset using Bhattacharyya Distance as Metric

the primary network QoS is safeguarded and the interference constraints are obeyed using the Transmit Margin that we have introduced. We have implemented our method in a real world large scale IEEE 802.11 WLAN and successfully established a reliable Secondary link between two nodes. Although we have made a number of assumptions like a quasi-stationarity of the packet statistics on a medium time scale, we have practically demonstrated the soundness and viability of the metrics used. Thus, we have achieved significant utilization of hitherto unused transmit opportunities. We hope to have introduced a new domain of cognition for CRNs which shows exciting potential for novel applications.

Chapter 3

Phi-divergence based Ensemble Goodness of Fit tests

3.1 Introduction

The problem of inference based decision making is conventionally treated as that of hypothesis testing for parametric models where the distributions are modeled using known and parametric probability functions which usually belong to the exponential family of distributions. Such a framework has worked remarkably well in the past including in a series of recent applications where the hypotheses to be tested are not well defined. Also, the robustness of parametric tests is often inferior to that of equivalent non parametric tests when there is uncertainty in the knowledge of the noise statistics or when the noise statistics are non-parametric. The penalty usually incurred for this increase in robustness is a decrease in the power of the test. Goodness of Fit tests are a particularly popular and robust class of inferential tests that have been applied for almost a century in the statistical community [41, 64]. But, the use of these tests in digital communications applications has historically been restricted to testing the fit of empirical models to data, i.e, model fitting. Recently, there has been an effort to study the performance of these tests for hypothesis testing applications, and highly encouraging results have been obtained [65–67].

3.1.1 Our Contributions

This work makes four major contributions towards developing ensemble phi-divergence based tests for spectrum sensing.

1. First, a generalized framework for inferential decision making based on phi-divergences is presented. It is shown how many other conventional goodness of fit measures are special cases of these statistics and the tailored design of new tests having desirable properties is introduced.

2. Second, extensive simulation results of the performance of this family of tests under Gaussian as well as non-Gaussian (impulsive) noise environments are presented.

3. Third, we develop a novel decision fusion method based on the statistical nature of the p-value metric that shows robust and predictable performance under variability in noise distributions.

4. Fourth, the combination of spatially separated tests under the assumption of independent but not necessarily identically distributed underlying distributions is studied, using a new summary test statistic.

There are two primary reasons for adopting a non-parametric goodness-of-fit test. First, it has a significantly reduced computational load as compared to complex parametric tests such as cyclostationarity detection [68], Maximum Likelihood detection, eigenvalue based detection [69] etc. No matrix inversions or Fourier transforms are needed. Instead, a simple distribution calculation followed by the use of a lookup table suffices. Second, such tests are inherently highly robust in the presence of unreliable information on the distributions under the hypothesis. Moreover, they work as well in the presence of completely arbitrary distributions. Third, the tests deliver satisfactory small sample performance, which allows the designer to effectively trade off performance versus sensing duration if desired. These tests have a number of other desirable properties that will be apparent in later sections.

3.1.2 Related Work

3.1.2.1 Non Parametric Statistics in Communications

Although parametric estimation and detection methods comprise the majority of proposed methods in digital communications, a significant variety of non-parametric statistical approaches coexist with them. There is a rich history of work, starting with the classical bibliography in [70] to recent works [68, 71, 72], but unlike the proposed work these cannot be applied to the use of goodness-of-fit tests nor to their distributed versions.

3.1.2.2 Goodness of Fit tests in Cognitive Radio literature

In this section we will review the use of Goodness-of-Fit tests in the literature. We will focus on aspects of hypothesis testing where the application domain is the problem of sensing white spaces in dynamic spectrum access systems [13, 73]. In [33, 65], a fast and robust spectrum sensing scheme is proposed using the Kolmogorov-Smirnov goodness of fit test. It is demonstrated through simulations that the KS test offers superior performance in and faster signal detection times as compared to traditional methods such as energy detection, eigenvalue-based detection and cyclostationarity detection. In the presence of a Gaussian noise, the KS test has been shown to be highly robust to uncertainty in background noise estimation as compared to the energy detection. Moreover, its performance is superb in the presence of non-Gaussian noise also, where other spectrum sensing methods often fail. The main drawback in their approach is that their interpretation of a goodness of fit test as a binary hypothesis test has been questioned in the statistical literature [74, 75]. Goodness-of-Fit tests are not meant to accept the null hypothesis H_0, but only reject it at a certain significance level. In other words, all the Kolmogorov-Smirnov test states is that the hypothesis that the noise is modeled by the estimated noise density can be rejected with a confidence level of α (usually 99.5 % etc). In contrast to the above mentioned approaches, our

proposed use of testing the uniformity of p-values for phi-divergence test does not encounter these conceptual difficulties. The test statistic can also exceed the threshold when either a) the assumed noise model is wrong as often happens in presence of impulsive non-Gaussian noise or b) there is another very weak non primary interferer that is subtly changing the noise distribution from the theoretical one. The latter situation can be treated using an approach similar to the techniques to detect sparse heterogeneity in mixtures and we will not consider that here [76] We will focus only on the first case in the rest of this chapter since in spectrum sensing applications the mischaracterization of noise statistics is the main problem.

Also, [66] recently proposed a Anderson Darling version of goodness of fit test for spectrum sensing but do not apply it to non-Gaussian noise models. The problem of reliable detection of gray space transmit opportunities using goodness-of-fit and other non-parametric techniques has been previously studied by the authors of this work [32–34] and by others [31] in the context of the Medium Access layer packet statistics.These works use only a single fixed Goodness-of-Fit test. Our proposed approach is significantly different in two ways, it uses an ensemble of tunable Goodness-of-Fit tests, and it reformulates the problem into a test for uniformity of p-values.

3.2 Inference Problem Formulation

We apply the proposed methods to the following inference problem. Consider the scenario where an unlicensed cognitive radio is trying to detect the presence of a licensed primary user via spectrum sensing. We model the general case where both the primary and secondary users have multiple antennas. Specifically, the MIMO channel is created by M_T transmit antennas and M_R receive antennas. We can express the generalized discrete-time

baseband MIMO channel with fading at a given cognitive radio as

$$\mathbf{y}[n] = \sum_{p=1}^{P} \sum_{l=0}^{L-1} \mathbf{H}_p[n,l]\mathbf{s}_p[n-l] = \mathbf{v}[n], \tag{3.1}$$

where $\mathbf{y}[n]$ is the received signal after sampling, P is the number of primary users transmitting over the sensed channel, the multipath delay in number of symbol intervals is L, $\mathbf{H}_p[n,l] \in \mathcal{C}^{M_T \times M_R}$ is the complex MIMO channel tap matrix. Also $\mathbf{s}_p[n-l] \in \mathcal{C}^{M_T}$ is the signal vector received at the cognitive radio antennas at time n and $\mathbf{v}[n] \in \mathcal{C}^{M_R}$ is the noise vector. For the special case of frequency flat fading with a block transmission of size T symbols per block, the channel taps are time invariant and eq (3.1) simplifies to,

$$\mathbf{Y} = \sqrt{\frac{E_s}{M_T}}\mathbf{HS} + \mathbf{V}. \tag{3.2}$$

Here, $\mathbf{Y} \triangleq [\mathbf{y}[n], n = 1, ..., T]$ is the $M_R \times T$ block of received signal vectors, E_s is the total average energy available at the transmitter over a single symbol period, $\mathbf{H}$ is the MIMO channel matrix. Note that the channel noise $\mathbf{V} \triangleq [\mathbf{v}[n], n = 1, ..., T]$ is allowed to take on arbitrary distributions. Also, the block formulation for the channel model is convenient as the tests that we propose operate on a block by block basis.

The goal of the spectrum sensing problem is to quickly detect if the channel under consideration is vacant and can be used for opportunistic transmission by the secondary user or if it is occupied by the primary user. The problem is structured such that the misclassification of a occupied channel as vacant is heavily penalized. This leads to the following formulation of the hypothesis testing problem.

$$\begin{aligned} &\mathcal{H}_0 : \text{Only background noise present} \\ &\mathcal{H}_1 : \text{Primary user signal + Noise present} \end{aligned} \tag{3.3}$$

3.3 Phi-Divergence based Goodness-of-Fit Tests

3.3.1 Goodness-of-Fit Procedures

A goodness-of-fit test is a procedure for testing how well a certain distribution fits a given observation [41, 64]. To be more specific, consider a continuous random variable $\mathbf{X}$ with distribution $\mathcal{F}(x)$ and let $X_1, X_2, ..., X_n$ be a random sample of independent and identically distributed random variables each following distribution $\mathcal{F}(x)$, with order statistics $X_{(1)} \leq X_{(2)} \leq ... \leq X_{(n)}$. To implement a goodness-of-fit test, we modify eq (3.3) to

$$\begin{aligned} &\mathcal{H}_0 : \mathcal{F}(x) = \mathcal{F}_0(x) \text{ (Null hypothesis)}, \\ &\mathcal{H}_1 : \mathcal{F}(x) \neq \mathcal{F}_0(x) \text{ (Alternative hypothesis)}. \end{aligned} \tag{3.4}$$

Here $\mathcal{F}_0(x)$ is the hypothesized null distribution function to be tested. The alternative hypothesis is transformed into a composite hypothesis that is defined as the complement of the null hypothesis. Although we consider the simple null hypothesis for the most parts, it is straightforward to extend the methods to the case of a composite null hypothesis where $\mathcal{F}_0(x)$ has parameters $\theta_0 \in \Omega_0$ We note here that the goodness-of-fit testing procedure is closely related to the tests for such *universal hypotheses* in information theory. The *Empirical Distribution Function* (edf) of $\mathbf{X}$ is defined as

$$\mathcal{F}_n(x) = \frac{1}{n} \sum_{i=1}^{n} \mathbb{I}(X_i < x), \qquad -\infty < x < \infty \tag{3.5}$$

where $\mathbb{I}(.)$ is the indicator function that evaluates to 1 if the condition in the braces is true, and is 0 otherwise. Also, the probability integral transformation theorem is stated below. The edf as defined in eq (3.5) combined with the probability integral transformation theorem leads directly to a number of powerful goodness-of-fit tests. See [77] for a generalized proof of the theorem.

Theorem 1. *Probability Integral Transformation*

Let a random variable $\mathbf{X}$ *have a distribution* $\mathcal{F}(x)$*. If* $\mathcal{F}$ *is continuous, the random variable*

Z produced by a transformation $Z = \mathcal{F}(X)$ has a uniform probability distribution over the interval $0 \leq z \leq 1$.

3.3.2 Phi-Divergences

In the rest of this chapter we propose a novel use of Phi-Divergences for the purpose of inference between two hypotheses. It has recently been shown that Phi Divergences are the optimal formulations for goodness-of-fit testing [78–81]. Many previous goodness-of-fit tests that have been proposed can be reduced to specialized cases of the phi-divergence statistic. Also, the Phi-Divergences can also be modified to include the standard distributional divergence measures like Kullback-Leibler divergence, Jensen divergence etc. Thus they provide a link between the metrics used for inference in statistical information theory and the non parametric inferential techniques used in goodness of fit based approaches. We will capitalize on these generalizations to allow us to come up with a wide and powerful family of goodness of fit statistics, out of which the best suited test can be chosen, using guidelines that we subsequently provide.

Let $\phi(x)$ be a convex function with domain $x \in [0, \infty)$ and range $\Re \cup \{\infty\}$. Then the supremum and integral versions of the Jager-Wellner Generalized Phi Divergences will be defined as

$$\mathcal{S}_n(\phi) = \sup_x K_\phi\big(\mathcal{F}_n(x), x\big), \tag{3.6}$$

$$\mathcal{T}_n(\phi) = \int_0^1 K_\phi\big(\mathcal{F}_n(x), x\big)\, dx. \tag{3.7}$$

To allow us to draw parallels to various information theoretic divergence measures and statistical goodness-of-fit tests, we will restrict ourselves to the following special class of ϕ-functions using the parameter $s \in \Re$

$$\phi_s(x) = \begin{cases} [1 - x - sx - x^s]/[s(1-s)] & s \neq 0, 1 \\ x(\log x - 1) + 1 & s = 1, \\ \log(1/x) + x - 1 & s = 0. \end{cases} \tag{3.8}$$

Also, with the kernel function used in eq (3.6) defined as in eq (3.9), we get the family of ϕ_s-divergences.

$$K_s(u, v) = v\phi_s(u/v) + (1 - v)\phi_s([1 - u]/[1 - v]) \tag{3.9}$$

After substituting $\phi_s(x)$ as defined in eq (3.8) into eq (3.9) above, we get,

$$K_s(u, v) = \frac{1}{s(1-s)}\left(1 - u^s v^{1-s} - (1-u)^s(1-v)^{1-s}\right). \tag{3.10}$$

Here, ϕ_s is continuous in $s \,\forall\, x \in (0, 1)$ and K_s is continuous in $s \,\forall\, (u, v) \in (0, 1)^2$. For each s, we obtain a unique goodness-of-fit test. It can be shown that a variety of previously proposed powerful goodness-of-fit tests can be obtained as described next.

3.3.3 Relation of Φ-Divergence Statistics to other Goodness-of-Fit Statistics

Φ-Divergence Statistics can be shown to include many other commonly used statistical tests as special cases. We will state a few special cases along with references for a more detailed treatment.

For $s = 2$, the Φ-divergence statistic $S_n(2)$ is proportional to the supremum form of the Anderson-Darling statistic [76].

For $s = 1$, the Φ-divergence statistic $S_n(1)$ reduces to the Berk-Jones statistic and for $s = 0$, it reduces to the reversed Berk-Jones statistic [82–84].

For $s = 1$, the Φ-divergence statistic $T_n(1)$ is the intergral version of the Berk-Jones statistic [85].

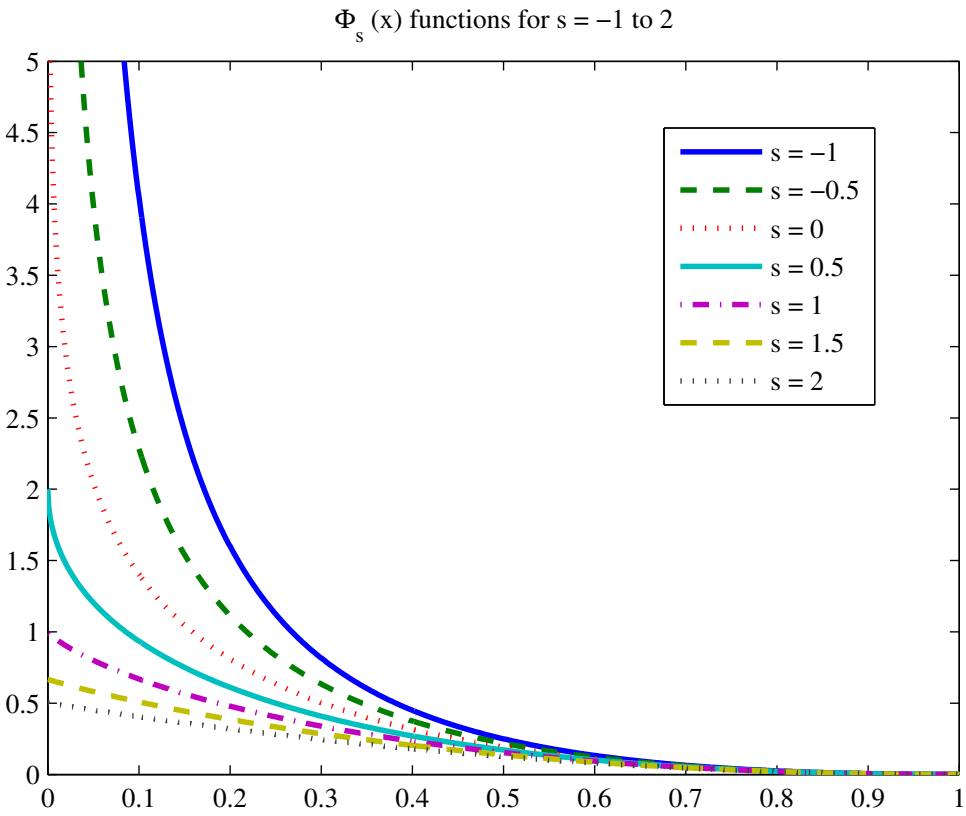

Figure 3.1: Φ function plots

For $s = 2$, the Φ-divergence statistic $S_n(1)$ reduces to the classical Anderson-Darling statistic. The corresponding Φ-divergence kernels are,

$$K_0(u,v) = v\, log\frac{u}{v} + (1-v)\, log\frac{1-u}{1-v}. \tag{3.11}$$

$$K_1(u,v) = u\, log\frac{u}{v} + (1-u)\, log\frac{1-u}{1-v}. \tag{3.12}$$

$$K_2(u,v) = \frac{1}{2}\,\frac{(u-v)^2}{v\,(1-v)}. \tag{3.13}$$

3.4 Phi-Divergence Tests for Spectrum Sensing

3.4.1 Handling Non-Gaussian Noise

Radio Frequency Interference (RFI) is a severe issue in modern spectrum sensing applications. The primary sources of RFI are non-communication sources of radiation such as microwave ovens, other wireless systems which are in close proximity, and the computational platform sources such as clock circuitry, co-located transceivers and power amplifiers which produce phase noise, clock offset noise etc. Ignoring RFI can lead to spurious decisions in favor of the signal being present, due to the impulsive noise. The non-parametric nature of the goodness-of-fit test becomes advantageous when there is such type of added RFI front end noise that is non-Gaussian in nature. The performance of conventional detection techniques degrades severely under such conditions, whereas as we show, the GoF tests are robustly able to handle such noise with minimum effect on performance.

Middleton Class A,B and C noise models are the most widely adopted non-Gaussian noise model and have been proven to model the non-Gaussianity accurately. We follow the bivariate Middleton Class A noise model as proposed in [86–88], which also explicitly accounts for the standard thermal noise through an additive Gaussian component. Narrowband impulsive noise is modeled as a series of independent events that are identically distributed. Also, the in-phase and quadrature components are usually modeled as i.i.d. The cases we will study here are

1. Magnitude based 1-D KS test with Gaussian noise
2. Magnitude based 1-D KS test with Middleton Class-A noise
3. **Φ**-Divergence based test with Gaussian noise for $s \in [-1, 2]$.
4. **Φ**-Divergence based test with Middleton Class-A noise for $s \in (-1, 2)$.

Let us consider the Middleton Class A noise for a 2×2 MIMO setting.The baseband noise at the two antennas is

$$\mathbf{N}_k = \mathbf{n}_{I,k} + j\mathbf{n}_{Q,k} \qquad k = 1, 2 \tag{3.14}$$

For each noise component, the joint spatial correlation between the two antennas is

$$f_{\mathbf{n}}(n_1, n_2) = \frac{e^{-A}}{2\pi|\mathbf{K}_0|^{\frac{1}{2}}} e^{\frac{\mathbf{n}^T\mathbf{K}_0^{-1}n}{2}} + \frac{1 - e^{-A}}{2\pi|\mathbf{K}_1|^{\frac{1}{2}}} e^{\frac{\mathbf{n}^T\mathbf{K}_1^{-1}n}{2}}. \tag{3.15}$$

The in-phase and quadrature noise components at both antennas are assumed to be jointly independent as in eq (3.16). Also, the individual components of the noise observations at the receive antennas are correlated with correlation coefficient κ.

$$f_{\mathbf{N}}(\mathbf{n}_I, \mathbf{n}_Q) = f_{\mathbf{n}_I}(n_{I_1}, n_{I_2}) \times f_{\mathbf{n}_Q}(n_{Q_1}, n_{Q_2}) \tag{3.16}$$

Also for $m = 0, 1$,

$$\mathbf{K}_m = \begin{pmatrix} (\sigma_{m,1})^2 & \kappa\sigma_{m,1}\sigma_{m,2} \\ \kappa\sigma_{m,1}\sigma_{m,2} & (\sigma_{m,2})^2 \end{pmatrix} \tag{3.17}$$

Here, A is the overlap index, defined as the product of the average duration of a standard interfering source emission and the expected number of emission events impinging on the receiver per second. Γ_1, Γ_2 denote the proportion of the Gaussian to the non Gaussian noise intensity per antenna and $(\sigma_{m,i})^2 = \frac{\frac{m}{A} + \Gamma_i}{1 + \Gamma_i}$. Usually, $A \in [10^{-2}, 1]$ and $\Gamma_1, \Gamma_2 \in [10^{-6}, 1]$.

3.5 Robust Fusion of Goodness of Fit Tests

Phi-divergences provide a powerful array of tests parameterized through s. As these are universal hypothesis tests, their behavior is controlled only in one direction, i.e testing for $\mathcal{H}_0$. The behavior of the test in rejecting $\mathcal{H}_0$ when $\mathcal{H}_1$ holds, i.e in the alternative hypothesis regime, is called the power of the test procedure (P_D). The power changes depending on the type of distribution we are testing for. As a result, there is no 'uniformly

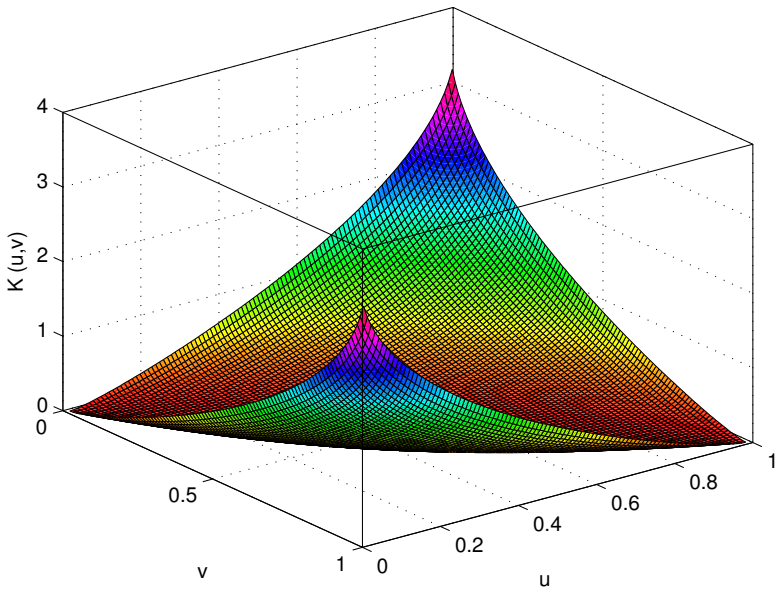

Figure 3.2: K(u,v) with s= 1/2

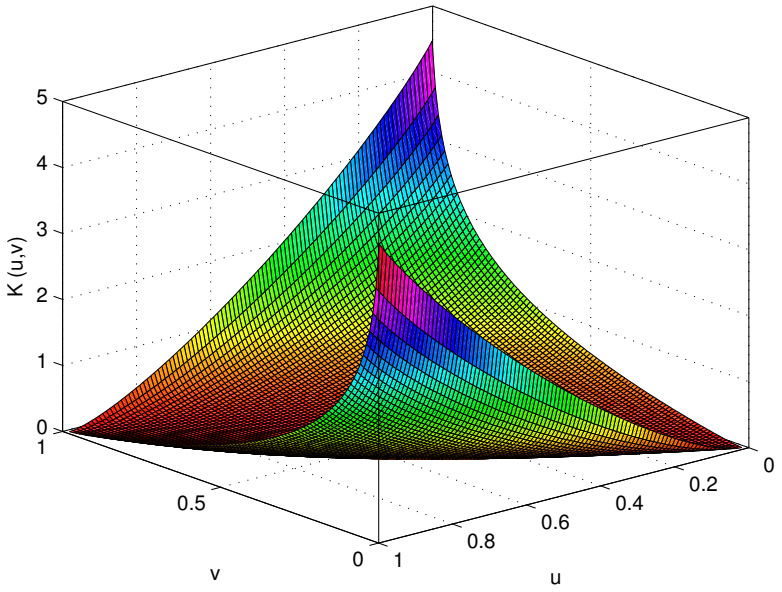

Figure 3.3: K(u,v) with s=1

most powerful' test from such a non-parametric setting, and different tests will be locally the most powerful, for a given set of alternate distributions. Depending on the structure of the distribution under the alternate hypothesis, the different goodness-of-fit tests vary

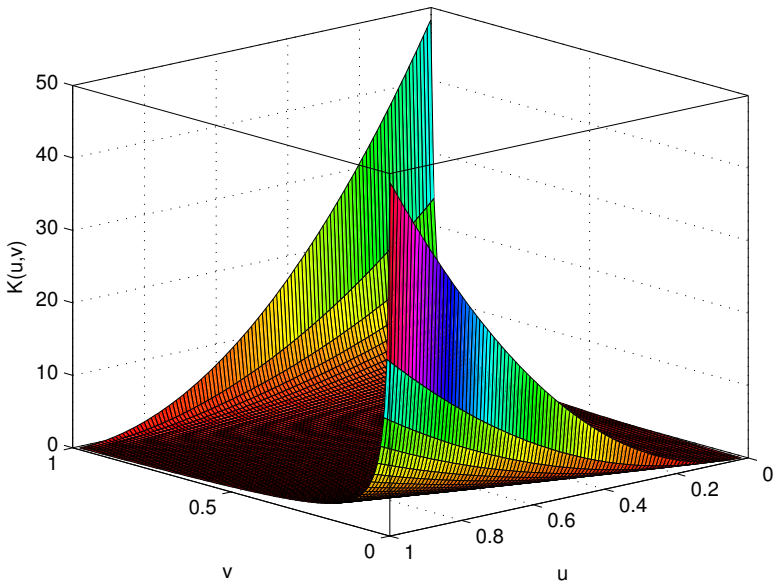

Figure 3.4: K(u,v) with s=2

greatly in power. Thus it is not possible to recommend a single test as an omnibus test over a range of SNRs as its performance may be surpassed by another test under different operating conditions.In cognizance of this fact, we propose to apply a battery of tests with uniformly spaced s using a novel Thresholded Extreme Value test. In this section, we will develop methodologies for the proper combination of such tests. Our results show that the combined test consistently outperforms individual tests, including the Kolmogorov Smirnov test. Our proposed Thresholded Extreme Value test is based on the following properties of the p-value.

3.5.1 p-value

In statistics, the p-value of a test is defined as the tail integral of the density of the test statistic. Consider a goodness-of-fit test with a test statistic $T(\mathbf{X})$. Let $Z_T(t)$ and $W_T(t)$ be the cumulative distributions of T under the null hypothesis ($\mathcal{H}_0$) and alternative hypothesis ($\mathcal{H}_1$) respectively. Then for a given observed test statistic $T(\mathbf{X}) = \tau$, the p-value

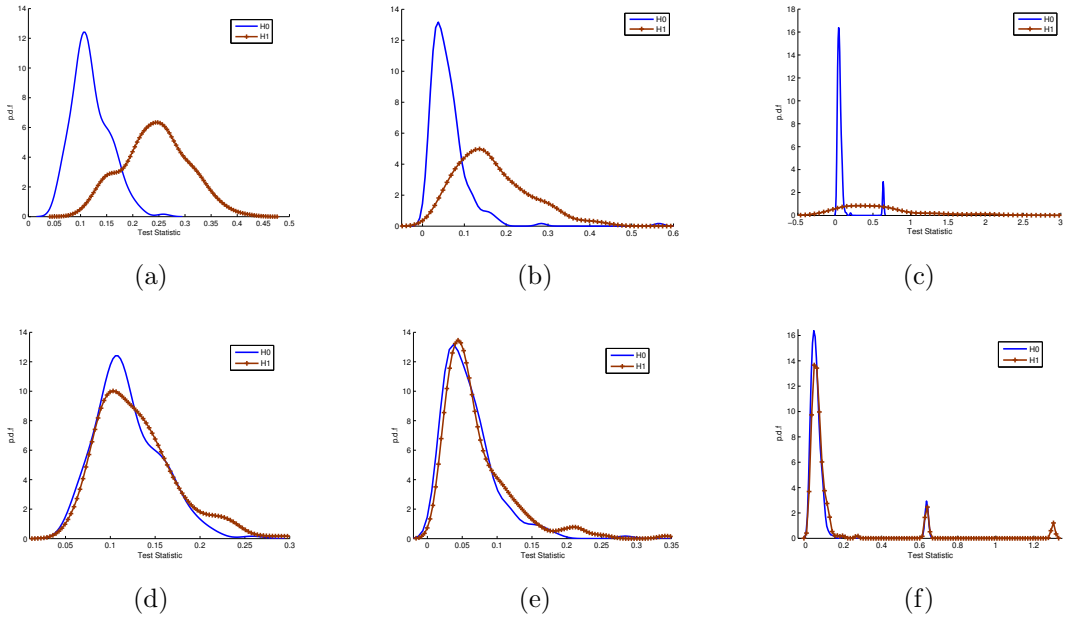

(a) (b) (c)

(d) (e) (f)

Figure 3.5: Distributions of the test statistics for the KL test and Phi-Divergence test

of the test is given as,

$$\rho(\tau) = \sup_{\theta \in \Omega_0} \mathrm{P}(T(\mathbf{X}) \geq \tau) \tag{3.18}$$

For the special case of a simple null hypothesis,

$$\rho(\tau) = \mathrm{P}(T > \tau | \mathcal{H}_0) = 1 - Z_T(\tau) = \int_{\tau}^{+\infty} \mathbf{z}_T(t)\, dt. \tag{3.19}$$

The p-value acts as an indicator of the confidence of the decision reached by the goodness-of-fit test. A low p-value indicates that we are highly unsure about rejecting the null hypothesis while a high p-value indicates that we are highly confident in rejecting the null hypothesis. For our purposes, the principle utility is that the p-value is obtained via an implicit probability integral transformation as we show in the Theorem below. As the p-values are distributed uniformly over $[0, 1]$ under the null hypothesis, we will compare the outputs of different types of goodness-of-fit tests that have mismatched ranges of their test statistics on a standardized $[0, 1]$ interval.

Theorem 2. *p-value distribution property*

The distribution of p-values for the null hypothesis is uniform over [0,1] for any test sample size.

Proof. Using the definition of p-value as in equation (3.19),

$$F_{\varrho}(\rho|H_0) = \mathbf{P}(\varrho \leq \rho) \tag{3.20}$$

$$= \mathbf{P}\Big\{\big(1 - Z_T(\tau)\big) \leq \rho\Big\} \tag{3.21}$$

$$= 1 - Z_T\Big\{Z_T^{-1}(1-\rho)\Big\} \tag{3.22}$$

$$= \rho. \tag{3.23}$$

$$\therefore F_{\varrho}(\rho|H_0) \sim \mathfrak{U}[0,1] \tag{3.24}$$

□

3.5.2 Ensemble of Φ-Divergence Test test

The Kolmogorov Smirnov test, Anderson-Darling test and other standard goodness-of-fit tests are individually sensitive to changes only in certain regions of the distribution and sacrifice high local power in order to attain medium power over the complete support of the cumulative distribution function (c.d.f). In contrast, the **Φ**-Divergence tests have been designed to be selective to changes in *different* regions of the c.d.f, and this selectivity is controlled via the tuning parameter s. Hence, the ensemble demonstrates a rake like property by being highly sensitive to changes over the complete support of the c.d.f. We have seen that the p-value measures the confidence of a given test under a set of specific operating conditions. Our approach is based on the observation in [89] that the distribution of the p-value under *both* hypothesis is essential to formulate a threshold. Out of the ensemble of the goodness-of-fit tests,we accept the decision of the test that has the most extreme p-value, i.e

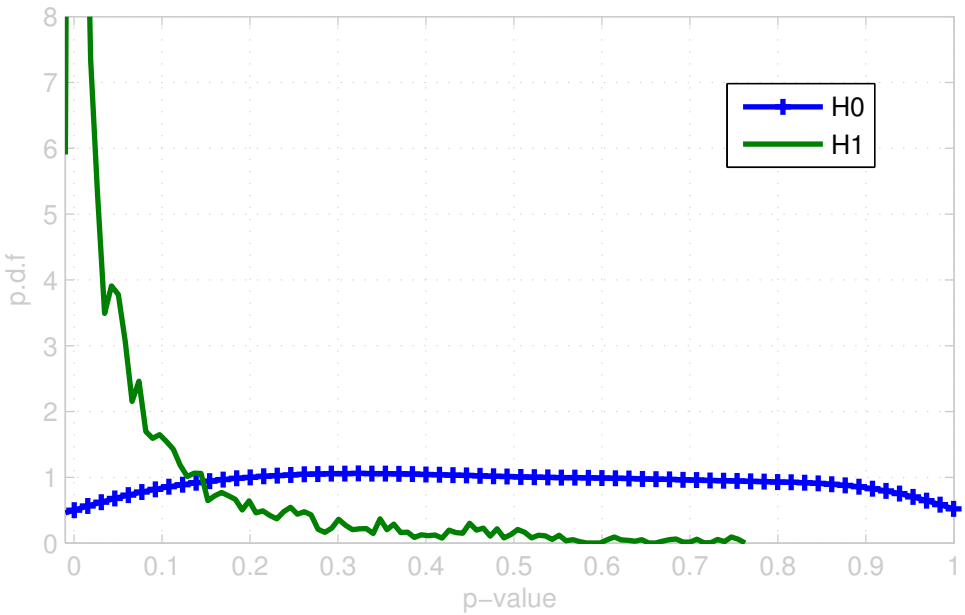

Figure 3.6: Distribution of p-values under H_1 and H_0 for SNR = -2 dB, test size = 50

, it has the highest confidence metric to support the decision. We will illustrate the process using the distribution of the p-values for SNR = 0 case, for the setup described in Results section. The distribution of p-values for the ensemble of tests is plotted in figure 3.6. The uniformity of the p-values under the null hypothesis is clearly seen, also the distribution under the alternative is highly skewed towards 0. The level of significance α to reject the null hypothesis is easily noted to be p-value = α. We will calculate a *second order P-value* defined as the upper tail integral of the alternate p-value distribution and threshold it a level β. Note that this differs from conventional p-value use in that the threshold depends via β on the distribution under the alternate hypothesis. After these rejection regions have been defined, the remaining area is subject to a *randomized test* (see Chp.3 , Lehmann [90] for a review of the randomized test concept). The randomized test randomly decides the outcome after normalizing with a predetermined prior distribution of the two hypothesis in the randomization region. Thus, the Ensemble Goodness-of Fit (EG) test based on **Φ**-Divergences is implemented as follows

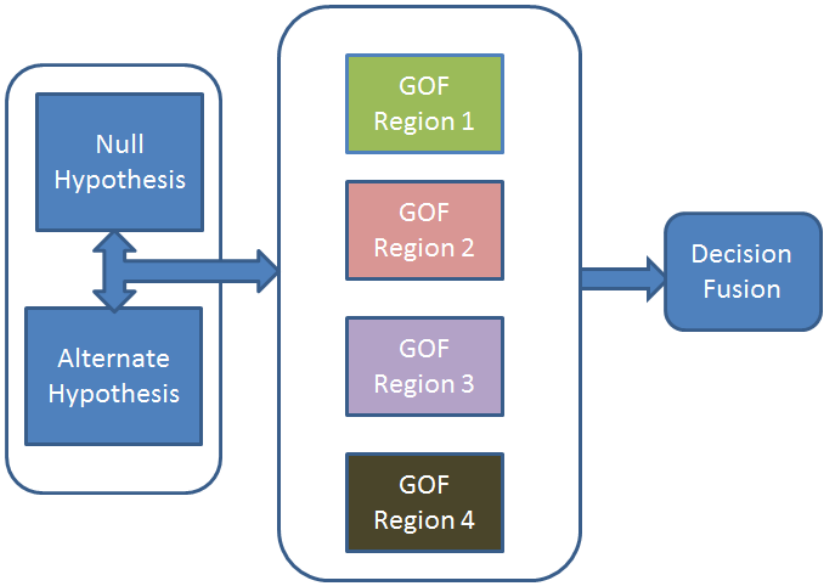

Figure 3.7: Block Diagram of Ensemble Goodness-of-Fit tests using tunable Phi-divergence statistics

1. Training phase: Calculate the distribution of p-values of all the test statistics under Null and Alternate hypotheses. Calculate the rejection region and the randomization region.

2. Test Phase: For the test sample, obtain test statistics for each test in the ensemble, and the corresponding p-values.

3. If the test p-value falls within a rejection region, pick the corresponding hypothesis.

4. Otherwise, randomly pick the hypothesis using the prior distribution and the magnitude of p-value.

5. If *any* test rejects the null hypothesis, then the EG test decides in favor of $\mathcal{H}_1$.

The consistently superior performance of this test is shown via experimental simulations in section 3.7. Here, we describe the rationale behind this particular approach.

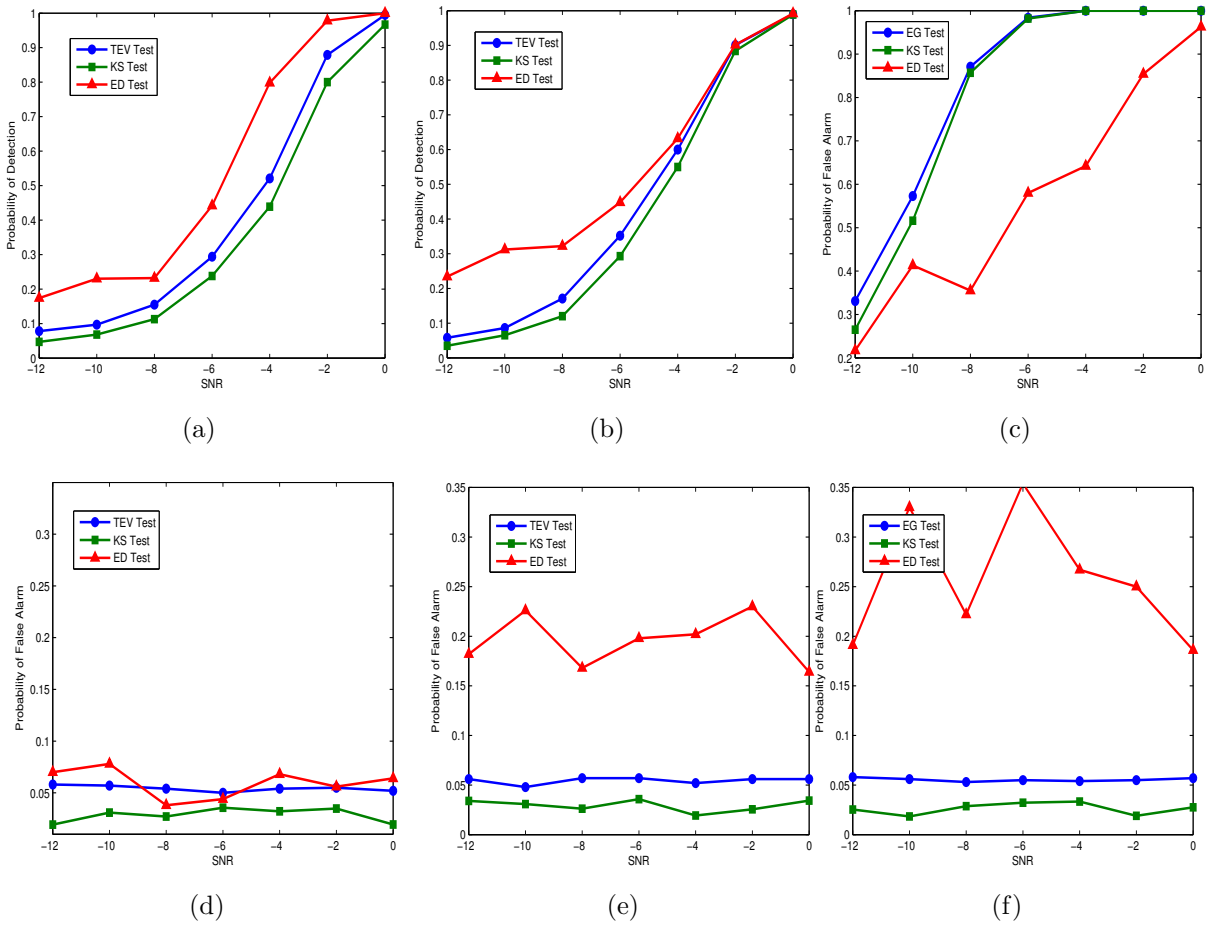

Figure 3.8: Performance of the various tests for test size = 50. Fig 3.8a : P_D for Gaussian noise, Fig 3.8b : P_D for Non-Gaussian noise with $\Gamma = 0.5$, Fig 3.8d : P_{FA} for Gaussian noise, Fig 3.8e : P_{FA} for non-Gaussian noise, Fig 3.8f : P_{FA} for Non-Gaussian noise with $\Gamma = 0.1$

Definition 1. *Consider random variables X and Y with cumulative distribution functions F_X and F_Y. Then, F_X will be said to* stochastically dominate *F_Y at the first order ($F_Y(y) \succ_1 F_X(y)$) if and only if $F_Y(y) \geq F_X(y)\ \forall y$. F_X strictly dominates F_Y with the first order if and only if $F_Y(y) \geq F_X(y)\ \forall\, y$ and $\exists y$ s.t $F_Y(y) > F_X(y)$*

Similarly, higher orders of stochastic dominance are defined on repeated integrals of the cumulative distribution as shown below. Using the definition of stochastic dominance and of rejection region, we can prove the following theorem.

Definition 2. *F_X will be said to stochastically dominate F_Y at the second order ($F_Y(y) \succ_2 F_X(y)$) if and only if*

$$\int_0^t F_Y(x)\,dx \geq \int_0^t F_X(x)\,dx \qquad \forall t \tag{3.25}$$

Lemma 1. *First order stochastic dominance implies second order stochastic dominance.*

Proof. Rearrange equation(3.25) as

$$\int_{-\infty}^t (F_Y(x) - F_X(x))\,dx \geq 0 \qquad \forall t. \tag{3.26}$$

. This is obviously true as first order dominance implies

$$F_Y(x) \geq F_X(x) \qquad \forall x \tag{3.27}$$

□

Now consider the ensemble goodness-of-fit test of size G, where the class of alternate hypothesis is right-tailed such that the expectation of the test statistic is larger under the alternate hypothesis than under the null hypothesis. Thus,

$$F_{1,i} \preceq_1 F_{0,i} \qquad i = 1, ..., G. \tag{3.28}$$

By Lemma 1 F_0 also dominates F_1 at the second order, i.e, $F_1 \preceq_2 F_0$. Also, by Theorem 2, $F_{0,i} \sim \mathfrak{U}(0,1) \forall i \in 1, ..., G$. Thus,

$$F_{1,i} \preceq_1 U \qquad i = 1, ..., G. \tag{3.29}$$

where, $U \sim \mathfrak{U}(0,1)$.

Thus for an ensemble of tests, we will define a piecewise alternate distribution using the method as shown below.

$$F_{1,alt}(y) = \max_{i=1,..,G} F_{1,i}(y) \, \forall y \in [0,1]. \tag{3.30}$$

This can be seen to be the convex hull of the individual p-value distributions under the alternate hypothesis. Doing so does not affect the behavior of the test under the null hypothesis, as the c.d.f is a uniform distribution as per Theorem above. Thus, by construction, this effective alternate distribution is stochastically dominant over all individual alternate distributions of the p-values in the ensemble. Hence, the performance of the ensemble goodness-of-fit test is superior to all its constituent tests.

Lemma 2. *The expectation of the p-value of the test under the alternative hypothesis is smaller than the expectation of the p-value of the test under the null hypothesis.*

Theorem 3. *If the test is unbiased, the c.d.f of the test statistic under the null hypothesis is always stochastically dominant over the c.d.f of the test statistic under the alternate hypothesis.*

3.5.3 Choice of Ensemble GoF test parameters

We will now give guidelines to design the ensemble Goodness-of-Fit test for a specific situation. The baseline test is the Kolmogorov-Smirnov test which is moderately sensitive to changes over the complete support for the density functions. If we known the exact

parametric form of the densities under the null and alternate hypotheses, then we can design a test that is tuned to the region of maximum change. In the absence of this knowledge, which is the situation studied here, the following guidelines allow us to design an ensemble Goodness-of-Fit test that delivers a good performance. The aim is to have the minimum number of tests in the ensemble to manage the implementation complexity.

1. Start with 3 tests for $s = -1, 0, 1$ that are sensitive to a change in left and right tails as well as the median of the density. This simple ensemble is sufficient for symmetric and relatively smooth densities.

2. Check if the performance of the ensemble is consistently improved over that of the baseline Kolmogorov-Smirnov test alone.

3. Gradually keep adding more tests to the ensemble to cover more and more regions of the densities till required performance is achieved. Note that we restrict the searchspace to values of $s = 0.5n$ where $n = -2...4$ which have been implemented in the R statistical software.

Summarizing the properties of the Ensemble Goodness-of-Fit test, we note that it first implements a parallelized ensemble of basic goodness-of-fit test, and then it reformulates this ensemble into a collection of p-values of the constituent tests. This reformulation allows us to test the goodness-of-fit for the uniformity of p-values. Thus we have decoupled the proposed ensemble test design and the design of the constituent goodness-of-fit test. Also, the theorem above shows the divergent behavior of the p-value distribution under the null and alternate hypotheses and this implies that the test will always function correctly. The exact performance gains delivered by the proposed test is shown in the Results section

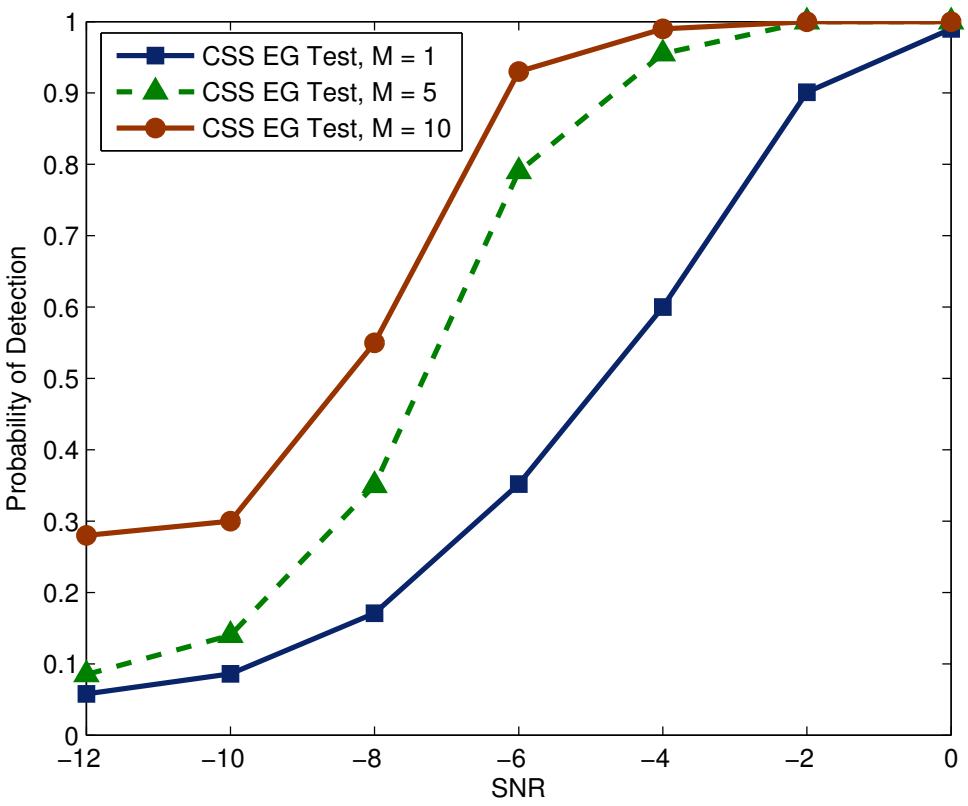

Figure 3.9: Probability of Detection for the CSS-EG test for N = 50

3.6 Collaborative Spatially separated Ensemble Goodness-of-Fit Tests

In this section consider a situation where the individual nonparametric tests are run at spatially separate locations. Such testing situations arise in the context of distributed spectrum sensing. While the EG test as proposed in the previous section works very well in comparison to the energy detector and the Kolmogorov Smirnov based test, those tests operate on the same data samples, i.e., they operate on completely dependent data, and it is not straightforward to extend them to the case of independent data. We propose a decision fusion based on the exchange of summary p-value statistic where each test operates with knowledge of only the local p-value statistics.

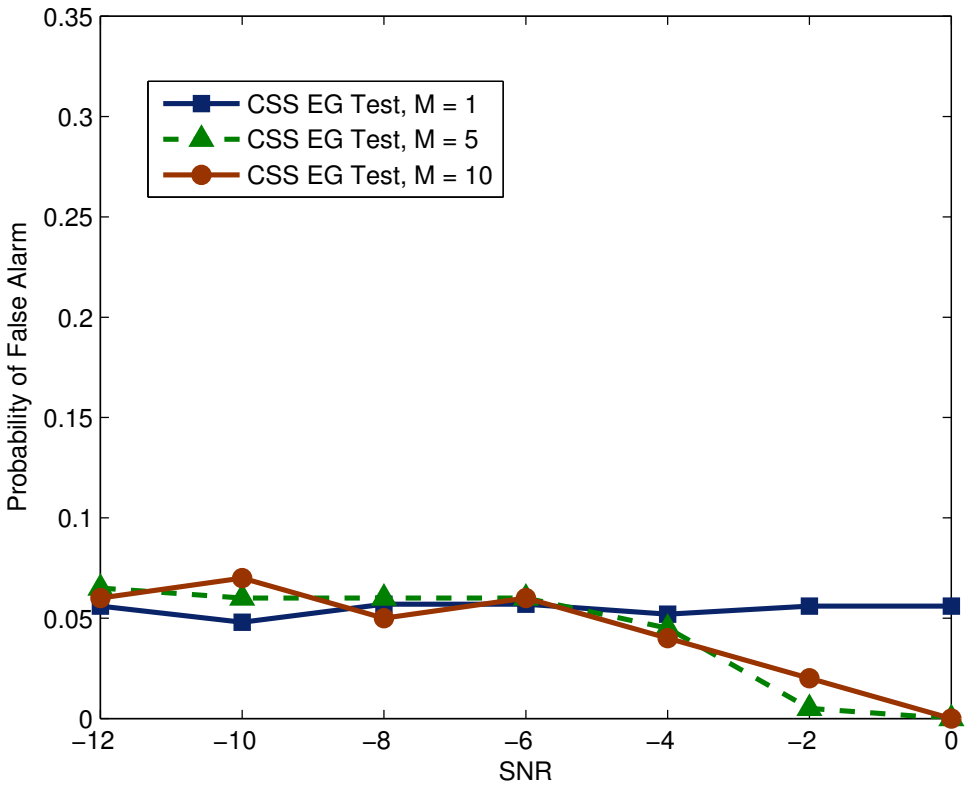

Figure 3.10: Probability of False Alarm for the CSS-EG test for N = 50

Let there be M locations in the network at each of which a subset of the G ensemble goodness-of-fit tests are performed with a test size N samples. If each sensing node has N_R receive antennas, then the test duration is N/N_R sampling instances. After each set of test samples is collected, the ensemble of goodness-of-fit tests are individually evaluated for their p-values. Let $\Theta_{0,k}(x)$ and $\Theta_{1,k}(x)$ be the empirical distributions of the p-values of the k^{th} test in the ensemble under the null and alternate hypothesis respectively. For each test, the CSS-EG test calculates the likelihood ratio of the evaluated p-value ρ_k as shown,

$$\lambda_{m,k}(\rho_{m,k}) = \frac{\Theta_{1,m,k}(\rho_{m,k})}{\Theta_{0,m,k}(\rho_{m,k})} \qquad k = 1, ..., G \; m = 1, ..., M. \tag{3.31}$$

The set of likelihood ratios are transmitted to a node designated as the fusion center. The set of likelihood ratios is two regions separated by the threshold ξ, which is chosen

using the Neyman-Pearson criterion for a fixed area under the set of combined hypothesis $\Theta_{0,k}(x)$ for $k = 1, ..., G$. Note the important fact that through the use of Theorem 2, the p-value distribution under the null hypothesis is known regardless of the size of the individual EG tests and the distribution of the p-values under the alternate distribution. Thus, the threshold can be set at the fusion center without the transfer of any side information from the individual nodes. Consequently, the Collaborative Spatially separated Ensemble Goodness-of-Fit Tests (CSS-EG) test operates with a high degree of flexibility in choosing the most powerful test for a given set of test samples, and fully leverages the non-parametric nature of goodness-of-fit procedures.

This test works extremely well in the situation where the sample size per test is very small but the number of locations where such tests that are conducted is reasonably large. The p-values under any test follow a fixed distribution under the two hypotheses. As effective small sample testing for uniformity is possible, it is possible to use such a test to robustly reach a decision. As we will show, the CSS-EG test works so well that it is to be preferred unless its implementation is unfeasible. The downsides to using this test are 1) the computational burden is higher, 2) the tuning of the test sample size and the threshold settings is not obvious, although we provide sufficient guidelines.

3.7 Results

In this section, we present the improvement in the performance of the **Φ**-Divergence based EG tests over the Kolmogorov-Smirnov test and the energy detector through simulation results under diverse settings.

3.7.1 Simulation Scenario

We consider a setup that consists of a single primary user in a frequency flat fading environment with a block transmission/reception of size T symbols per block. The primary transmitter and the secondary receiver have 2 antennas each, i.e, $N_T, N_R = 2$. Thus the test size is $N = N_R \times T$ complex samples. Quadrature Phase Shift Keying modulation is employed and the noise is circularly complex Gaussian with a spatial correlation coefficient of 0.2 between the two antennas. At the initiation of the testing period in the absence of the primary signal, a sequence of training samples is obtained with a duration of $N = 100$ complex samples. These training samples are used to estimate the distribution of the test samples under the null hypothesis. This density estimation step is performed using a Gaussian kernel as shown below. The bandwidth of the kernel is set to be 0.1 times the bandwidth provided by the Sheather-Jones bandwidth estimation procedure. Such a setting provides the correct smoothing of the density. In the case of the energy detector test, the training samples are necessary to estimate the variance of the noise distribution.

3.7.1.1 Handling Complex Data

The goodness-of-fit tests have been defined over the support of real numbers $\mathfrak{R}$ whereas the baseband I-Q test samples are complex numbers $\mathfrak{C}$. One approach to apply the goodness-of-fit tests to complex data is via the use of two dimensional KS tests [91–93]. But, such tests impose a significant overhead in terms of the computational complexity which is $O(n^3)$, or under simplifying assumptions, it reduces to $O(n^2)$. Also, the theory of two dimensional tests has not yet been extended to GoF tests other than the Kolmogorov Smirnov test. It has previously been proposed that amongst all the variants of the Kolmogorov Smirnov test, the 1-dimensional test that considers the magnitude of the received samples provides the best performance [65]. Our simulations provided similar results for the $\mathbf{\Phi}$-Divergence based goodness-of-fit tests for $s \in (-1, 2)$, and we will only focus on the

relative performance of the tests that operate on the magnitudes of the received complex samples.

After the training phase, each goodness-of-fit test statistic is evaluated using equation (3.10). Also, the corresponding p-value is calculated using the distribution of the test statistic that is approximated with high accuracy using the Noe recursion relations [78, 94]. Note that the p-values can be pre-calculated and stored in look-up tables. Only the p-values are used in later processing and act as the summary statistic. For individual goodness-of-fit tests, the level of significance α for the test is decided *a priori*, that corresponds to the probability of falsely rejecting the null hypothesis (P_{FA}). If the p-value is less than α, the null hypothesis is rejected. The energy detector test calculates the energy of the received samples as $\mathbf{YY^H}$ and compares it to a threshold given by

3.7.1.2 Test Power for individual Goodness-of-Fit test

The power of a statistical test is the measure of its discriminatory power under an alternative hypothesis. We compare the powers of the Φ-Divergence based goodness of fit test against the Kolmogorov Smirnov test using Monte Carlo methods. The figure shows the distribution of the test statistics for 3 representative tests in the ensemble over 10^6 trials for each hypothesis. The null hypothesis is, without loss of generalization, assumed to be an uniform distribution. The alternate hypothesis is a chi-squared distribution followed by the received statistic. These distributions are converted into the equivalent p-value distributions using Theorem 1.

3.7.2 Ensemble Goodness-of Fit (EG) test based on Φ-Divergences

The EG test thresholds are implemented as per the algorithm described in Section 3.5.2 for the following specifications. The ensemble consists of 7 **Φ**-divergence tests in addi-

tion to the Kolmogorov-Smirnov test for values of s $= -1, -0.5, 0, 0.5, 1, 1.5, 2$. This ensemble is found to comprehensively improve on the performance of each individual test, including the Kolmogorov-Smirnov test, but is not the only possible configuration. Any number of tests can be chosen to form the ensemble. The value of $s = 0$ gives maximum weight to changes in central portion of the density function. And changing the value of s away from 0 gives increasing weight to changes in the tail areas of the density function. Also, the behavior of the phi-divergence is well characterized for any choice of s in the range $[-1, 2]$ and there is support for implementing this in the R statistical software package. While, we have chosen s with a spacing of 0.5, a finer spacing will give better performance but also increase the computational load. The performance of the Ensemble Goodness-of-Fit test is shown in figure 3.8 for a test sample size of $N = 50$, i.e, the received block size $T = 25$. The level of significance for Probability of False Alarm is set as $\alpha = 0.05$ and the second order threshold for Probability of Missed Detection is set to be $\beta = 0.1$ using the method described in Section 3.5.2. The p-value corresponding to β is calculated empirically for each SNR level and noise distribution. The interim region is setup as the randomized testing region. Figure (3.8a) and figure (3.8d) plot the P_D and P_{FA} performance in presence of Gaussian noise. The Signal-to-Noise Ratio is varied from -12 dB to 0 dB. As the noise realization for the energy detector follows the model exactly, its performance is better than that of the goodness-of-fit tests. Also, the Ensemble Goodness-of-Fit test uniformly outperforms the Kolmogorov-Smirnov test alone. This behavior is expected because of the rake like selectivity property of the test mentioned in Section 3.5.2, and can be seen through all operating conditions. Thus, the EG test is a consistent upper bound to the Kolmogorov-Smirnov test. Figure (3.8b) and figure (3.8e) plot the P_D and P_{FA} performance in presence of Middleton Class A noise mixture distribution. The Middleton noise has a $\Gamma = 0.5$ at both antennas and $A = 0.2$. Γ controls the ratio of the Gaussian noise component to the Non-Gaussian noise component in the mixture distribution. For such a mixture with a dominant Gaussian noise, the power of

the goodness-of-fit tests as measured by the P_D is now better than that for Gaussian noise alone, and matches that of the Energy detector at SNR > -4 dB. But, the critical point to note here is that false alarm events, given by P_{FA}, are significantly higher for the energy detector. Thus the design parameters are violated for the ED test while the EG test and the KS test still satisfy the P_{FA} design constraints.

3.8 Conclusion

We have shown that nonparametric goodness-of-fit tests provide a robust solution to the problem of severe degradation of the performance of parametric tests like the energy detector. A systematic approach to design a nonparametric test suited to the particular set of alternative hypothesis is proposed via using the Φ-divergence based goodness-of-fit tests. These are are parameterized through s, and for all values of s, accurate procedures to calculate the test tables exist. Also, the Ensemble Goodness-of-Fit test that comprises of these Φ-divergence tests is shown through extensive simulations to consistently outperform the individual goodness-of-fit tests, including the Kolmogorov-Smirnov test. We have also derived the Collaborative Spatially Separated EG method that leverages the unique properties of the p-value summary metric to perform rapid distributed decision fusion.

Chapter 4

Sequential Approaches to Spectrum Sensing

4.1 Introduction

We have seen how Cognitive Radio (CR) provides an effective framework for opportunistic and efficient reuse of the scarce spectrum resources, e.g, [9], [13]. The process of detection of spectral holes is the key enabler of Dynamic Spectrum Access (DSA) in cognitive radio networks. A variety of methods for DSA have been proposed in the literature such as energy detection, cyclostationarity based detection, eigenvalue based detection and wide band spectrum sensing, see for example [95], [96]. These spectrum sensing methods are classified into two categories: blind methods which work irrespective of the nature and type of PU transmission and non-blind methods which exploit knowledge of the nature of PU transmission. The energy detector is a blind method. It makes a decision based on the estimate of the energy in the received signal. In contrast, non-blind techniques are based on feature detection. Except for energy detection, these methods aim to deliver performance improvement at the expense of significantly larger sensing times. We will focus on efficient implementations of the Energy Detector (ED).

4.1.1 Related Work

The ED was recently popularized in the context of IEEE 802.22 Cognitive Radio Networks [97]. These networks are required to detect the primary user at extremely low Signal to Noise Ratios (SNRs) of upto -25db. Another constraint is the small upper limit

(on the order of milliseconds) on the sensing window. There exists a large body of work which investigates the performance of the energy detector, e.g, [13], [98], [99] etc. As the structure of the signal being detected is not known, matched filters cannot be implemented and energy detectors are commonly used [100]. But, it has been shown that energy detector performance degrades under lognormal shadowing [101, 102] though collaborative detection methods have been proposed to improve the robustness of spectrum sensing to shadowing [103]. In this chapter we investigate the behavior of spectrum sensing under sequential detection schemes. A variety of distributed sequential detection methods based on information transfer between the nodes, or between the node and a fusion center at each time step of the sequential detection have been proposed for sensor networks [104]. For cognitive radios, extremely reliable and fast detection of the primary user is critical which makes transfer of information between the secondary users and the central node at each time step as assumed in these works inviable. In contrast our approach proposes a hierarchical sequential detection scheme wherein sequential detection of the classical kind is carried on at the level of secondary users followed by a second level of sequential detection at the central node. The authors of this work were amongst the first to implement a sequential approach to energy detection for spectrum sensing [105], [106]. Other sequential based approaches have since been proposed all of which have the goal of reducing the sensing time [107], [108], [109] but none of them address the significant overhead reduction and performance gains achieved by hierarchical tests that we study here.

4.1.2 Our Contributions

In this chapter we formulate a novel Sequential Energy Detector, characterize its performance gains and demonstrate a throughput increase of 2 to 6 times over the Fixed Size ED test as measured using the Relative Efficiency of the test. Also the issue of sensitivity of the Sequential Test to primary signal variance estimation is addressed at length. Specif-

ically, we develop an Iterative Hybrid Bayesian method to robustly estimate the primary signal variance.The rest of this chapter is organized as follows. In Section 4.2 we introduce the assumptions. We review the conventional Fixed Sample Size (FSS) ED and the basic Sequential Test in Section 4.3. The novel SEquential Energy Detection (SEED) test is introduced in Section 4.4 & the Iterative Hybrid Bayesian Update method in Section 4.5.

4.2 Notation and Assumptions

In this section we formulate the sequential detection problem. The channel is modeled as per eqn. (4.1) for $n = 1, \ldots$.

$$x(n) = hs(n) + v(n) \ : H1 \quad \& \quad x(n) = v(n) \ : H0 \tag{4.1}$$

Here, $s(n)$ is the Primary User (PU) signal, $v(n)$ is the Additive White Gaussian Noise (A.W.G.N), $x(n)$ is the signal received at the CR and h is the instantaneous channel gain. Also, $\bar{x} = [x(1)x(2)...x(n)]$. We make the following assumptions:

A.1 s(n) is independent identically distributed (i.i.d) zero mean circularly complex Gaussian with variance σ_s^2. $s(n) \sim N(0, \sigma_s^2)$.

A.2 v(n) is i.i.d zero mean circularly complex Gaussian with variance σ_v^2 distributed as $\sim N(0, \sigma_v^2)$.

A.3 h is constant and normalized to unity throughout the test duration.

A.4 s(n) and v(n) are mutually independent.

A.5 Perfect knowledge of the noise variance σ_v^2 at the CR end.

4.3 Review of ED and Sequential Detector

The sequential test is most naturally introduced as an extension of the FSS energy detector. Here we will summarize the structure of the conventional ED as described in [110]. For the problem setting described above of an non deterministic signal in white Gaussian noise, it is known that the energy detector is the optimal test [110]. The test is given as,

$$\text{Decide } H0 \text{ or } H1 \text{ as} \quad \lambda(\bar{x}) = \frac{f(\bar{x}|H1)}{f(\bar{x}|H0)} \lessgtr \gamma. \tag{4.2}$$

$$\lambda(\bar{x}) = \frac{\frac{1}{(2\pi(\sigma_s^2+\sigma_v^2))^{N/2}} \exp\left(-\frac{1}{2(\sigma_s^2+\sigma_v^2)}\right) \sum_{n=1}^{N} |x(n)|^2\Big)}{\frac{1}{(2\pi(\sigma_v^2))^{N/2}} \exp\left(-\frac{1}{2\sigma_v^2} \sum_{n=1}^{N} |x(n)|^2\right)}. \tag{4.3}$$

$$\lambda_L(\bar{x}) = \frac{N}{2} \ln\left(\frac{\sigma_s^2}{\sigma_s^2+\sigma_v^2}\right) + \frac{1}{2}\frac{\sigma_s^2}{(\sigma_s^2+\sigma_v^2)} \sum_{n=1}^{N} |x(n)|^2. \tag{4.4}$$

As the functional λ is monotonic, the log likelihood ratio is expressed as shown above. The FSS ED takes the form as shown in eqn. (4.5). $T(\bar{x})$ is the sum of Gaussian random variables and obeys a χ^2 distribution as in eqn. (4.6).

$$T(\bar{x}) = \sum_{n=1}^{N} |x(n)|^2 \lessgtr \gamma. \tag{4.5}$$

$$\frac{T(\bar{x})}{\sigma_s^2+\sigma_v^2} \sim \chi^2_{2N} \ : H1 \quad \& \quad \frac{T(\bar{x})}{\sigma_v^2} \sim \chi^2_{2N} \ : H0 \tag{4.6}$$

It has been shown that the number of samples (N) required for a given P_D and P_{FA} is $\propto SNR^{-2}$. Thus, the energy detector has the drawback that at SNRs $\ll 1$, it requires a large number of samples. We will show later that sequential tests reduce the expected number of samples required to maintain the same P_D and P_{FA} as the ED by more than 50%.

4.3.1 Threshold Calculation

Let $Q_{\chi^2_{2N}}$ be the tail integral of the χ^2_{2N} distribution. Then, we can express eqn. (4.6) as

$$P_{FA} = Q_{\chi^2_{2N}}(\frac{\gamma'}{\sigma_v^2}) \quad \& \quad P_D = Q_{\chi^2_{2N}}(\frac{\gamma'}{\sigma_s^2 + \sigma_v^2}). \tag{4.7}$$

Let $\gamma"_1 = \frac{\gamma'}{\sigma_v^2}$ and $\gamma"_2 = \frac{\gamma'}{\sigma_s^2+\sigma_v^2}$. Fixed Point Iteration is used to solve for the threshold for given a value of P_D as in eqn. (4.8) and similarly for P_{FA}.

$$\gamma"_{j+1} = -\ln P_D + \ln\left[1 + \sum_{i=1}^{N-1} \frac{(\gamma"_j)^i}{i}\right]. \tag{4.8}$$

4.3.2 Sequential Probability Ratio Test

We introduced a Sequential Probability Ratio Test (SPRT) formulation of the energy detector in [105], [106]. This sequential approach was refined and extended by [108], [111], [109] etc. In this section we will review the SPRT test. An actual observed sample run of the SPRT scheme is shown in Fig. 4.1. Unlike the energy detector which always waits for a predecided number of samples to be received before calculating the test statistic, here the samples are accepted sequentially and at each time step i, the likelihood ratio λ_i is calculated. This likelihood ratio is compared with two thresholds, lower threshold A and upper threshold B, as in eqn. (4.9).

$$\text{If} \quad \lambda_i \leq A \quad \text{Decide H0} \tag{4.9}$$

$$\text{If} \quad \lambda_i \geq B \quad \text{Decide H1} \tag{4.10}$$

$$\text{Else accept next sample.} \tag{4.11}$$

These thresholds are computed using the Wald approximations in eqn. (4.12) based on the Wald-Wolfowitz theorem, which is a fundamental result in the theory of sequential

detection and states that the SPRT has the minimum expected sample size amongst all other likelihood ratio tests for a given fixed P_D and P_{FA} [112].

$$A = \frac{1 - P_D}{1 - P_{FA}} \quad \& \quad B = \frac{P_D}{P_{FA}}. \tag{4.12}$$

4.4 SEquential Energy Detector: SEED

The SPRT test has the flaws of high complexity, large variability and sensitivity to inaccurate signal power estimates. To deal with these issues, we shall now develop the novel low complexity SEED test and formulate the Min-M SEED test. The likelihood ratio λ_i is a ratio of two central χ^2_{2i} random variables with $2i$ degrees of freedom since the $x(n)$ are complex variables. The probability distribution of $y_i = T_i(\bar{x}) = \sum_{n=1}^{i} x(n)x^*(n)$ as in eqn. (4.5) with each $x \sim N(0, \sigma^2)$ and $y_i > 0$ is given by [113] as,

$$f_Y(y_i) = \frac{1}{2\sigma^2\Gamma(i)} \left(\frac{y_i}{2\sigma^2}\right)^{i-1} \exp\left(-\frac{y_i}{2\sigma^2}\right). \tag{4.13}$$

$\Gamma(i)$ is the gamma function. Using eqn. (4.13) we express λ_i as,

$$\begin{aligned}
\lambda_i &= \frac{\frac{1}{2(\sigma_s^2+\sigma_v^2)\Gamma(i)} \left(\frac{y_i}{2(\sigma_s^2+\sigma_v^2)}\right)^{i-1} \exp\left(-\frac{y_i}{2(\sigma_s^2+\sigma_v^2)}\right)}{\frac{1}{2\sigma_v^2\Gamma(i)} \left(\frac{y_i}{2\sigma_v^2}\right)^{i-1} \exp\left(-\frac{y_i}{2\sigma_v^2}\right)} \\
&= \left(\frac{\sigma_v^2}{(\sigma_s^2 + \sigma_v^2)}\right)^{i} \exp\left(-\frac{y_i}{2}\left[\frac{1}{\sigma_s^2 + \sigma_v^2} - \frac{1}{\sigma_v^2}\right]\right) \\
&= \zeta^i \exp(y_i\beta).
\end{aligned} \tag{4.14}$$

$$\text{where} \quad \zeta = \frac{\sigma_v^2}{(\sigma_s^2 + \sigma_v^2)} \quad \& \quad \beta = -\frac{\sigma_s^2}{2\sigma_v^2(\sigma_s^2 + \sigma_v^2)}. \tag{4.15}$$

Thus, we can iteratively update the λ_i as

$$\begin{aligned}
\ln \lambda_{i+1} &= (i+1)\ln\zeta + y_{i+1}\beta \\
&= i\ln\zeta + \ln\zeta + \beta(y_i + x(i+1)x^*(i+1)) \\
&= \ln\lambda_i + \ln\zeta + \beta x(i+1)x^*(i+1).
\end{aligned} \tag{4.16}$$

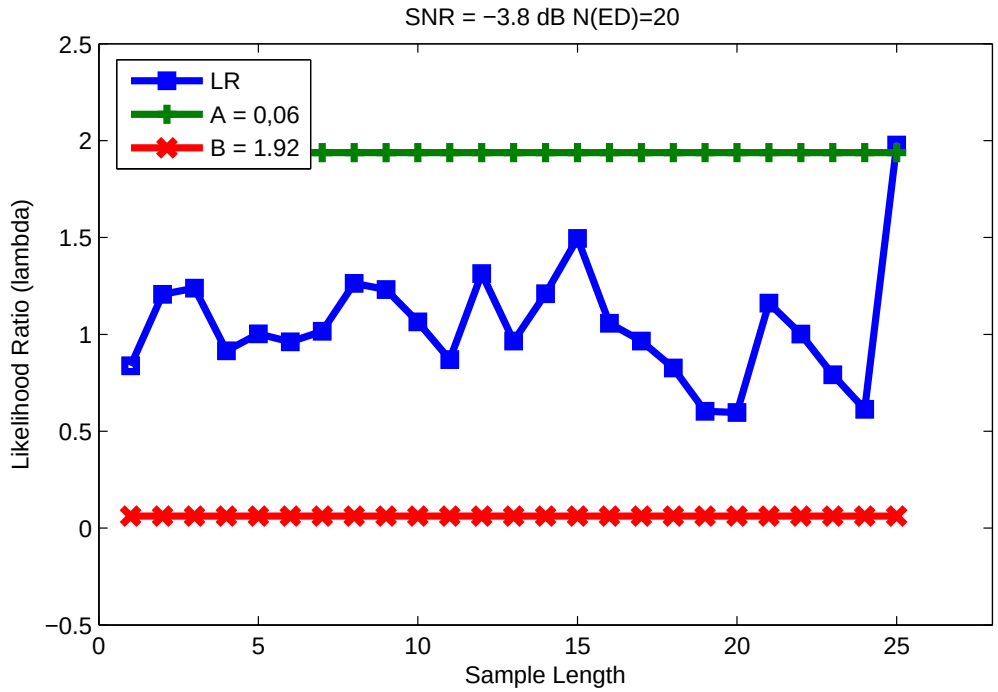

Figure 4.1: Sample Run of the Sequential Test Statistic

Eqn. (4.16) shows that the test statistic update term is linear in complexity as $\ln \zeta$ and β are constants. This formulation allows a natural simplification of the implementation of the SEED test and avoids the approximations made by [109] and others. We use this iterative log likelihood ratio update formula to reduce the computational complexity. The χ^2 distribution converges asymptotically to the Normal distribution as per the Central Limit Theorem. The χ^2 distribution is commonly approximated by the equivalent normal distribution for a sample size greater than 20. Figure 4.2 plots the Kullback-Leibler distance between the χ^2 distribution and its approximation. It is seen that the approximation is highly inaccurate for $N < 15$. Also, our SEED test operates for the most part in this low sample region and hence use of the normal approximation introduces large errors in analysis of sequential tests which we avoid here.

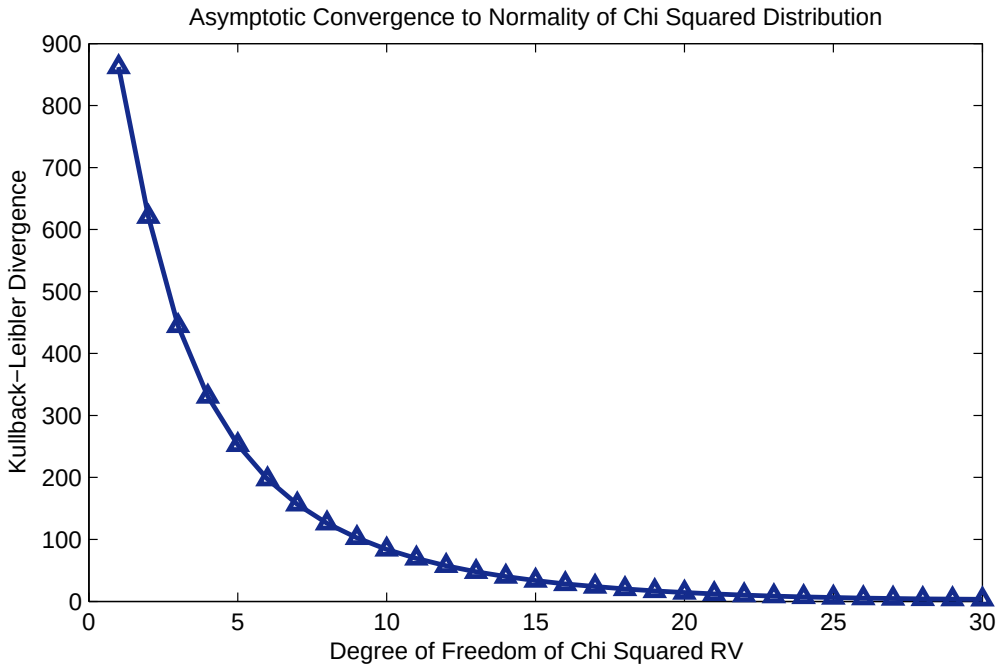

Figure 4.2: χ^2 Distribution Approximation

4.4.1 SEED Performance Evaluation

The stopping time of a sequential test is a random variable. The relative performance gain delivered by a sequential test can be succinctly characterized by comparing the expected value of the sequential test duration to the fixed size of the energy detector. Let N_{SEED} be the Average Sample Number (ASN) of the sequential test and N_{ED} be the size of the energy detector. The Relative Efficiency, η, of a sequential test over a fixed sample size test is defined as the ratio of the expected sample size (i.e ASN) of the sequential test to the sample size of the fixed sample size test with the same size and power.

$$\eta = N_{ED}/N_{SEED}. \tag{4.17}$$

The plots shown in Fig.4.3 for a fixed SNR were obtained as follows. For a given P_D and N_{ED}, the energy detector threshold γ" is found. Using the fixed point iteration in eqn.(4.8) the corresponding P_{FA} is calculated. Once we get the P_{FA} and P_D, we can construct the

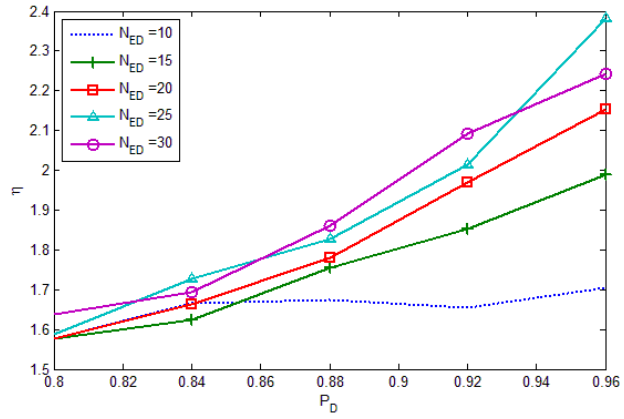

(a)

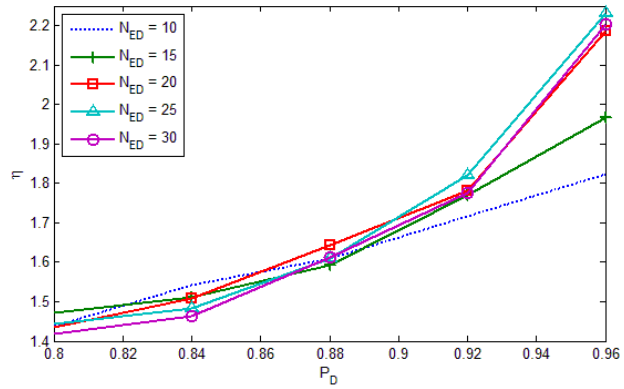

(b)

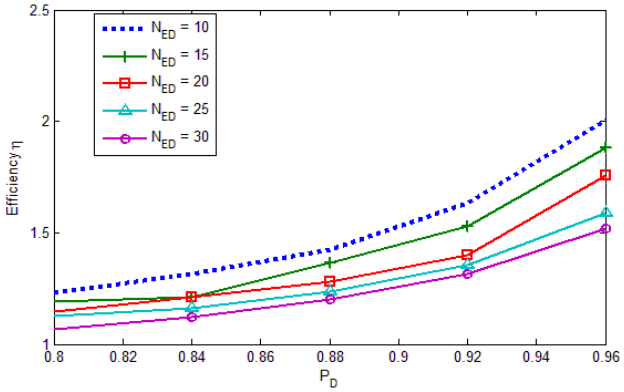

(c)

Figure 4.3: Relative Efficiency of Seed vs ED for increasing P_D with (a) -5 dB SNR (b) -3 dB SNR and (c) 3 dB SNR

equivalent SEED test and obtain the ASN using which the Relative Efficiency of the SEED test is calculated. The plots show that at high P_D values for low (negative) SNRs, η increases as the size of corresponding ED test increases. But, in the high SNR domain, η decreases as the size of ED test increases. This is because the fixed sample size ED test has very good performance in the high SNR region and fares poorly in the low SNR operating region.

4.4.2 Problems with Wald Approximations and the Min-M SEED

The thresholds A and B are derived under the assumption that the test statistic does not overshoot the threshold boundary at the sequential test stopping time. But this condition usually doesn't hold in practice and the design values of P_{FA} and P_D for the SEED test are not obtained. We introduce a novel variation called the Min-M SEED test in which a minimum of M samples are always collected before the test can terminate. This reduces the effect of spurious values and brings the design values of P_{FA} and P_D in line with the practically obtained values but the cost paid is a reduction in the relative efficiency of SEED test. The plots in Fig.4.3 implement a Min-1 SEED while Fig.4.4 uses the standard SEED. The higher variability and the higher efficiencies are easily noticed in Fig.4.4.

4.5 Signal Variance Estimation

Figures 4.3 and 4.4 demonstrate the significant throughput gain of the SEED test over the FSS ED test and provide compelling evidence in favor of its widespread adoption. However, there is an important drawback to the sequential testing methodology. In designing the ED, we require only an accurate knowledge of the noise variance to calculate the ED thresholds using eqn. (4.7) as its P_D and P_{FA} are interdependent. By contrast, in the SEED test, we need perfect knowledge of both the primary signal power and the noise variance to setup the test thresholds. In practice, the primary user signal is assumed to be completely

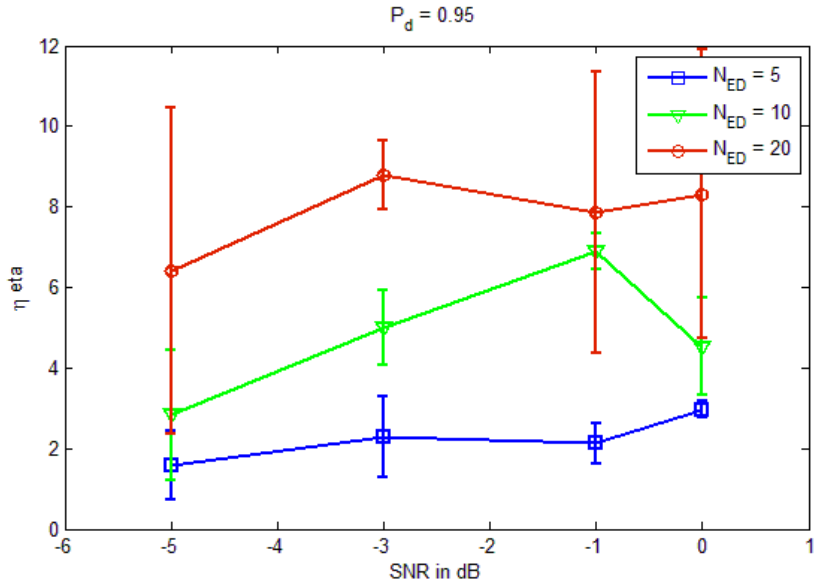

Figure 4.4: SNR vs η for a $P_d = 0.95$

unknown. Moreover, we have at most approximate estimates of the distance from the PU transmitter, the propagation loss factor and the channel gain. These constraints introduce high variability in the signal power estimates at the CR.

4.5.1 Sensitivity to Signal Variance Estimate

Eqn. (4.13) shows the dependence of λ_i on the signal variance σ_s^2 and can be used to calculate the sensitivity of the likelihood ratio to the estimated $\hat{\sigma}_s^2$. Unfortunately, this dependence is not amenable to analysis and is demonstrated here via simulations. Fig. 4.5 plots the percentage change in the efficiency of the SEED test as increasing error is introduced in the estimate of signal power $\hat{\sigma}_s^2$. There is a performance degradation of almost 15% for a 30% estimation error.

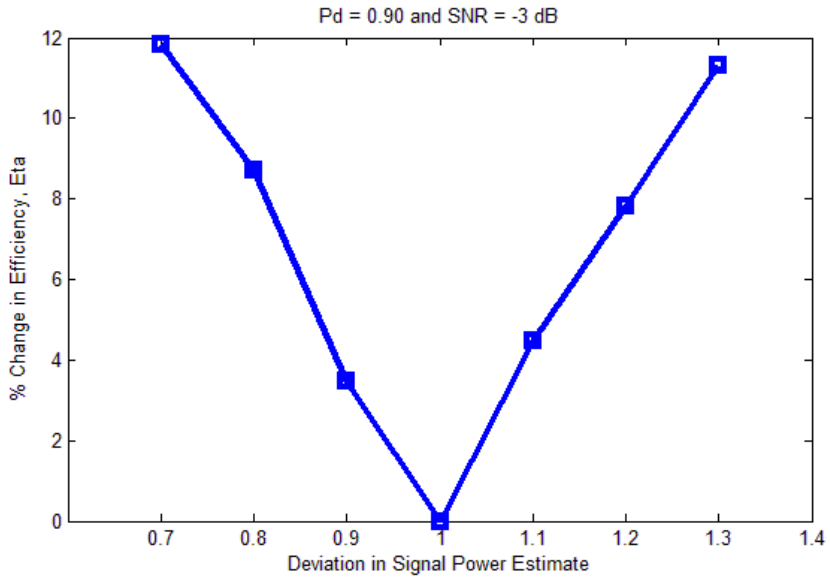

Figure 4.5: % Deviation in η vs % Deviation in σ_s^2

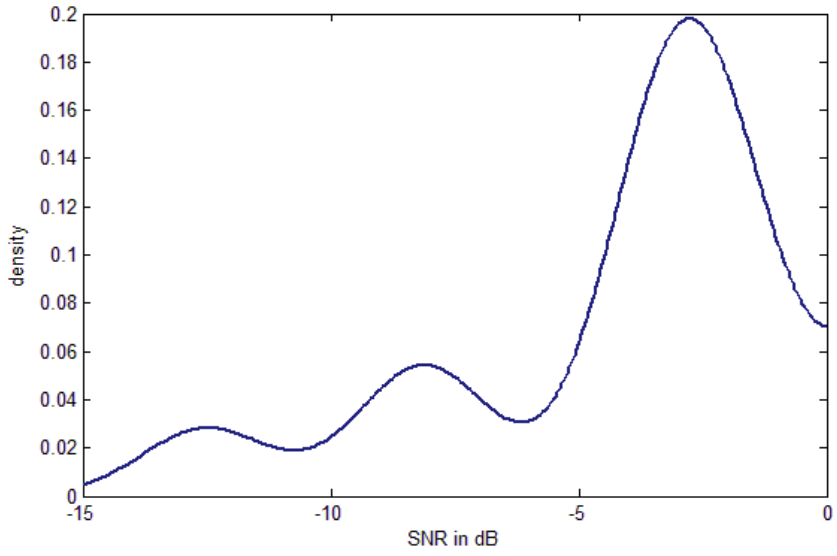

Figure 4.6: The Predicted Distribution of PU SNR values after 10 runs

4.5.2 Hybrid Iterative Bayesian Estimation of σ_s^2

To deal with the high sensitivity to inaccurate estimates of σ_s^2 as explained above, we introduce a Hybrid Iterative Bayesian Estimator. This method learns and maintains a

distribution for $\hat{\sigma}_s^2$. This prior distribution is used to estimate the future value of the signal energy and the estimate is refined as more and more samples are collected. Before we explain the method in detail, we note that the signal variance has to be estimated from the sporadic small intervals when a detection event occurs. In contrast, the problem of noise variance estimation has been extensively studied, see for e.g [114], and accurate estimates can be obtained by out-of-band sensing. We assume perfect knowledge of noise variance in order to isolate the effects of signal variance on the SEED test.

4.5.2.1 Initialization

The instantaneous value of σ_s^2 depends on the shadowing and fading of the channel. Also, Fig. 4.3 shows that the efficiency of the test improves with SNR and the IEEE 802.22 standard has stringent specifications for detection of low power TV signals in the negative SNR region. Considering these factors, the σ_s^2 estimator is initialized conservatively using a uniform distribution over [-20dB, 0dB] as the informative prior. Once the prior has been initialized, it will be updated every time the SEED algorithm produces a detection event.

4.5.2.2 Update

As the SEED test progresses, it will produce detection events. From the channel model, $\sigma_x^2 = \sigma_s^2 + \sigma_v^2$. Thus the estimator of the signal variance is $\hat{\sigma}_{s,old}^2 = \hat{\sigma}_x^2 - \sigma_v^2$. The updated posterior distribution $f(x)$ is obtained via adding a Gaussian kernel centered at the obtained $\hat{\sigma}_s^2$. We implement this as a Kernel Density Estimator with a Gaussian Kernel. $f(x) = \sum_{i=1}^{N} K(x, X_i, t)$ where $K(x, X_i, t) = \frac{1}{\sqrt{2\pi t}} \exp\left(-\frac{(x-X_i)^2}{2t}\right)$. t is the estimator bandwidth selected by the data-dependent Sheather-Jones method [115], [116]. Thus, the posterior distribution tends towards a Mixture of Gaussian formulation. We use a unique variation in which the older kernels are assigned exponentially decreasing weights to account for the time varying received signal power.

Table 4.1: Performance of SNR Prediction in 10 Iterations

SNR	**Mean Predicted SNR**	**% Deviation in η**
-3.0dB	-4.2	3.6
-10.0dB	-9.2	5.4
-15.0dB	-17.1	6.9

4.5.2.3 Prediction

A sample drawn probabilistically from the updated posterior distribution is the predicted value of the signal power $\hat{\sigma}^2_{s,new}$ and is used to initialize the next iteration of the SEED test. This probabilistic approach as opposed to the use of the mean of the posterior increases the robustness of the estimation procedure and helps avoid local attractor points. The efficiency error reduction through the prediction performance is shown in Table 4.1 .

4.6 Distributed Sequential Detection

In Section 4.4 we have formulated the sequential SED test that runs at an individual CR node. A typical CR has a single antenna which can be used for either sensing or transmitting and the secondary transmissions prevent other CRs from detecting PU signals. The necessity for spectrum sensing to be interleaved with secondary transmission has led to the adoption of a Quiet Period (QP). The QP is a synchronized time interval when all secondary transmissions cease. We have seen in the last section that Sequential Tests are uniquely suited for Cognitive Radio Networks which need to minimize sensing overhead while attaining a specified detection performance. There is a need to adopt a holistic approach to the goal of minimization of sensing overhead. Let $d_k = 0, 1$ be the decision of the k^{th}

CR whose SED terminates at time T_k. Also, T_{BS} is the DSED termination time at the base station and is the system sensing overhead. At one end is the policy where the base station simply decides the same as the first CR to report. We show in Section 4.8 that such a 'one shot' strategy has very poor performance in terms of P_{FA}. At the other end is the policy where the base station waits for all CRs to terminate their SED tests and report before it decides. But this can take a very long time in the worst case as the termination time of the SED is a random variable. Assuming all CRs stop sensing at T_{BS}, the system sensing overhead is bounded as $\min_{k\in[1,N]} T_k < T_{BS} < \max_{k\in[1,N]} T_k$. There exists a tradeoff between the two extreme sensing strategies which can be formulated as shown below.

$$\min T_{BS} \; s.t \quad P_D > P_{D,target} \;\&\; P_{FA} < P_{FA,target}. \tag{4.18}$$

4.6.1 Doubly Sequential Energy Detection (DSED)

The novel Doubly Sequential Energy Detection (DSED) test that we propose here minimizes the sensing overhead while maintaining the target P_{FA} and P_D. In the DSED test, a sequential SED test runs at each CR node and a variable time is required by the Base Station to reach a final decision. It does not stop sensing when the first CR reaches a decision. Instead, sensing is continued till more and more CRs terminate and sufficient data is available to the base station to be able to reach a decision with a pre-fixed certainty. Thus, the base station can be interpreted as running a second sequential test. We shall call this unique structure a Doubly Sequential Test.

The termination time of the sequential test is a random variable. Unfortunately, an exhaustive mathematical formulation of the Doubly Sequential structure is intractable. In this section we will mainly characterize the DSED performance through simulations and provide supporting theoretical results where possible. Let $Z = \log \frac{f_1(y)}{f_0(y)}$. In the SED, $y = T(\bar{x}) = \sum_{n=1}^{M} |x(n)|^2$. Wald has derived the following lower bounds for the expectation of

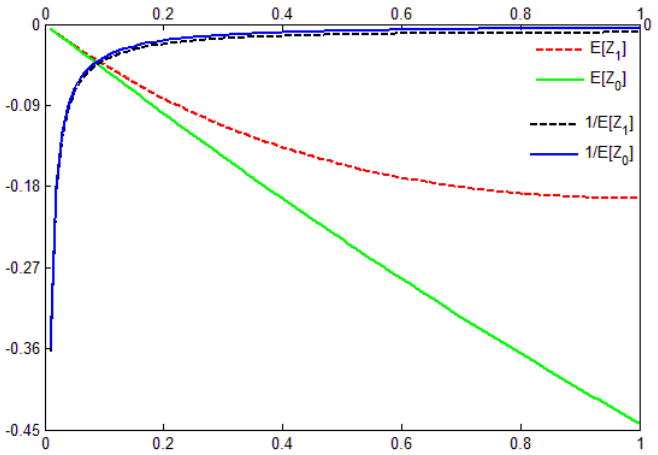

Figure 4.7: Plot of $E[Z_k]$ vs SNR (linear scale)

the average sample number as shown below [112]. Note that the termination behavior is different under the two hypotheses.

$$E_0 N \geq \frac{1}{E_0 Z}\left[(1-\alpha_0)\log\frac{\alpha_1}{1-\alpha_0} + \alpha_0\frac{1-\alpha_1}{\alpha_0}\right], \tag{4.19}$$

$$E_1 N \geq \frac{1}{E_1 Z}\left[\alpha_1\log\frac{\alpha_1}{1-\alpha_0} + (1-\alpha_1)\frac{1-\alpha_1}{\alpha_0}\right]. \tag{4.20}$$

We will assume here that there is negligible overshoot of the test statistic at the termination time. With this assumption, we replace the inequalities in (4.19) and (4.20) with the approximate equalities. Using the threshold formulas, we obtain the expected values of the termination time as given below.

$$E_0[N] = \frac{1}{E_0[Z_i]}\left[\frac{B-1}{B-A}\log A + \frac{1-A}{B-A}\log B\right], \tag{4.21}$$

$$E_1[N] = \frac{1}{E_1[Z_i]}\left[\frac{A(B-1)}{B-A}\log A + \frac{B(1-A)}{B-A}\log B\right].$$

Using (4.14) the Log Likelihood Ratio Z of the SED test becomes $Z = \sum_{k=1}^{i} Z_i$, i.e, a sum of i.i.d statistics Z_i,

$$Z_i = \ln \zeta + \beta x(i+1)x^*(i+1). \tag{4.22}$$

Taking the expectation of (4.22), with $k = 0\ , 1$ corresponding to the hypothesis H_0 and H_1 respectively,

$$E_k[Z] = E\left[\log \zeta + y_i \beta\right] = \log \zeta + \sigma_x^2 \beta. \tag{4.23}$$

After further simplification with $\sigma_x^2 = \sigma_s^2 + \sigma_v^2$ for H_1 and $\sigma_x^2 = \sigma_v^2$ for H_0, we get the following relations.

$$\begin{aligned} E_0[Z_i] &= -log(1+\gamma) + \frac{\gamma}{2(1+\gamma)} && : H_0 \\ E_1[Z_i] &= -log(1+\gamma) + 2\gamma && : H_1 \end{aligned} \tag{4.24}$$

Equations (4.21) and (4.24) shown that the distribution of the termination time depends on the P_D, the P_{FA} and the SNR of the system. The behavior of $E_k[Z_i]$ for SNR $\gamma < 1$ is plotted in Figure 4.7. We note that for $\gamma < 0.1$, i.e, $\gamma < \ -10$ dB, the SED stopping time significantly deteriorates for a fixed P_D and P_{FA}. This behavior has two important consequences. 1) The SED is a truncated sequential test and is forced to stop and reach a decision after the maximum sensing duration. As the SNR decreases, the test reaches truncation more often and the delivered P_D suffers as seen in Figure 4.8. 2) When shadowing is taken into consideration, there is a spread observed in the SNRs. This means that the earliest CRs to terminate are highly likely to be the ones that have an extreme value of the SNR and this behavior is exploited in the Distributed SED. In the next section we present strategies for the termination of the DSED at the Base Station.

4.7 Termination Criteria at Base Station

4.7.1 One Shot Detection

This is the simplest strategy where the base station terminates the DSED when the first CR terminates and communicates its decision, i.e, $T_{BS} = T_1$, i.e, the base station reaches a final decision in a one-shot manner. While this is an effective strategy for the scenario of i.i.d observations at each CR, the system performance is severely degraded under log-normal shadowing. The degradation occurs because the overall system performance is dictated by the earliest CR to reach a decision, which is often the one that also experiences a false alarm due to extreme value of γ as explained in the last section. The simulation results verify that the the sensing time is reduced but detection performance severely degrades.

4.7.2 First-M-Positive Detection

In First-M-Positive Detection, the Base Station continues the DSED test till it has received M decisions in favor of a particular hypothesis. The test then terminates and that particular hypothesis is the DSED decision. Heuristically, we found that setting $M \geq 4$ delivers good performance. We observe that this choice of M depends only upon the shadowing present and does not scale with the number of nodes in the secondary network. This strategy exploits the lower stopping times at high SNRs as in Fig. 4.7 to terminate faster while at the same time it increases the robustness against extreme shadowing values.

$$T_{BS} = \arg\min_{k} \left(\sum_{i=1}^{k} \mathbb{1}_{[d_i=1]} = M \right) \wedge \left(\sum_{i=1}^{k} \mathbb{1}_{[d_i=0]} = M \right).$$

4.7.3 Wait-Till-T_{Th} Detection

The Base Station waits till it receives the first decision after a duration T_{Th} has passed. The final decision is made in favor of the majority of individual CR decisions. Here,

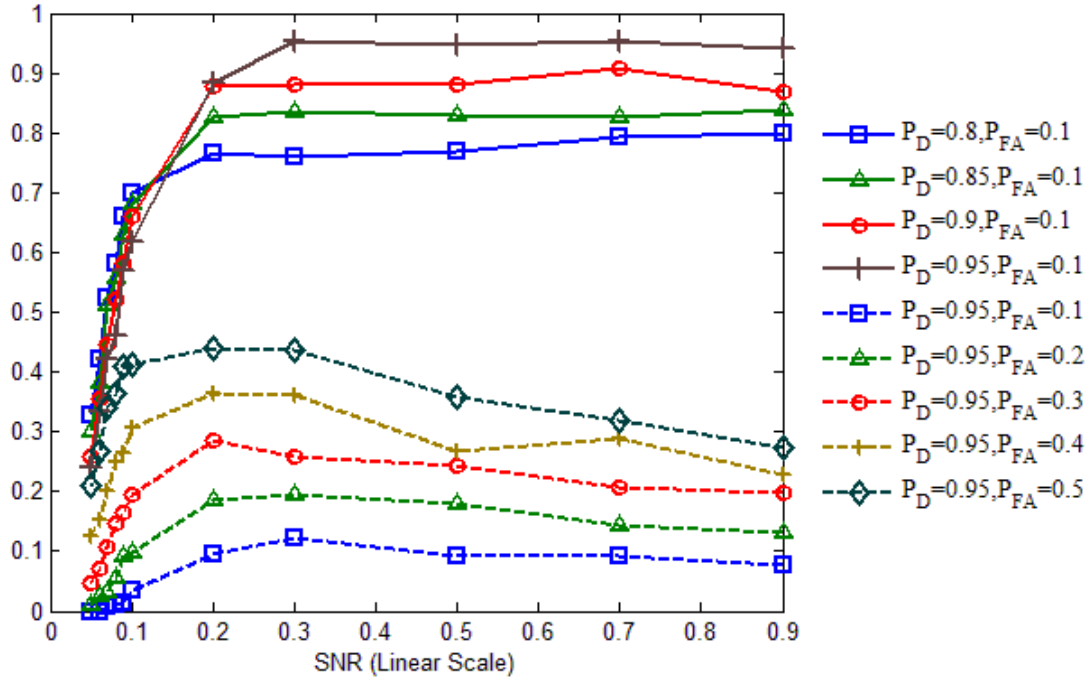

Figure 4.8: Behavior of P_D and P_{FA} vs SNR for SED Test

$T_{BS} = \arg\min_k T_k \geq T_{Th}$. The time T is set to be equal to the expected value of the test termination time as predicted by (4.21) or set to the mean of the empirical termination time distribution shown in Figure 4.10.

4.8 Experimental Results

The performance curves for the SED test are plotted in Figure 4.8. The P_D and P_{FA} values that we use to set the thresholds of the sequential test are called Design Values while the actual P_D and P_{FA} obtained via Monte Carlo simulation are called Delivered Values. The upper set of curves show effect of SNR on the delivered values of P_D for increasing P_{FA} design values while the lower set of curves similarly plot the delivered P_{FA} for increasing design values of P_D. It is seen that the SED test matches its design specifications upto a SNR

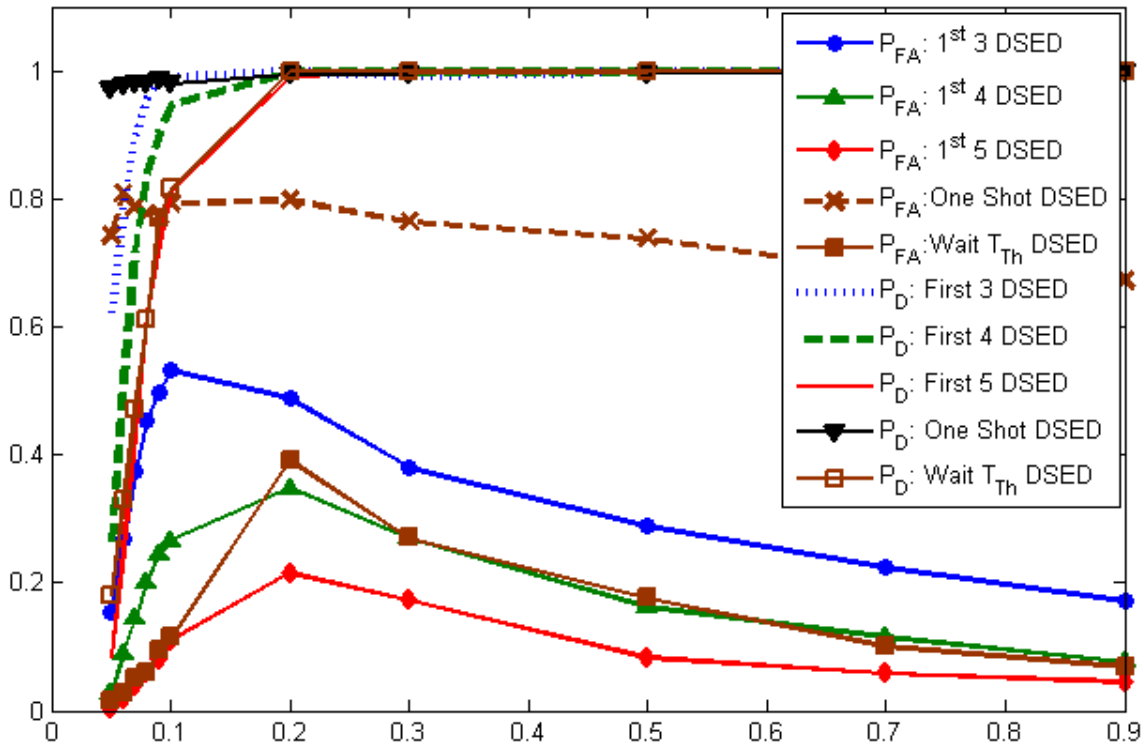

Figure 4.9: Behavior of P_D and P_{FA} vs SNR for DSED Test

of 0.2 (-7 dB), below which the delivered P_D precipitously declines while the delivered P_{FA} is always upper bounded by the designed P_{FA}. In contrast, Figure 4.9 shows the substantial performance improvement in the DSED with First-M-Positive Detection. The delivered P_D equals 1 till $\gamma = 0.2$ and the P_D is still > 0.8 upto SNR $\gamma = 0.05$ (-13 dB). The delivered P_{FA} is slightly higher than that for the SED test and the curves demonstrate that setting $M = 4$ gives the best tradeoff between the delivered P_D and P_{FA} values. Comparable performance is obtained via the Wait Till T_{Th} DSED but it is more difficult to tune. Also Figure 4.9 shows the poor performance of the One Shot DSED as predicted in Section 4.7. The delivered P_{FA} values are extremely high and hence there is need for the better DSED strategies we have studied.

The distribution of the termination time of the DSED test is concentrated towards

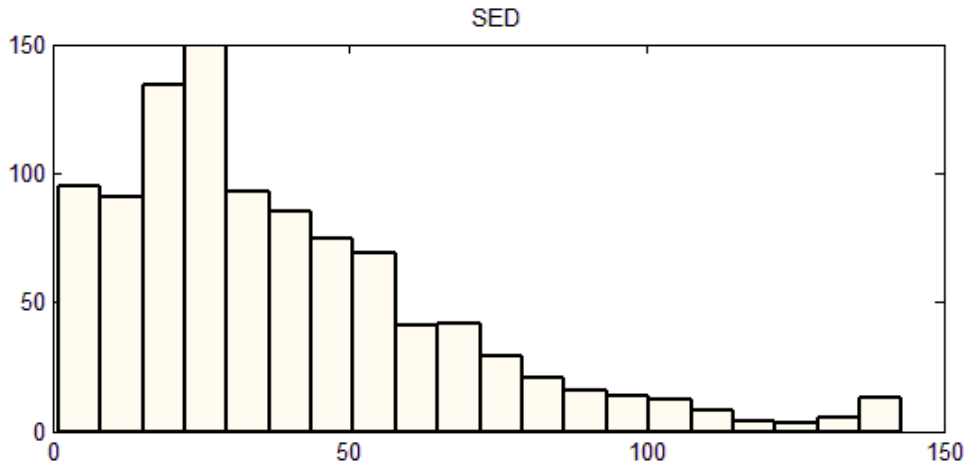

Figure 4.10: Distribution of Termination Time for SED Test

Table 4.2: Efficiency Comparison of DSED Tests

Method	η **For** H_1	η **For** H_0
SED Test	3.73	2.77
One Shot DSED	31.56	16.04
Wait-T_{Th} DSED	2.53	1.86
First-M DSED (M=4)	7.33	2.92

faster stopping time as compared to the SED test. As seen in Figures (4.10) and (4.11), only the CRs that terminate their SED test early contribute to the Base Station's decision and thus cause the beneficial skew in the resultant DSED distribution. Table 4.2 compares the sensing efficiencies of the proposed tests for a SNR of -5 dB. The First-M test outperforms the Wait-T_{Th} DSED test, while the poor detection performance of One Shot DSED makes it infeasible. The DSED sensing durations are different for the two hypothesis and the overall delivered η is 2 to 8.

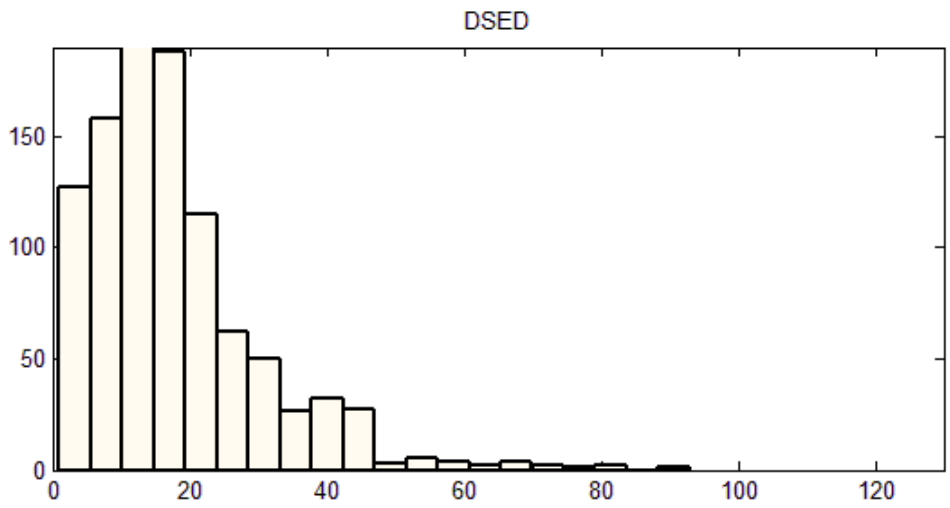

Figure 4.11: Distribution of Termination Time for DSED Test

4.9 Case Study 1- Sequential Sensing applied to the IEEE 802.22 Standard

The IEEE 802.22 Standard is the first practical implementation of the cognitive radio technology [97, 117]. It is based on dynamic spectrum sensing and opportunistic access of the bands that are not currently in use by TV transmitters. It exploits the fact that the average TV market in the United States uses around 7 of the allotted 67 high power channels. FFT based pilot sensing of the TV signal is recommended in the standard. The sensing is carried out by averaging over a fixed number of multiple dwells (6-10). We propose a sequential version of the scheme where the number of dwells required is dynamically varying according to the fidelity of the received signal. We show via simulation that the proposed sequential sensing strategy yields a throughput gain and reduces system overhead

4.9.1 FFT based Pilot Detection of ATSC signals

The FFT based pilot sensing method is a non-blind technique which meets the sensing requirements of the 802.22 draft standard [118]. It uses the pilot present in ATSC DTV signals. The ATSC signal has an 8-VSB (Vestigial Side Band) modulation with signal levels of (-7,-5,-3,-1, 1, 3, 5, 7). For efficient carrier recovery at the receiving end, a pilot is added to the signal through a DC offset of 1.25. In this section, we will focus only on ATSC signals. The pilot is transmitted at a much higher SNR than the rest of the ATSC TV signal. This is the main advantage of sensing only the pilot, as we can operate at a more favorable point on the operating characteristics curve of the energy detector. We take the FFT of the captured signal over a period of 1 ms or 5 ms, called a dwell. The power in the signal at a particular frequency (say, the pilot frequency) is estimated as the square of the corresponding frequency bin in its FFT. It can be easily shown that the pilot power follows a Chi-squared distribution with 2 degrees of freedom. The hypothesis testing problem is to decide between a central Chi Square and a non-central Chi square distribution with a non centrality parameter equal to the SNR at the pilot frequency.

$$H0 \sim \chi_2^2(0) \tag{4.25}$$

$$H1 \sim \chi_2^2(\lambda_{pilot}) \tag{4.26}$$

The test reduces to comparing the power in the bin corresponding to the pilot frequency to a threshold. The threshold is calculated using the Neyman-Pearson theorem to meet the required values for the probability of missed detection (PMD) and probability of false alarm (PFA). Calculation of the threshold requires the knowledge/estimation of the SNR at the pilot frequency, as do all energy detectors. We assume that a perfect estimate of the SNR is available for deriving the tests. The effect of uncertainty in knowledge of the SNR is neglected. If the signal is in a deep fade or is very weak, a single dwell may give

erroneous results. Multiple dwells have to be used in practical implementations to improve the detection performance [119].

4.9.2 Sequential Sensing of ATSC Pilot

In the multiple-dwell implementation of pilot sensing, the number of dwells is fixed a priori, usually between 6 -10. We will now formulate a sequential implementation of the pilot sensing scheme, where depending upon the uncertainty of the decision, a variable number of dwells will be required. We will develop the sequential pilot sensing method in a similar manner to our development of the SED test in last section. The sequential probability ratio test (SPRT) allows us to arbitrarily specify the PMD and PFA we would like the system to operate at, by the virtue of the variable run length of the test. We keep accepting new samples till we can make a decision with a satisfactory certainty. The performance of a SPRT is measured in terms of the average sample number (the average number of dwells) required. At each iteration of the sequential test, we update the likelihood ratio, which is a function of all the samples received within that time. The updated likelihood ratio is compared with upper and lower thresholds. If either threshold is exceeded, we stop the test and reach a decision. Otherwise we accept more samples till we are in a position to decide. Also,the Walds approximations give us the thresholds.

4.9.2.1 Preprocessing of ATSC signal captures

The ATSC signal has a bandwidth of 6 MHz and the pilot is at the lower edge of the band as shown in Figure 4.12. The IEEE 802.22 standard prescribes a database of 12 ATSC signal captures under varying real world multi-path fading, frequency offsets and other distortions. The signal is sampled at 21.52 Msamples/sec and down converted to a low central IF of 5.38 MHz (one fourth the sampling rate). An 8 MHz bandwidth IF filter was used when capturing the signals.

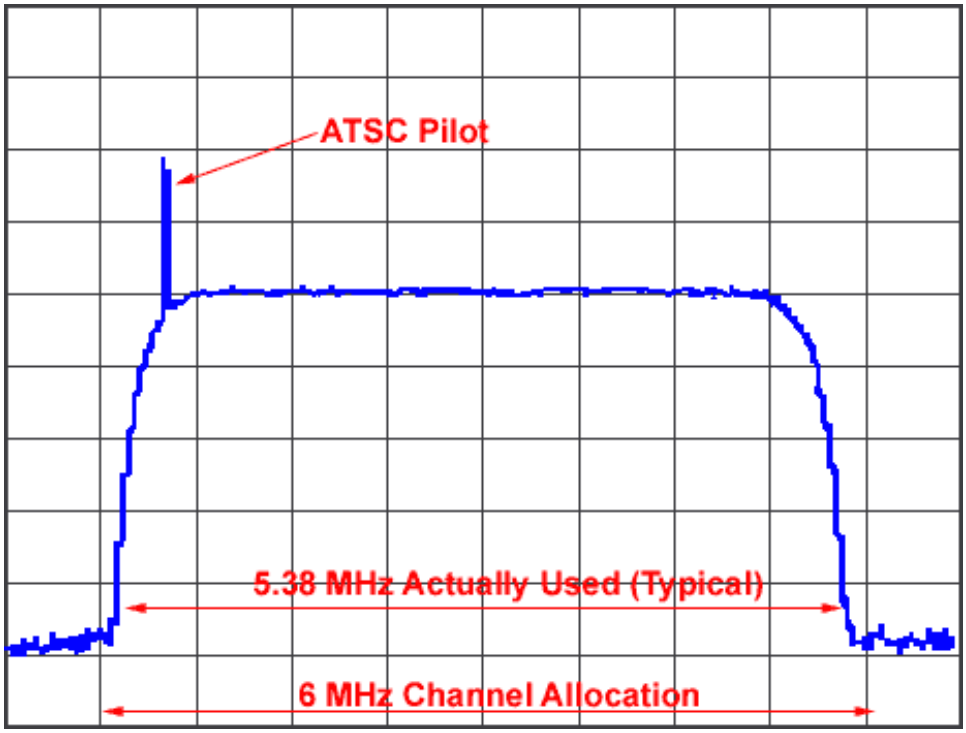

Figure 4.12: Spectral Density of an ATSC channel

We follow the 802.22 standard recommended steps (1-4) [120] and then implement our proposed sequential test.

A.1 Filter the signal using a passband filter with a 6 MHz bandwidth with a center frequency of $f_{IF} = 5.38$MHz. The filter is a brick wall filter.

A.2 Add the filtered noise and the scaled and filtered signal.

A.3 Estimate pilot frequency as the peak in the FFT nearest to the nominal pilot frequency of 2.69MHz.

A.4 We need prior knowledge of the pilot power, the noise power at the pilot frequency and the pilot SNR to run the test. We will estimate them by averaging over a large number of realizations of the signal.

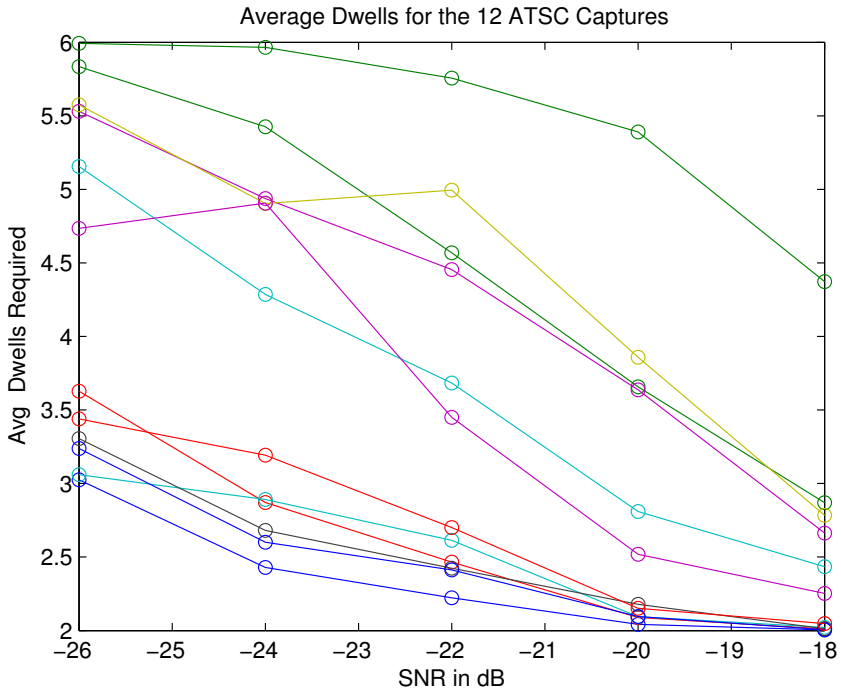

Figure 4.13: Average dwells required for detection of ATSC signal vs SNR

4.9.3 Simulation Results

The sequential pilot sensing test has been set up for a nominal PD of 0.99 (PMD = 0.01) and a PFA of 0.01 where PMD is probability of missed detection defined as 1 - PD. These have been chosen to meet the best performance of the multiple dwell test in order to be able to compare our performance with that of the non sequential test reported in [119]. In practice, the actual PD and PFA as measured are different from the values used for test setup. This is because we use a truncated sequential test and the Wald-Wolfowitz theorem doesn't hold. Also, the independence of the AWGN samples is destroyed by noise shaping at the receiving filter. Inspite of these variations, the average performance of the test remains at least as good as that of the non sequential test in most situations. The test is run for a thousand iterations and the number of dwells required in each iteration is averaged. Figures 4.15a and 4.15b plot the actual delivered performance of the test. Note that the number of

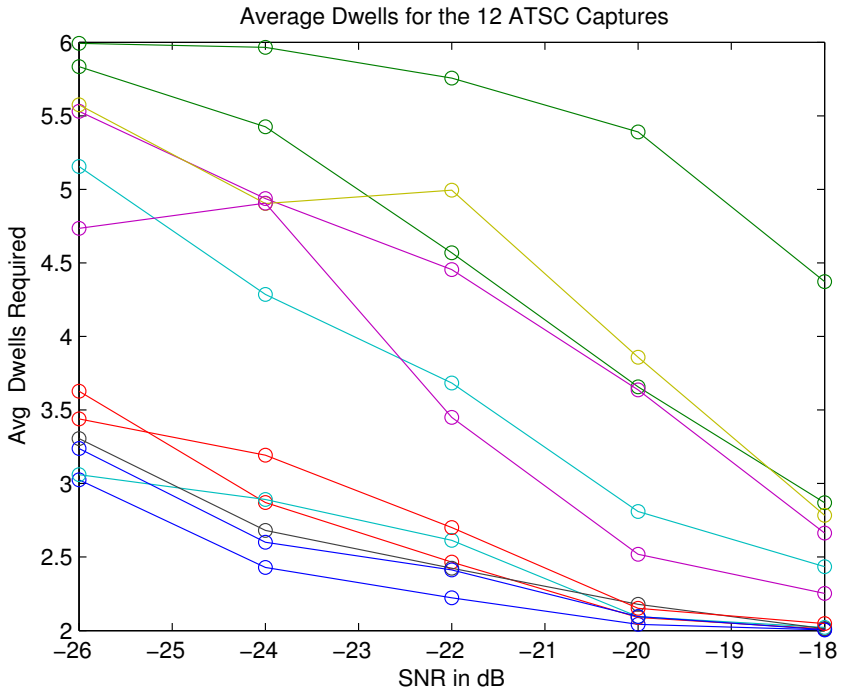

Figure 4.14: Distribution of the dwells required for sensing

dwells required is not constant but varies dynamically. Note also that the proposed sequential test outperforms the fixed sample size test and yields a lower probability of missed detection. We have set up the test to run for a minimum of two dwells. The average dwell number increases as the SNR is decreased from -18 dB to -26 dB. Figure 4.13 shows the average number of dwells required over the range of SNRs for sequential pilot detection. Also, the spread of the dwells is plotted in the histogram for a SNR of -26 dB is plotted in Figure 4.14.

4.10 Conclusion

In this chapter we proposed a novel sequential energy detector (SED) which delivers significant reduction in sensing time as compared to the conventional fixed sample size energy detector. We also formulated a Doubly Sequential Test (DSED) as a distributed version of the SED test and characterized its performance. It was demonstrated that the DSED

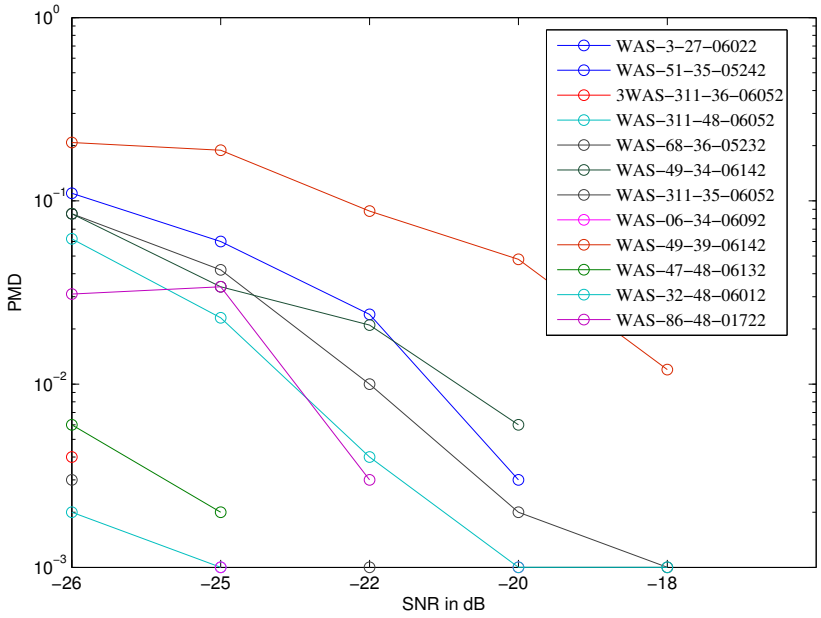

(a)

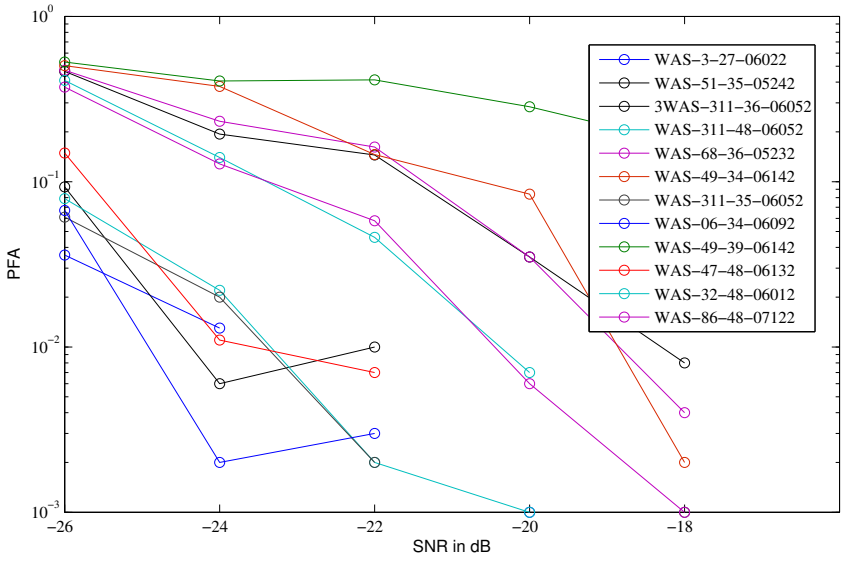

(b)

Figure 4.15: The behavior with respect to SNR for (a) delivered probability of missed detection P_{MD} and (b) the delivered probability of false alarm P_{FA}

Table 4.3: Selected IEEE 802.22 Requirements

Parameter	**Digital TV channel detection value**
Channel detection time	$\leq 2sec$
Channel move time (in service)	2 sec
Interference detection threshold	-116 dBm

Table 4.4: Average dwells required across all 12 ATSC Captures and Average Throughput Increase

ATSC SNR (in dB)	**Average Dwells(max of 6)**	**Throughput Increase**
-18	2.456	2.44
-20	2.876	2.08
-22	3.478	1.72
-24	3.924	1.52
-26	4.376	1.37

provides improved sensing performance at lower SNRs while matching the efficiency gain via drastically reduced sensing times. Thus, Doubly Sequential Tests are uniquely suited for Cognitive Radio Networks which need to minimize sensing overhead while attaining a specified detection performance. The novel SEED sequential detector has been shown to deliver substantial efficiency gains over the fixed sample size Energy Detector. Also, the deleterious effect of uncertainty in signal power estimates at the CR end on the performance of sequential tests have been quantified and an Iterative Probabilistic Update method has

been developed to robustly estimate the variance and thus improve the SEED test performance. The superior performance of the family of sequential energy detectors has been comprehensively studied from the perspective of Dynamic Spectrum Access applications.

Chapter 5

Conclusion

In this thesis we have presented various techniques for sensing and accessing the latent capacity in wireless channels. We will now briefly revisit the salient points of these techniques, elaborate on how the techniques fit into a comprehensive network sensing and access framework, and point out avenues for expanding on our contributions within and beyond the scope of cognitive radios.

Conventional Opportunistic Spectrum Access methodologies seek out opportunities for the unlicensed secondary transmissions at the physical layer. The current models such as white space, interference temperature limits and others are examples of this physical layer based outlook towards cognitive radios. In Chapter 2 we introduced a novel transmission opportunity sensing paradigm which senses the opportunities at the MAC layer of the primary network in contrast to most previous work. We developed a suite of transmit opportunity detection methods that effectively exploit the gray space present in high traffic packet networks. Our methods adopted a holistic view of the primary network and could proactively decide the maximum safe transmit power that does not affect the nodes in the primary network. This was achieved via an implicit feedback mechanism from the Primary network to the Secondary network. This is the first time that such a Primary User - Secondary User feedback link has been shown to naturally arise in the framework of Opportunistic Spectrum Access. This was achieved in part via use of primary network packet statistics such as packet lengths and interarrival durations to rapidly and robustly perform change detection in the

primary network's Quality of Service. Our field testing of these methods on real world deployments of IEEE 802.11 campus wireless LANs demonstrate the potential of this approach towards Opportunistic Spectrum Access.

In Chapter 3 we focused on the problem of detecting the presence or absence of a licensed user on a specific channel. We addressed the more complex spectrum sensing setup where the noise statistics are either completely arbitrary or a mixture of Gaussian and impulsive noise. It has long been known that uncertainty in estimation of noise statistics, time variability of the noise statistics or presence of significant non Gaussian interferers drastically deteriorates the presence of conventional white space sensing methods. We demonstrated here that using a nonparametric formulation delivers superior performance gains over the more popular parametric spectrum sensing tests. The unique aspect of this work was our use of goodness of fit tests for the purpose of inference in a non-parametric setting. We provided the first comprehensive framework for decision fusion of an ensemble of goodness-of-fit testing procedures through an Ensemble Goodness-of-Fit test. Also, for the first time we introduced a generalized family of functionals and kernels called $\mathbf{\Phi}$-divergences which allow us to formulate goodness-of-fit tests that are parameterized by a single parameter. The performance of these tests is simulated under Gaussian and non-Gaussian noise in a MIMO setting. We show that under uncertainty in the noise statistics or non-Gaussianity in the noise, the performance of non-parametric tests in general, and phi-divergence based goodness-of-fit tests in particular, is significantly superior to that of the energy detector with reduced implementation complexity. In particular, the false alarm rates of our proposed tests is maintained at a fixed level over a wide variation in the channel noise distributions. Additionally, we proposed a new and effective collaborative spatially separated version of the test for robust combining of tests in a distributed spectrum sensing setting via use of p-values of the test statistics and quantified the significant collaboration gains achieved.

It is critically important during spectrum sensing to detect the presence of the primary

user as rapidly as possibly so as to be able to vacate the channel and minimize the interference caused to the licensed channel users. With this goal in mind, in Chapter 4 we developed the sequential energy detection problem in the context of spectrum sensing for cognitive radio networks. We formulated a novel Sequential Energy Detector and provide a comprehensive study of its performance. Also, the sensitivity of such Sequential Test procedures to errors in primary signal energy estimation is uniquely addressed in this work. Through simulations it was demonstrated that our Sequential version of the energy detector delivers a significant throughput improvement of 2 to 6 times over the fixed sample size test while maintaining equivalent operating characteristics as measured by the Probabilities of Detection and False Alarm. We applied our sequential energy detection test to demonstrate the throughput gains for a case study of sensing real world capture of ATSC television signals under adverse channel conditions within the framework of the IEEE 802.22 standard via the FFT based pilot energy sensing technique. Finally, we further extended the sequential testing framework to a doubly hierarchical setting with each CR performing sequential detection and the fusion center performing a second tier of hard sequential test on the sequentially transmitted decisions of these individual nodes.

There is an overarching themes common to the three principal contributions summarized above. The real world wireless channel is a complex messy entity. It is erroneously oversimplified for ease of analysis and for elegance of the theoretical formulations thus achieved. Dealing with this real world complexity and nonidealities requires that the researcher be prepared to go beyond his/her toy models. To give a specific example, most modeling in cognitive radios assumes that the background noise is additive, white and Gaussian. In practice, only the thermal noise follows those properties, and in addition to thermal noise, there is a significance presence of other noise such as front end non-linearities, spikes due to engines, leakage from microwave ovens, cross channel interference and narrowband interference from Bluetooth, wireless sensors and other low power pervasive communication devices, natural

sources such as lightning etc. Also, even the distribution of the AWGN noise can only be imperfectly estimated and such imperfect estimation bounds the performance of spectrum sensing methods like the energy detector. In a blind sensing environment as is typical in cognitive radio settings, we cannot even assume to know the power statistics of the primary users unless we tailor the cognitive radio to learn each type of primary transmission at each frequency band of interest, which is a task of high magnitude of complexity. Summing up, the tidy little *parametric models* of the signals of the primary users and background noise statistics are almost always not usable in the real world, and the parameters are seldom known to us exactly, as is required to tune those models. In our work, we recommend a shift in perspective towards *nonparametric* modeling of Opportunistic Spectrum Access scenarios. Such nonparametric models are perfectly suited for use when the probability distributions are known with uncertainty, varying slowly over time or completely arbitrary.

Finally, we conclude by pointing out that the paradigm of Opportunistic Spectrum Access is only the first tentative step towards the vision of a world of intelligent and flexibly reconfigurable radios that seamlessly roam over the entire frequency band and integrate into a single universal wireless network. Cognitive radios built on a foundation of advanced Software Defined Radio technology show tremendous potential to achieve this goal. Today the wireless world is divided into hundreds of distinct principalities and fiefdoms, with each ruled by a combination of particular wireless technology, standard and intellectual property strongholds. A state of such fragmentation coupled with a regulatory reluctance to overhaul the spectrum policies and the potent inertia of the vested interests of legacy technologies are formidable obstacles to a seamless and borderless wireless future. It is the fervent hope of the authors that the new generation of smart Cognitive Radios and the associated technology policies and standards will help us achieve the holy grail of a truly universal communications network.

Appendices

Appendix A

Abbreviations

ACK	Acknowledgment
AD	Anderson Darling test
AIMSE	Asymptotic Integrated Mean Square Error
ATSC	Advanced Television Systems Committee
AMC	Adaptive Modulation and Coding
BER	Bit Error Rate
BPSK	Binary Phase Shift Keying
CAP	Channel Capture
CDF	Cumulative Distribution Function
CR	Cognitive Radio.
CRN	Cognitive Radio Network
CSS-EG	Collaborative Spatially Separated EG test
CTS	Clear To Send
CvM	Cramer von Mises test

DSA	Dynamic Spectrum Access
DSED	Doubly Sequential Energy Detection
DTV	Digital Television
ED	Energy Detector
EG	Ensemble Goodness-of-Fit test
e.d.f	Empirical Distribution Function
ETSI	The European Telecommunications Standards Institute
FCC	Federal Communications Commission
FFT	Fast Fourier Transform
FSS	Fixed Sample Size test
GoF	Goodness of Fit
IT	Interference Temperature
KDE	Kernel Density Estimation
KL	Kullback Leibler divergence
KS	Kolmogorov Smirnov test
MAC	Medium Access Control
MIMO	Multiple Input Multiple Output
OFCOM	Office of Communications
OSA	Opportunistic Spectrum Access

PBN	Packet Based Network
PDF	Probability Density Function
PER	Packet Error Rate
PFA	Probability of False Alarm
PHY	Physical Layer
PMD	Probability of Misdetection
ProTOMAC	Proactive Transmit Opportunity at MAC layer
PU	Primary User
QoS	Quality of Service
QP	Quiet Period
RFI	Radio Frequency Interference
RTS	Request To Send
SED	Sequential Energy Detection
SEED	Sequential Energy Detector
SDR	Software Defined Radio
SNR	Signal to Noise Ratio
SPRT	Sequential Probability Ratio Test
SPTF	Spectrum Policy Task Force
SU	Secondary User

TEV	Thresholded Extreme Value test
TM	Transmit Margin
USRP	Universal Software Radio Peripheral
WRAN	Wireless Regional Area Network
WLAN	Wireless Local Area Network

Bibliography

[1] V. Valenta, R. Marsalek, G. Baudoin, M. Villegas, M. Suarez, and F. Robert, "Survey on spectrum utilization in europe: Measurements, analyses and observations," pp. 1–5, 2010.

[2] M. McHenry, P. Tenhula, D. McCloskey, D. Roberson, and C. Hood, "Chicago spectrum occupancy measurements & analysis and a long-term studies proposal," p. 1, 2006.

[3] M. Islam, C. Koh, S. Oh, X. Qing, Y. Lai, C. Wang, Y. Liang, B. Toh, F. Chin, G. Tan *et al.*, "Spectrum survey in singapore: Occupancy measurements and analyses," pp. 1–7, 2008.

[4] S. Pagadarai and A. Wyglinski, "A quantitative assessment of wireless spectrum measurements for dynamic spectrum access," in *Cognitive Radio Oriented Wireless Networks and Communications, 2009. CROWNCOM'09. 4th International Conference on*. IEEE, 2009, pp. 1–5.

[5] J. Mitola *et al.*, "Cognitive radio: An integrated agent architecture for software defined radio," *Doctor of Technology, Royal Inst. Technol.(KTH), Stockholm, Sweden*, pp. 271–350, 2000.

[6] E. FCC, "Docket no. 03-108," *Facilitating opportunities for flexible, efficient, and reliable spectrum use employing cognitive radio technologies, FCC Report and Order adopted (March 10, 2005)*, 2005.

[7] J. Hoffmeyer, "Ieee 1900 and itu-r standardization activities in advanced radio systems and spectrum management," in *Consumer Communications and Networking Conference, 2007. CCNC 2007. 4th IEEE.* IEEE, 2007, pp. 1159–1163.

[8] "Comments of the national telecommunications and information administration on fcc et docket no. 03-108: facilitating opportunities for flexible, efficient, and reliable spectrum use employing cognitive radio technologies," February 15, 2005.

[9] S. Haykin, "Cognitive radio: brain-empowered wireless communications," *IEEE J. Sel. Areas Commun.*, vol. 23, no. 2, pp. 201–220, Feb. 2005.

[10] B. Fette, *Cognitive radio technology.* Academic Press, 2009.

[11] P. Marshall, "Extending the reach of cognitive radio," *Proceedings of the IEEE*, vol. 97, no. 4, pp. 612–625, 2009.

[12] I. Akyildiz, W. Lee, M. Vuran, and S. Mohanty, "Next generation/dynamic spectrum access/cognitive radio wireless networks: a survey," *Computer Networks*, vol. 50, no. 13, pp. 2127–2159, 2006.

[13] T. Yucek and H. Arslan, "A survey of spectrum sensing algorithms for cognitive radio applications," *Communications Surveys & Tutorials, IEEE*, vol. 11, no. 1, pp. 116–130, 2009.

[14] A. Goldsmith, S. Jafar, I. Maric, and S. Srinivasa, "Breaking spectrum gridlock with cognitive radios: An information theoretic perspective," *Proceedings of the IEEE*, vol. 97, no. 5, pp. 894–914, 2009.

[15] G. Scutari and D. Palomar, "Mimo cognitive radio: A game theoretical approach," *Signal Processing, IEEE Transactions on*, vol. 58, no. 2, pp. 761–780, 2010.

[16] C. Clancy, J. Hecker, E. Stuntebeck, and T. O'Shea, "Applications of machine learning to cognitive radio networks," *Wireless Communications, IEEE*, vol. 14, no. 4, pp. 47–52, 2007.

[17] Q. Zhao and B. Sadler, "A Survey of Dynamic Spectrum Access," *IEEE Signal Process Mag.*, vol. 24, no. 3, pp. 79–89, 2007.

[18] G. Bianchi, "Performance analysis of the IEEE 802. 11 distributed coordination function," *IEEE Journal on selected areas in communications*, vol. 18, no. 3, pp. 535–547, 2000.

[19] H. Wang and N. Moayeri, "Finite-state markov channel-a useful model for radio communication channels," *Vehicular Technology, IEEE Transactions on*, vol. 44, no. 1, pp. 163–171, 1995.

[20] I. Nikiforov, "A generalized change detection problem," *IEEE Trans. Inf. Theory*, vol. 41, no. 1, pp. 171–187, 1995.

[21] J. Chamberland and V. Veeravalli, "Wireless sensors in distributed detection applications," *IEEE Signal Processing Magazine*, vol. 24, no. 3, p. 16, 2007.

[22] A. Tartakovsky, B. Rozovskii, R. Blazek, and H. Kim, "A Novel Approach to Detection of Intrusions in Computer Networks via Adaptive Sequential and Batch-Sequential Change-Point Detection Methods," *IEEE Trans. Signal Process.*, vol. 54, no. 9, p. 3372, 2006.

[23] A. Adya, P. Bahl, R. Chandra, and L. Qiu, "Architecture and techniques for diagnosing faults in IEEE 802.11 infrastructure networks," in *Proceedings of the 10th annual international conference on Mobile computing and networking*. ACM New York, NY, USA, 2004, pp. 30–44.

[24] S. Rayanchu, A. Mishra, D. Agrawal, S. Saha, and S. Banerjee, "Diagnosing wireless packet losses in 802.11: Separating collision from weak signal," in *IEEE INFOCOM 2008. The 27th Conference on Computer Communications*, 2008, pp. 735–743.

[25] D. Giustiniano, D. Malone, D. Leith, and K. Papagiannaki, "Experimental assessment of 802.11 MAC layer channel estimators," *IEEE Commun. Lett.*, vol. 11, no. 12, pp. 961–963, 2007.

[26] FCC, "Docket No 03-322 Notice of Proposed Rule Making and Order," 2003.

[27] E. Adamopoulou, K. Demestichas, and M. Theologou, "Enhanced estimation of configuration capabilities in cognitive radio," *IEEE Commun. Mag.*, vol. 46, no. 4, pp. 56–63, 2008.

[28] I. Akyildiz, W. Lee, M. Vuran, and S. Mohanty, "NeXt generation/dynamic spectrum access/cognitive radio wireless networks: A survey," *Computer Networks*, vol. 50, no. 13, pp. 2127–2159, 2006.

[29] L. Giupponi and A. Perez-Neira, "Fuzzy-based Spectrum Handoff in Cognitive Radio Networks," in *3rd International Conference on Cognitive Radio Oriented Wireless Networks and Communications. CrownCom 2008.*, 2008, pp. 1–6.

[30] Y. Xing, C. Mathur, M. Haleem, R. Chandramouli, and K. Subbalakshmi, "Dynamic Spectrum Access with QoS and Interference Temperature Constraints," *IEEE Trans. Mob. Comput.*, pp. 423–433, 2007.

[31] H. Rahul, N. Kushman, D. Katabi, C. Sodini, and F. Edalat, "Learning to share: narrowband-friendly wideband networks," *ACM SIGCOMM Computer Communication Review*, vol. 38, no. 4, pp. 147–158, 2008.

[32] N. Kundargi and A. Tewfik, "A novel parallelized goodness-of-Fit test based Dynamic Spectrum access technique for Cognitive Radio Networks," in *Communications, Control and Signal Processing (ISCCSP), 2010 4th Int. Symposium on.* IEEE, pp. 1–5.

[33] ——, "A nonparametric sequential kolmogorov-smirnov test for transmit opportunity detection at the MAC layer," in *Signal Processing Advances in Wireless Communications, 2009. SPAWC'09. IEEE 10th Workshop on.* IEEE, 2009, pp. 101–105.

[34] ——, "ProTOMAC: Proactive Transmit Opportunity Detection at the MAC Layer for Cognitive Radios," in *IEEE International Conference on Communications (ICC), 2010.*

[35] S. Kim, E. Dall'Anese, and G. Giannakis, "Cooperative spectrum sensing for cognitive radios using kriged kalman filtering," *Selected Topics in Signal Processing, IEEE Journal of*, no. 99, pp. 1–1, 2011.

[36] M. Papadopouli, H. Shen, E. Raftopoulos, M. Ploumidis, and F. Hernandez-Campus, "Short-term traffic forecasting in a campus-wide wireless network," in *Personal, Indoor and Mobile Radio Communications, 2005. PIMRC 2005. IEEE 16th International Symposium on*, vol. 3. IEEE, 2005, pp. 1446–1452.

[37] C. Sarr, C. Chaudet, G. Chelius, and I. Lassous, "Bandwidth Estimation for IEEE 802.11-Based Ad Hoc Networks," *IEEE Trans. Mob. Comput.*, vol. 7, no. 10, pp. 1228–1241, 2008.

[38] A. Toledo and X. Wang, "Robust Detection of MAC Layer Denial-of-Service Attacks in CSMA/CA Wireless Networks," *IEEE Trans. Inf. Forensics Secur.*, vol. 3, no. 3, pp. 347–358, 2008.

[39] N. Kundargi and A. Tewfik, "Sensing of Transmission Opportunities at the Medium Access Control Layer for Cognitive Radio Networks," in *3rd International Conference on Wireless VITAE*, 2009.

[40] R. D'Agostino and M. Stephens, "Goodness-of-fit techniques," *Marcel Dekker, Inc. New York, NY, USA*, p. 560, 1986.

[41] M. Stephens, "EDF statistics for goodness of fit and some comparisons," *Journal of the American Statistical Association*, vol. 69, no. 347, pp. 730–737, 1974.

[42] W. Conover, *Practical Nonparametric Statistics*. Wiley, 1999.

[43] D. Quade, "On the Asymptotic Power of the One-Sample Kolmogorov-Smirnov Tests," *Ann. Math. Statist*, vol. 36, no. 3, pp. 1000–1018, 1964.

[44] A. Kolmogoroff, "Sulla determinazione empirica di una legge di distribuzione," *Giorn. 1st. Ital. Attuari*, vol. 4, pp. 83–91, 1933.

[45] J. Durbin, *Distribution Theory for Tests Based on the Sample Distribution Function*. Society for Industrial Mathematics, 1973.

[46] F. Massey, "The Kolmogorov-Smirnov test for goodness of fit," *Journal of the American Statistical Association*, vol. 46, no. 253, pp. 68–78, 1951.

[47] A. Stuart, J. Ord, and S. Arnold, "Kendalls Advanced Theory of Statistics, vol. 2A," *London: Edward Arnold*, 1999.

[48] D. Hawkins, "Retrospective and sequential tests for a change in distribution based on kolmogorov-smirnov-type statistics," *Sequential Analysis*, vol. 7, no. 1, pp. 23–51, 1988.

[49] D. Darling, "The Kolmogorov-Smirnov, Cramer-von Mises Tests," *Ann. Math. Statist*, vol. 28, no. 4, pp. 823–838, 1957.

[50] T. Anderson and D. Darling, "A test of goodness of fit," *Journal of the American Statistical Association*, pp. 765–769, 1954.

[51] J. Rodriguez and A. Viollaz, "A Cramer: von Mises type goodness of fit test with assymetric weight function," *Communications in statistics. Theory and methods*, vol. 24, no. 4, pp. 1095–1120, 1995.

[52] M. Basseville, "Distance measures for signal processing and pattern recognition," *Signal Processing*, vol. 18, no. 4, pp. 349–369, 1989.

[53] S. Ali and S. Silvey, "A general class of coefficients of divergence of one distribution from another," *J. Roy. Statist. Soc. Ser. B*, vol. 28, no. 131-142, p. 213, 1966.

[54] S. Kullback and R. Leibler, "On information and sufficiency," *Annals of Mathematical Statistics*, vol. 22, no. 1, pp. 79–86, 1951.

[55] H. Jeffreys, "An Invariant Form for the Prior Probability in Estimation Problems," *Proceedings of the Royal Society of London. Series A, Mathematical and Physical Sciences (1934-1990)*, vol. 186, no. 1007, pp. 453–461, 1946.

[56] H. Chernoff, "A measure of asymptotic efficiency for tests of a hypothesis based on the sum of observations," *Annals of Mathematical Statistics*, vol. 23, no. 4, pp. 493–507, 1952.

[57] P. Halmos, *Measure Theory*. Springer-Verlag Berlin and Heidelberg GmbH & Co. K, 1974.

[58] A. Bhattacharyya, "On a measure of divergence between two statistical populations defined by their probability distributions," *Bull. Calcutta Math. Soc*, vol. 35, no. 99-109, p. 4, 1943.

[59] T. Kailath, "The Divergence and Bhattacharyya Distance Measures in Signal Selection," *IEEE Trans. Commun.*, vol. 15, no. 1, pp. 52–60, 1967.

[60] B. Park, B. Turlach, C. for Operations Research, and Econometrics, "Practical performance of several data driven bandwidth selectors," *Computational Statistics Quarterly*, vol. 7, pp. 251–251, 1992.

[61] A. Conti, D. Dardari, G. Pasolini, and O. Andrisano, "Bluetooth and IEEE 802.11 b coexistence: analytical performance evaluation in fading channels," *IEEE J. Sel. Areas Commun.*, vol. 21, no. 2, pp. 259–269, 2003.

[62] M. Ettus, "USRP User and Developer Gadauide," *Ettus Research LLC, Febuary*, 2005.

[63] E. Blossom, "Gnu radio: tools for exploring the radio frequency spectrum," *Linux Journal*, vol. 2004, no. 122, p. 4, 2004.

[64] R. D'Agostino and M. Stephens, *Goodness-of-fit techniques*. CRC, 1986.

[65] G. Zhang, X. Wang, Y. Liang, and J. Liu, "Fast and robust spectrum sensing via Kolmogorov-Smirnov test," *Communications, IEEE Transactions on*, vol. 58, no. 12, pp. 3410–3416, 2010.

[66] H. Wang, E. Yang, Z. Zhao, and W. Zhang, "Spectrum sensing in cognitive radio using goodness of fit testing," *Wireless Communications, IEEE Transactions on*, vol. 8, no. 11, pp. 5427–5430, 2009.

[67] A. Glen, L. Leemis, and D. Barr, "Order statistics in goodness-of-fit testing," *Reliability, IEEE Transactions on*, vol. 50, no. 2, pp. 209–213, 2001.

[68] J. Lundén, S. Kassam, and V. Koivunen, "Robust nonparametric cyclic correlation-based spectrum sensing for cognitive radio," *Signal Processing, IEEE Transactions on*, vol. 58, no. 1, pp. 38–52, 2010.

[69] Y. Zeng and Y. Liang, "Eigenvalue-based spectrum sensing algorithms for cognitive radio," *Communications, IEEE Transactions on*, vol. 57, no. 6, pp. 1784–1793, 2009.

[70] S. Kassam, "A bibliography on nonparametric detection," *IEEE Transactions on Information Theory*, vol. 26, pp. 595–602, 1980.

[71] B. Seyfe and A. Sharafat, "Signed-rank nonparametric multiuser detection in non-Gaussian channels," *Information Theory, IEEE Transactions on*, vol. 51, no. 4, pp. 1478–1486, 2005.

[72] H. Chen, P. Varshney, S. Kay, and J. Michels, "Noise enhanced nonparametric detection," *Information Theory, IEEE Transactions on*, vol. 55, no. 2, pp. 499–506, 2009.

[73] Y. Zeng, Y. Liang, A. Hoang, and R. Zhang, "A review on spectrum sensing for cognitive radio: challenges and solutions," *EURASIP Journal on Advances in Signal Processing*, vol. 2010, pp. 2–2, 2010.

[74] M. Schervish, "P Values: What They Are and What They Are Not." *The American Statistician*, vol. 50, no. 3, 1996.

[75] J. Hoenig and D. Heisey, "The abuse of power," *The American Statistician*, vol. 55, no. 1, pp. 19–24, 2001.

[76] D. Donoho and J. Jin, "Higher criticism for detecting sparse heterogeneous mixtures," *The Annals of Statistics*, vol. 32, no. 3, pp. 962–994, 2004.

[77] J. Angus, "The probability integral transform and related results," *SIAM review*, vol. 36, no. 4, pp. 652–654, 1994.

[78] L. Jager and J. Wellner, "Goodness-of-fit tests via phi-divergences," *The Annals of Statistics*, vol. 35, no. 5, pp. 2018–2053, 2007.

[79] N. Cressie, "Multinomial goodness-of-fit tests," *Journal of the Royal Statistical Society. Series B (Methodological)*, vol. 46, no. 3, pp. 440–464, 1984.

[80] F. Liese and I. Vajda, "On divergences and informations in statistics and information theory," *Information Theory, IEEE Transactions on*, vol. 52, no. 10, pp. 4394–4412, 2006.

[81] I. Vajda, *Theory of statistical inference and information*. Kluwer Academic Publishers Boston, 1989.

[82] R. Berk and D. Jones, "Goodness-of-fit test statistics that dominate the kolmogorov statistics," *Probability Theory and Related Fields*, vol. 47, no. 1, pp. 47–59, 1979.

[83] J. Wellner and V. Koltchinskii, "A note on the asymptotic distribution of berk-jones type statistics under the null hypothesis," *High Dimensional Probability III*, pp. 321–332, 2003.

[84] L. Jager and J. Wellner, "A new goodness of fit test: the reversed berk-jones statistic," 2004.

[85] J. Einmahl and I. McKeague, "Empirical likelihood based hypothesis testing," *Bernoulli*, vol. 9, no. 2, pp. 267–290, 2003.

[86] D. Middleton, "Non-Gaussian noise models in signal processing for telecommunications: New methods an results for class A and class B noise models," *Information Theory, IEEE Transactions on*, vol. 45, no. 4, pp. 1129–1149, 1999.

[87] A. Chopra, K. Gulati, B. Evans, K. Tinsley, and C. Sreerama, "Performance bounds of MIMO receivers in the presence of radio frequency interference," in *IEEE International Conference on Acoustics, Speech and Signal Processing*, 2009, pp. 2817–2820.

[88] L. Liu and M. Amin, "Performance analysis of GPS receivers in non-Gaussian noise incorporating precorrelation filter and sampling rate," *Signal Processing, IEEE Transactions on*, vol. 56, no. 3, pp. 990–1004, 2008.

[89] R. Donahue, "A Note on Information Seldom Reported Via the P Value." *The American Statistician*, vol. 53, no. 4, 1999.

[90] E. Lehmann and J. Romano, *Testing statistical hypotheses*. Springer Verlag, 2005.

[91] S. Metchev and G. JE, "A two-dimensional Kolmogorov–Smirnov test for crowded field source detection: ROSAT sources in NGC 6397," *Monthly Notices of the Royal Astronomical Society*, vol. 335, no. 1, pp. 73–83, 2002.

[92] R. Lopes, I. Reid, and P. Hobson, "The two-dimensional Kolmogorov-Smirnov test," in *XI International Workshop on Advanced Computing and Analysis Techniques in Physics Research, Nikhef, Amsterdam, the Netherlands, April 23-27, 2007*, 2007.

[93] G. Fasano and A. Franceschini, "A multidimensional version of the Kolmogorov-Smirnov test," *Monthly Notices of the Royal Astronomical Society*, vol. 225, pp. 155–170, 1987.

[94] M. Noe, "The calculation of distributions of two-sided Kolmogorov-Smirnov type statistics," *The Annals of Mathematical Statistics*, vol. 43, no. 1, pp. 58–64, 1972.

[95] K. Kim, I. Akbar, K. Bae, J. Urn, C. Spooner, and J. Reed, "Cyclostationary approaches to signal detection and classification in cognitive radio," in *2nd IEEE International Symposium on New Frontiers in Dynamic Spectrum Access Networks, 2007. DySPAN 2007*, 2007, pp. 212–215.

[96] Z. Quan, S. Cui, A. Sayed, and H. Poor, "Optimal Multiband Joint Detection for Spectrum Sensing in Cognitive Radio Networks," *IEEE Trans. Signal Process.*, vol. 57, no. 3, pp. 1128–1140, 2009.

[97] C. Cordeiro, K. Challapali, and D. Birru, "IEEE 802.22: An Introduction To The First Wireless Standard Based On Cognitive Radios," *Journal of Communications*, vol. 1, no. 1, pp. 38–47, 2006.

[98] A. Sahai, N. Hoven, and R. Tandra, "Some Fundamental Limits on Cognitive Radio," in *Allerton Conference on Communication, Control, and Computing*, 2004.

[99] D. Cabric, A. Tkachenko, and R. Brodersen, "Experimental Study of Spectrum Sensing Based on Energy Detection and Network Cooperation," in *1st International Workshop on Technology and Policy for Accessing Spectrum, TAPAS.*, 2006.

[100] H. Urkowitz, "Energy detection of unknown deterministic signals," *Proceedings of the IEEE*, vol. 55, no. 4, pp. 523–531, 1967.

[101] D. Cabric, S. Mishra, and R. Brodersen, "Implementation issues in spectrum sensing for cognitive radios," in *Signals, Systems and Computers, 2004. Conference Record of the Thirty-Eighth Asilomar Conference on*, vol. 1. Ieee, 2004, pp. 772–776.

[102] S. Chang, "Analysis of proposed sensing schemes: Ieee 802.22-06/0032r0," 2006.

[103] A. Ghasemi and E. Sousa, "Collaborative spectrum sensing for opportunistic access in fading environments," in *First IEEE International Symposium on New Frontiers in Dynamic Spectrum Access Networks, 2005. DySPAN.*, 2005, pp. 131–136.

[104] R. Blum, S. Kassam, and H. Poor, "Distributed detection with multiple sensors I. Advanced topics," *Proceedings of the IEEE*, vol. 85, no. 1, pp. 64–79, 1997.

[105] N. Kundargi and A. Tewfik, "Hierarchical Sequential Detection In The Context Of Dynamic Spectrum Access For Cognitive Radios," in *14th IEEE International Conference on Electronics, Circuits and Systems. ICECS*, 2007.

[106] ——, "Sequential pilot sensing of ATSC signals in IEEE 802.22 cognitive radio networks," *IEEE International Conference on Acoustics, Speech and Signal Processing. ICASSP*, 2008.

[107] T. Lai, "Sequential analysis: some classical problems and new challenges," *Statistica Sinica*, vol. 11, no. 2, pp. 303–350, 2001.

[108] L. Lai, Y. Fan, and H. Poor, "Quickest Detection in Cognitive Radio: A Sequential Change Detection Framework," in *IEEE Global Telecommunications Conference. GLOBECOM*, 2008.

[109] Y. Xin, H. Zhang, Z. Ho, V. Lau, R. Cheng, V. Mordachev, and S. Loyka, "A Simple Sequential Spectrum Sensing Scheme for Cognitive Radio," *Arxiv preprint arXiv:0905.4684*, 2009.

[110] S. Kay, *Fundamentals of Statistical Signal Processing*. Prentice Hall PTR, 1993.

[111] R. Chen, J. Park, and K. Bian, "Robust Distributed Spectrum Sensing in Cognitive Radio Networks," in *27th IEEE Conference on Computer Communications, INFOCOM 2008.*

[112] A. Wald, *Sequential analysis*. Dover Publications, 2004.

[113] M. Simon, *Probability Distributions Involving Gaussian Random Variables: A Handbook for Engineers and Scientists*. Kluwer Academic Publishers, 2002.

[114] J. Coon, M. Sandell, M. Beach, J. McGeehan, and T. Bristol, "Channel and Noise Variance Estimation and Tracking Algorithms for Unique-word Based Single-carrier Systems," *IEEE Transactions on Wireless Communications*, vol. 5, no. 6, pp. 1488–1496, 2006.

[115] Z. Botev, "Nonparametric Density Estimation via Diffusion Mixing," *The University of Queensland, Postgraduate Series, Nov*, 2007.

[116] P. Hall, S. Sheather, M. Jones, and J. Marron, "On Optimal Data-based Bandwidth Selection in Kernel Density Estimation," *Biometrika*, vol. 78, no. 2, pp. 263–269, 1991.

[117] C. Stevenson, G. Chouinard, Z. Lei, W. Hu, S. Shellhammer, and W. Caldwell, "Ieee 802.22: The first cognitive radio wireless regional area network standard," *Communications Magazine, IEEE*, vol. 47, no. 1, pp. 130–138, 2009.

[118] M. Ghosh, "Text on fft-based pilot sensing-for informative annex on sensing techniques," in *IEEE 802.22 Meeting Doc*, 2007.

[119] C. Cordeiro, M. Ghosh, D. Cavalcanti, and K. Challapali, "Spectrum sensing for dynamic spectrum access of tv bands," in *Cognitive Radio Oriented Wireless Networks and Communications, 2007. CrownCom 2007. 2nd International Conference on.* IEEE, 2007, pp. 225–233.

[120] S. Mathur, R. Tandra, S. Shellhammer, and M. Ghosh, "Initial signal processing of captured dtv signals for evaluation of detection algorithms," *IEEE 802.22-06/0158r4*, 2006.